# Basic studies and functional design
# of fluorinated polymer/ionic liquid composites

## Akiko Tsurumaki

# Abstract

Materials based on polymers have gathered much attention due to their thermal stability and mechanical stability.　Among them, fluorinated polymers have attracted a wide attention for their extreme inertness to chemicals.　Due to the inertness of fluorinated polymers, adduct will bleed out from fluorinated matrices when their composites are designed.　In order to prevent this, affinity between additives and fluorinated polymers are needed to be controlled.　On the other hand, ionic liquids (ILs) have been recognized as potential additives for polymers due to their unique property set such as high ionic conductivity, possibility of design, and thermal stability.　Since there are numerous combination of cations and anions, there is a strong expectation to design functional additives for polymers including fluorinated polymers using the ILs.　However, there is no strategy to design ILs as additives for fluorinated polymers.　In this dissertation, affinity between ILs and fluorinated polymers will be analyzed and factors to control the affinity will be discussed.　Then, these results will be extended to functional design of homogeneous composites based on fluorinated polymers (*e.g.* poly(tetrafluoroethylene) (PTFE)) and ILs.

# Preface

This dissertation is original and independent work by the author, Akiko Tsurumaki.

<div align="right">

Akiko Tsurumaki

March 2015

</div>

Table of contents

Chapter 1

# Polymer composites containing ionic liquids

## 1-1.　Ion conductive materials

Ion conductive materials are critical components involved in balancing energy and safety specifications of energy devices.　With the growth of the market in energy devices, there is a strong request to improve credibility and stability of ion conductive material.　Accordingly, many kinds of ion conductive materials containing volatile organic solvent have been replaced to the non-volatile substances.　Here I account of the developments of polymer electrolyte aiming improvements in terms of credibility, thermal- and electrochemical-stability.

### 1-1-1.　Classification

**Electrolyte solution**

　　　　Electrolyte solution can be divided into aqueous and non-aqueous ones.　Aqueous electrolytes, such as $H_2SO_4$ aq. for voltaic cell and KCl aq. for conductivity standard, are prepared by dissolving salts to $H_2O$.　The electrolytes enhance high ionic conductivity as the additive salts are dissociated into ions accompanying donor-acceptor and ion-dipole interactions with $H_2O$. Since the electrolyte contains $H_2O$, the effect of moisture on the ionic conductivity and stability of the electrolyte is not noteworthy.　However, the potential window for this electrolyte is limited to ~1.23 V vs. SHE due to the hydrogen evolution around -0.83 V vs SHE at the cathodic side and oxygen evolution around 0.40 V vs. SHE at the anodic side [1].　Additionally, since aqueous media is corrosive to alkaline metal, the aqueous electrolytes are not suitable for lithium ion battery. Due to these properties, the aqueous electrolytes have been applied to super capacitor [2] and lithium-air battery [3].

　　　　Non-aqueous electrolytes based on aprotic organic solvents have been developed in parallel to the development of the aqueous ones.　These electrolytes have the following characteristics:

　　　　1: Ion conductive comparable to aqueous electrolytes
　　　　2: Stable against to the anode materials, *e.g.* metallic lithium
　　　　3: Remarkable cathodic limit arising from aprotic properties of the solvents
　　　　4: Tolerative against high potential as high as 5.5 V [4]
　　　　5: Suppressive of reaction between fluoro anions and water

　　　　Due to their remarkable electrochemical stabilities, various non-aqueous electrolytes have been applied for lithium ion batteries which are required 4 V as a working voltage.　**Figure 1-1** shows structure of aprotic solvents particularly used as the electrolytes for lithium ion batteries.　**Table 1-1** summarizes the physicochemical properties of selected solvents.　Non-

aqueous electrolytes usually consist of ester or ether groups in order to dissociate additive salts via dipoles.   Among these solvents, ethylene carbonate (EC) and propylene carbonate (PC) have large dielectric permittivity and effectively dissociate additive salts.   On the other hand, ether-based solvents, such as tetrahydrofuran (THF) and dimethoxyethane (DME), have lower dielectric permittivity, but have lower viscosity compared to ester based solvents and result in sufficient ionic conductivity.   Physicochemical properties of the electrolyte solution can be controlled by mixing several solvents.   For example, dimethyl carbonate (DMC) is added to lower melting point ($T_m$) of EC, and DME is added to lower viscosity of carbonate solutions.
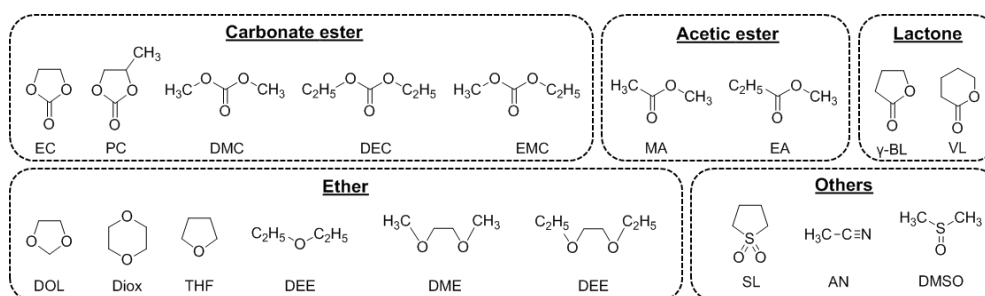


**Figure 1-1.**   Structure of aprotic solvents for non-aqueous electrolytes.

**Table 1-1.**   Physicochemical properties of aprotic solvents for electrolytes [5].
($T_m$: melting point, $T_b$: boiling point, $\varepsilon$: dielectric permittivity, $\eta$: viscosity)

| Solvent | Abbreviation | $T_m$ /°C | $T_b$ /°C | $\varepsilon$ | $\eta$ / cP |
|---------|-------------|-----------|-----------|---------------|-------------|
| Ethylene carbonate @40 °C | EC | 36.5 | 238 | 90.4 | 1.9 |
| Propylene carbonate | PC | -54.5 | 242 | 65.0 | 2.51 |
| Dimethyl carbonate | DMC | 3 | 90 | 3.1 | 0.59 |
| Diethyl carbonate | DEC | -43.0 | 126.8 | 2.8 @ 20 °C | 0.75 |
| Tetrahydrofuran | THF | -108.5 | 66.0 | 7.4 | 0.46 |
| Dimethoxyethane | DME | -58 | 84.5 | 7.1 | 0.41 |

As for additive salts for non-aqueous electrolyte, lithium salts containing fluoro anion, such as lithium bis(trifluoromethanesulfonyl)imide (Li[Tf$_2$N]), LiPF$_6$, LiBF$_4$, LiAsF$_6$, LiCF$_3$CO$_2$, and LiCF$_3$SO$_3$ have been applied.   These salts are stable in the non-aqueous system, in spite of the fact that fluoro anion is undesirable for aqueous electrolyte, because it may react with H$_2$O as shown in following steps [6].

$LiPF_6 \rightleftarrows Li^+ + PF_6^-$ ...(ionization)

$LiPF_6 \rightleftarrows LiF + PF_5$ ...(step 1)

$PF_5 + H_2O \rightleftarrows POF_3 + 2HF$ ... (step 2)
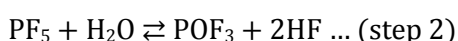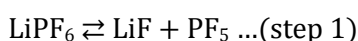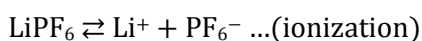
Furthermore, $POF_3$ is possible to react with water in a following step [7].

$$POF_3 + H_2O \rightarrow POF_2(OH) + HF \ldots (step \; 3)$$
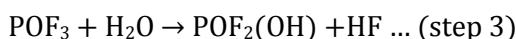
As shown in step 1, nonionized $LiPF_6$ dissociate to $PF_5$ and $LiF$, and $PF_5$ reacts with water (step 2). The solvents having large dielectric permittivity (see **Table 1-1**) ionize effectively $LiPF_6$, thereby suppressing the reaction with $H_2O$.   The non-aqueous electrolyte solution (*e.g.* LP 30 consisting 1M $LiPF_6$ in EC/DMC 1:1(v/v) is available from BASF Corporation) are widely used not only in laboratory scale but also in industry field.

### Solid state electrolytes

Inorganic solid electrolytes are also examined in contrast with liquids electrolyte consisting of organic solvent and inorganic/organic salts.   Replacement of organic solvent with inorganic crystal promises to widen a temperature range of working and improve thermal stability of the electrolytes.   $\beta$-Alumina containing sodium ion is one of the earliest solid state electrolytes [8].   The formula of is $\beta$-Alumina $Na_2O\text{-}11Al_2O_3$ and sodium ions migrate spinel-type block of aluminum and oxygen ions [9].   They show ionic conductivity exceeding $10^{-3}$ S cm$^{-1}$ at room temperature in the crystalline state.   However, this material is hygroscopic and difficult to prepare at ambient condition.   As subsequent work, solid solution containing alkali metal ion has been developed and ionic conductivity comparable to $\beta$-Alumina system is obtained (**Figure 1-2**) [10].
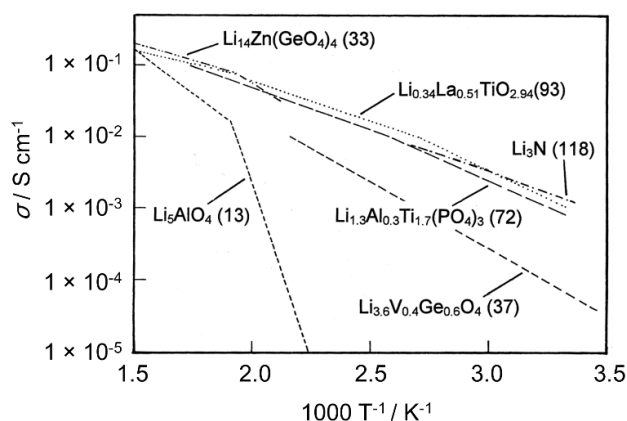


**Figure 1-2.**  Ionic conductivity of several solid state electrolytes [10].

### Polymer electrolytes
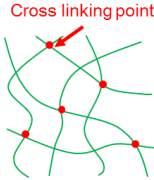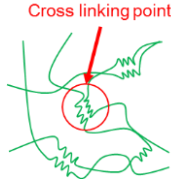
Beside the development of liquid-type electrolytes, conductivity enhancement in polymer matrices has been motivated after a pioneering work by P.V. Wright on the polyether-alkali metal salts complexes [11].   Mechanisms of ion conduction and factors to control conductivity of the polyether-based polymer electrolytes are summarized in following sections.

The polymer electrolytes are classified into dry and gel-like polymer electrolytes. The original polymer electrolytes based on poly(ethylene oxide) (PEO) and NaSCN result in 4.5:1 complex and are classified to dry polymer electrolytes [12]. This electrolyte show ionic conductivity around $10^{-8}$ S cm$^{-1}$ at room temperature. To improve ionic conductivity of these polymer electrolytes, many attempts have been made. As ionic conductivity of dry polymer electrolytes depend on the crystallinity of PEO matrices; *i.e.* low glass transition temperature ($T_g$) is required for high ionic conductivity, the matrices having branch structure with PEO oligomers have been developed. For example, PEO having (2-methoxy)ethyl glycidyl as side chain (PMEGE), shows the ionic conductivity of $3 \times 10^{-5}$ S cm$^{-1}$ when the polymer dissolves LiClO$_4$ (**Table 1-2**). This improvement derived from lowering $T_g$ motived to design gel polymer electrolytes.

**Table 1-2.** Systems of polymer electrolytes and their conductivity at 20 °C
(adopted from ref [13]).

| Host polymer matrices | Repeat unit | Complex with LiClO$_4$ (as example) | Conductivity / S cm$^{-1}$ |
|---|---|---|---|
| **Linear** | | | |
| Poly(ethylene oxide) (PEO) | $-[CH_2CH_2O]_n-$ | (PEO)$_8$-LiClO$_4$ | $10^{-8}$ |
| Poly(oxymethylene) (POM) | $-[CH_2O]_n-$ | (POM)-LiClO$_4$ | $10^{-8}$ |
| Poly(propylene oxide) (PPO) | $-[CH(CH_3)CH_2O]_n-$ | (PPO)$_8$-LiClO$_4$ | $10^{-8}$ |
| Poly(dimethyl siloxane) (DMS) | $-[Si(CH_3)_2-O]_n-$ | (DMS)-LiClO$_4$ | $10^{-4}$ |
| **Branched** | | | |
| Comb branched ethers *e.g.* Poly[(2-methoxy)ethyl glycidyl ether] (PMEGE) | $-[CH_2CH(CH_2(OCH_2CH_2)_2OCH_3)O]_n-$ | (PMEGE)$_8$-LiClO$_4$ | $10^{-5}$ |
| Comb-branched methacrylates *e.g.* Poly[methoxy poly(ethylene glycol)methacrylate] (PMG) | $-[C(CH_3)(CO_2(CH_2CH_2O)_xCH_3)CH_2]_n-$ | (PMG)$_{22}$- LiCF$_3$SO$_3$ (EO:Li$^+$ = 18:1) | $3 \times 10^{-5}$ |
| Polysiloxanes *e.g.* PEO-grafted polysiloxane | $-[Si(CH_3)(CH_2CH_2PEO)-O]_n-$ | PGPS- LiClO$_4$ | $10^{-4}$ |

**Table 1-3.** Differences of properties depending on the bond type.

| Properties | Bond type | |
|---|---|---|
| | Chemical crosslinks | Physical crosslinks |
| Typical structure | | |
| Thermal stability | Morphologically stable but thermal decomposition due to crosslinking point can occur | Fluidize at high temperature |
| Mechanical stability | Increase with crosslinking density | Normally high |
| Trigger of ion conduction | Segmental motion of matrices | Amorphous phase plasticized with electrolyte solution |
| Ionic conductivity | Desired | Acceptable |
| Electrochemical stability | Acceptable ~ Desired | Excellent |
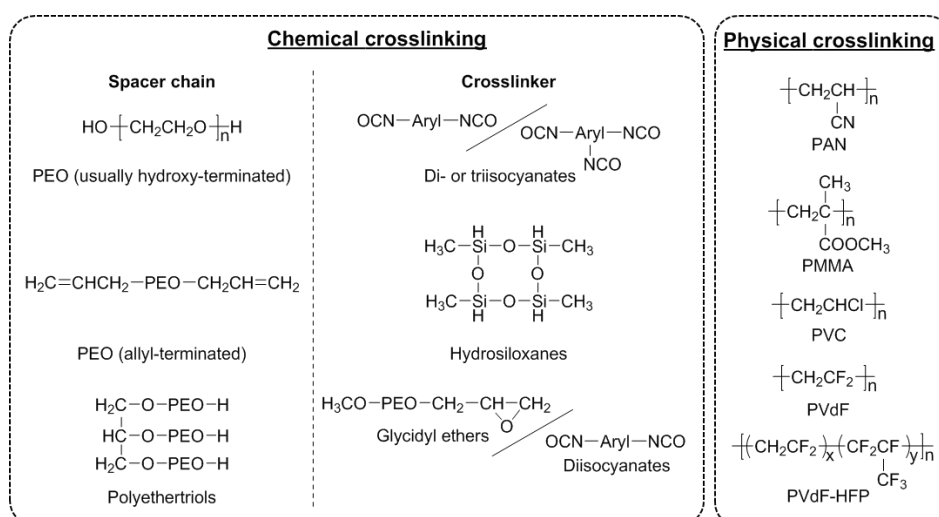
**Figure 1-3.** Structure of polymer matrices for gel electrolytes [3c, 14].

The gel polymer electrolytes can be obtained as a result of either chemical crosslinks or physical crosslinks.    Chemical crosslinks in gel polymer electrolytes can lead to the formation of irreversible gels (**Table 1-3**, left).    For example, the gels based on hydroxyl-terminated polyethers crosslinked with di- or tri-isocyanates, allyl-terminated polyethers crosslinked with hydrosiloxanes, and polyethertriols crosslinked with diisocyanates or glycidyl ethers have been developed (**Figure 1-3**, left).    These suffer from breaking of crosslinking points upon heating, stressing, adding chemicals, and applying voltage; however, particular chemical gels used as battery electrolytes are essentially stable.    The mechanical stability of chemical gels is improved

depending on crosslinking density.   As a tradeoff, the higher crosslinking density results in the lower ionic conductivity, since the ion migration of these materials are triggered by segmental motion of spacer chain, and increasing crosslinking density collaterally bring increase of $T_g$.   In contrast, physical crosslinks lead to the formation of entanglement network of polymers (**Table 1-3**, right).   For this case, PEO as well as poly(acrylonitrile) (PAN), poly(methyl methacrylate) (PMMA), poly(vinyl chloride) (PVC), poly(vinylidene fluoride) (PVdF), and poly(vinylidene fluoride-*co*-hexafluoropropylene) (PVdF-HFP) are used as matrices (**Figure 1-3**, right).   These polymer matrices are also used for dry polymer electrolytes, but mostly swelled with some carbonate solvents and applied as gel polymer electrolytes.   These polymers have linear structure, and they change their morphology around $T_m$ (*e.g.* PAN: $T_m = 317$ °C and PVdF: $T_m = 171$ °C).   The morphology also changes when the polymer matrices are mixed excess electrolyte solution.     For instance, gel electrolytes based on PVdF-HFP with 60 % of LiPF$_6$-EC-PC mixture shows a balanced properties in terms of elasticity and ionic conductivity, although the composite containing > 60 % of the solution results in viscous electrolyte solution (**Figure 1-4**) [15].   In order to improve mechanical stability, the polymer having higher molecular weight are used regardless of the increase in $T_g$, since the polymer matrices for physical gel are plasticized with carbonate solution.   For this case, factors to control plasticization of polymers, such as compatibility between polymers and electrolyte solutions, their mixing ratio, and curing temperature, have to be considered.   With respect to high mechanical stability and acceptable thermal stability, many gel electrolytes have been developed in this system.
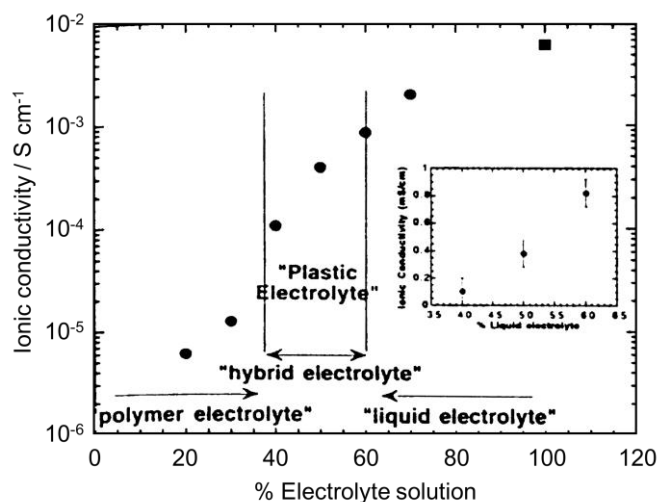


**Figure 1-4.**  Ionic conductivity of gel electrolyte based on PVdF–12% HFP and 1 M LiPF$_6$ in EC-PC mixture [15].

### 1-1-2. Ion conduction based on segmental motion of polymer matrices

PEO has been recognized to form complex with various salts via ion-dipole interactions [16]. In 1975, P. V. Wright discovered conductivity of PEO–salts composites [11]. In this paper, direct current conductivities for PEO-NaSCN, -NaI, -KSCN, and –NH$_4$SCN composites were demonstrated in order to discuss the structure of their coordinations in the amorphous phase. At that time, highest conductivity was found to be 10$^{-7}$ ohm$^{-1}$ cm$^{-1}$ for PEO-NaI. In 1979, M. Armand addressed the development of polyethers as electrolytes for the battery application [12]. In this paper, they discussed with the effect of cation species, salt concentration, and crystallinity of PEO on the conductivity of PEO-alkali metal salt complexes. For the PEO-NaSCN complex, the conductivity change as a function of temperature showed good agreement with the Arrhenius model (**Figure 1-5**, second left) [12]. This complex was crystalline through the temperature range, but showed a transition around 65 $^o$C, and activation energy for ionic conductivity changed around the transition temperature. For the PEO-CsSCN and PEO-LiSCN composites (**Figure 1-5**, far left and far right), the composites behaved like viscous liquids on the microscopic scale, and temperature dependence of conductivity followed the Vogel-Tamman-Fulcher (VTF) model, indicating remarkable agreement with the free-volume theory for the mechanism of conductivity. This suggests that ions dissociated in these composites migrate in the amorphous phase. Mixed behavior of the Arrhenius and the VTF is also observed for the PEO-KSCN composite. This composite showed $T_m$ around 80 $^o$C and gave highly conductive elastomeric phase.
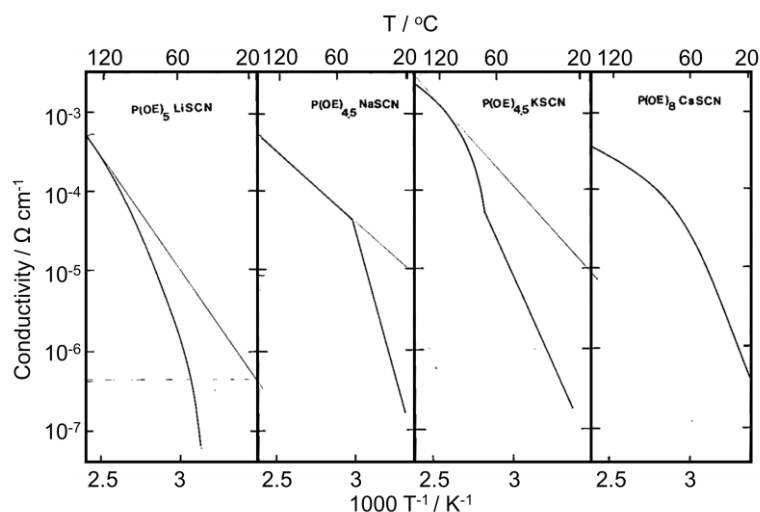


**Figure 1-5.** Conductivity of PEO-alkali thiocyanate composites.
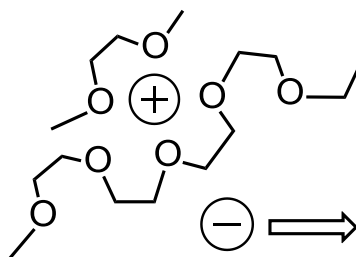
**Figure 1-6.**  Ion conduction model in amorphous phase of PEO-salts composites.

In the solid state electrolytes, ions having kinetic energies greater than the activation energies can migrate in the crystals state, and the Arrhenius model is applied to explain the mechanisms of ion conduction.   The ionic conduction in crystalline PEO composites can also be interpreted in the same manner.   On the other hand, for the ionic conduction in amorphous PEO composites, some specific ideas based on the VTF model have been summarized in 1980s.   In the amorphous phase, ion conduction process is dependent on the complex formation via mutual motion of ether oxgens from two or more polymer chains (**Figure 1-6**) [17].   The formation of coordination has been confirmed by the Raman measurements from of cation-dependent vibration bands [18].   The typical structure of the composite is 4:1, but the 6:1 complex is of greater interest as their conductivity increasing significantly on raising the polymer content from 3:1 to 6:1 [19].

**Table 1-4.**  Complex formation of various alkali metal salts and PEO or PPO [17].

| Ion species | PEO | | | | | | PPO | | | | | |
|:---:|:---:|:---:|:---:|:---:|:---:|:---:|:---:|:---:|:---:|:---:|:---:|:---:|
| | $Li^+$ | $Na^+$ | $K^+$ | $Rb^+$ | $Cs^+$ | $NH_4^+$ | $Li^+$ | $Na^+$ | $K^+$ | $Rb^+$ | $Cs^+$ | $NH_4^+$ |
| $F^-$ | ✕ | ✕ | ✕ | ✕ | ✕ | ✕ | ✕ | ✕ | ✕ | ✕ | ✕ | ✕ |
| $Cl^-$ | ○ | ✕ | ✕ | ✕ | ✕ | ✕ | ✕ | ✕ | ✕ | ✕ | ✕ | ✕ |
| $Br^-$ | ○ | ○ | ✕ | ✕ | ✕ | ✕ | ✕ | ✕ | ✕ | ✕ | ✕ | ✕ |
| $I^-$ | ○ | ○ | ○ | ○ | ○ | ○ | ○ | ✕ | ✕ | ✕ | ✕ | ✕ |
| $SCN^-$ | ○ | ○ | ○ | ○ | ○ | ○ | ○ | ○ | ✕ | ✕ | ✕ | ✕ |
| $ClO_4^-$ | ○ | ○ | ○ | ○ | ○ | ○ | ○ | ○ | ✕ | ✕ | ✕ | ✕ |
| $CF_3SO_3^-$ | ○ | ○ | ○ | ○ | ○ | ○ | ○ | ○ | ✕ | ✕ | ✕ | ✕ |
| $AsF_6^-$ | ○ | ○ | ○ | ○ | ○ | ○ | ○ | ○ | ✕ | ✕ | ✕ | ✕ |
| $BO_4^-$ | ○ | ○ | ○ | ○ | ○ | ○ | ○ | ○ | ✕ | ✕ | ✕ | ✕ |

The PEO-salts complexes are formed only when the solvation energy compete cohesive energy of PEO and lattice energy of salts.    The effect of cohesive energy of polymers clearly come out when the solubility of salts into PEO and PPO are compared (**Table 1-4**) [20].    Since the electron donor properties of both ethers are comparable, the difference of solubility are issued by the difference of the cohesive energies of the polymer matrix.    For the case of PPO, the steric hindrance by methyl group increase cohesive energy, thus reducing the interaction with adduct.  Hard and soft, acids and bases (HSAB) theory [21] has been applied to discuss the competition between cation-PEO and –anion interaction [20].    PEO is classified as a hard base and dissolves inorganic salts having hard acids such as Li salts and Na salts.    Among these salts, LiF, NaF, and NaCl are insoluble to PEO.    Since F and Cl are also hard base, cation-anion interaction compete the PEO-cation interaction.    The HSAB theory has also proven helpful in considering the ionic conductivity of PEO/inorganic salt complex.

### 1-1-3.    Polymer electrolytes consisting polyethers

PEO tend to crystallize below 60 ℃, conductivity higher than $10^{-4}$ S cm$^{-1}$ are obtained at around $60 \sim 80$ ℃.    In order to improve ionic conductivity as well as cation transference number for the purpose of alkali metal batteries, many attempts to design novel PEO-salts composites have been made.    There are two major tasks in developing these polymer electrolytes: design of polymer matrix and design of additives.

Ion conduction in polyethers are realized by segmental motion of polyethers.    Thus, low molecular weight of polyethers stimulate low $T_g$ and high ionic conductivity.    As a tradeoff, to improve mechanical stability of polyether-based film, polyethers with higher molecular weight is favorable.    To overcome this drawback, branched polyether matrices have been designed.    The ionic conductivity of these branched polyethers is larger than that of linear polyether hundred times or more (see **Table 1-2**).    In the field of lithium ion batteries, conductivity of lithium cation is required to be improved.    For this purpose, negative charges of salts were fixed to poleyhter matrices.    As anion-fixed polymer electrolytes such as poly[(oligo(oxyethylene)methacrylate)-*co*-(alkali-metal methacrylate)] and alkali-metal salts of poly[(ω-carboxy)oligo(oxyethylene) methacrylate] have been reported [22].    These polymer electrolytes allow single-ion conduction because all the anion charges are fixed on the main chain.    In spite of the single ionic properties of these polymers, the ionic conductivity is not particularly high because of the lower carrier ion density.    Further improvement is needed in this area.

To improve thermal-, electrical-, and mechanical-properties, addition of inorganic filler is attractive.    The nanometer-sized $TiO_2$ and $AlO_3$ are added to PEO as solid plasticizers which kinetically inhibit crystallization of PEO [23].    Thus, the composite of PEO-based electrolyte such as PEO-LiClO$_4$ composite containing powder of these inorganic fillers enhance conductivity of 10-

[4] S cm$^{-1}$ at 50 $^o$C and 10$^{-5}$ at 30 $^o$C.  Two important feature of this system are increase of Li transport number and low interfacial resistance in contact with Li metal.  Decrease of the interfacial resistance would be caused by the formation of homogeneous interface induced by the filler addition.

### 1-1-4.  Ionic liquids as alternative additive salts

#### Basics of ILs

In recent years, ionic liquids (ILs), which are molten salts below 100 $^o$C, have been proposed as potential candidates for new additive salts.   The first paper which state the possibility to design room temperature molten salts was reported by Walden in 1914 [24].   Aside from low stability against water, ethylamine nitrate (mostly abbreviated as EAN) was reported to have $T_m$ of 12 $^o$C. In 1992, 1-ethyl-3-methylimidazolium BF$_4$ ([C$_2$mim]BF$_4$, $T_m$ = 15 $^o$C) and [C$_2$mim]CH$_3$CO$_2$ ($T_m$ = -45 $^o$C) was reported as air- and moisture-stable ILs.   This discovery accelerated a development of ILs, and ILs have been applied to organic reactions [25], biochemistry fields [26], and electronics fields [27].   The advantage of ILs is that at least a million binary ILs are possible to design.   For comparison, about 600 molecular solvents are in use today [28].   Here I summarize particular characteristics of ILs and typical ions used as component of ILs (**Figure 1-7**).   .

Typically [29]
 ・Remain liquid state in a wide range of temperature
 ・Have high ion density
 ・Possess high thermal stability and negligible vapor pressure
 ・Show high heat capacity

Possibly
 ・Have high ionic conductivity without molecular solvents even at ambient temperature
 ・Functionalized to show high polarity, hydrophobicity, or affinity with other materials
   Not all ILs complete these properties, however, ILs having dual function such as hydrophobic- and polar-ILs are possible to design [30].
 ・Recursive use
 ・Realize low viscosity for particular ILs; *e.g.* 1-allyl-3-methylimidazolium dicyanoborate ([Amim][DCA]) has viscosity of 12.4 cP [31]
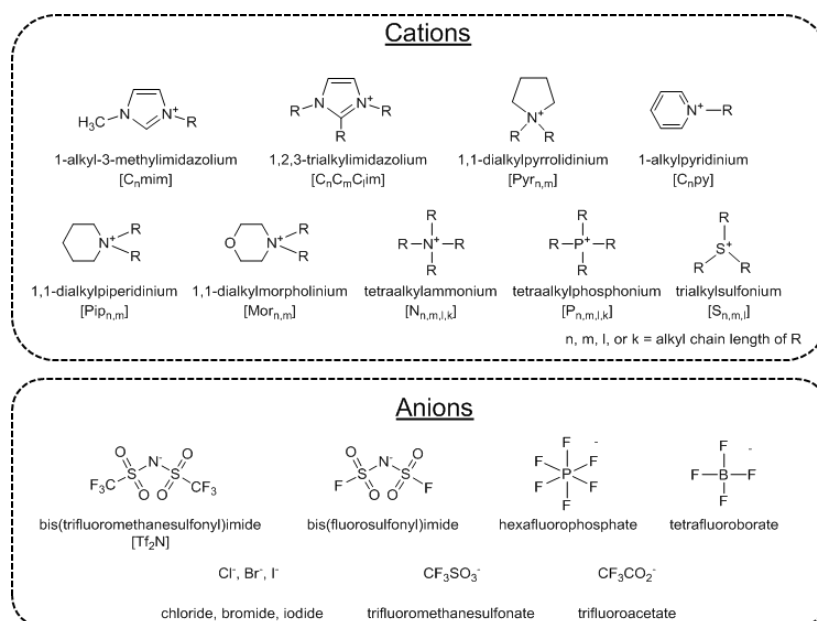
**Figure 1-7.**    Some common ions used in ILs and their abbreviations.

## ILs for additive salts for polyethers

Here I compare polyether-inorganic salt composites and polyether-IL composites.    For the case of the composites with inorganic salts, salts are dissociated into ions via ion-dipole interaction, and enhance ionic conductivity activated from segmental motion of polyether.    On the other hand, the composites with ILs, there exist larger amount of free ions regardless of interaction due to $T_g$ of the ILs.    Higher ionic conductivity is easily obtained by using ILs.    Due to their low $T_g$ of ILs, ILs themselves are intrinsically conductive and show enhanced conductivity compared to inorganic systems.

## ILs for electrochemistry

There are an increasing number of ILs as a novel electrolyte system for electrochemical devices such as lithium batteries, capacitors, fuel cells, and solar cells respect to their considerable ionic conductivity, stability even under high-voltage, non-volatility and flame-resistant nature. The most important - and interesting-point of ILs is that they provide many mobile ions in a polymer matrix without molecular solvents.    An imidazolium-based IL (*e.g.* 1-ethyl-3-methylimidazolium bis(trifluoromethanesulfonyl)imide; [C$_2$mim][Tf$_2$N]) has been studied because of its low viscosity and relatively high ionic conductivity.    However, imidazolium-based ILs are not suitable for lithium batteries because of their cathodic limit (1 V vs. Li$^+$/Li) arising from acidic protons on the imidazolium ring [32].    Therefore, the challenge is to increase cathodic stability by using aliphatic cations such as pyrrolidinium [33], quaternary phosphonium [34], and

quaternary ammonium [35]. These cations are combined with Fluorinated ions such as [Tf$_2$N], bis(fluorosulfonyl)imide ([FSI]), BF$_4$, and PF$_6$. Systems based on *N-n*-propyl-*N*-methylpyrrolidinium [FSI] ([Py$_{13}$][FSI]) mixed with LiTFSI displayed an excellent reversible capacity of ~144 mAh g$^{-1}$ at C/2 and negligible capacity fade over several hundred cycles with lithium iron phosphate [36]. Further improvement is still on going, as the addition of Li salts to an IL usually leads to an increase in viscosity due to enhanced ion-ion interactions [37]. The formation of hybrid electrolytes based on mixtures of ILs and standard carbonate solvents is beneficial to the viscosity, formation of SEI, and relative cycle performance while retaining less-flammability [38]. The presence of carbonate solution, especially EC also assists the formation of the solid electrolyte interface (SEI), which protects and enhances ion transfer on the graphite surface [39]. A Li[Tf$_2$N] doped piperidinium-based IL was reported to have discharge capacities of 140 and 100 mAh g$^{-1}$ with lithium cobalt oxide, with and without carbonate solvents respectively [40]. Moreover, the idea of using IL-Li salt mixtures or their further mixture with alkyl carbonate solutions in order to form a solid-state polymer electrolyte has been successfully demonstrated, achieving safety and stability. Focusing on ionic conductivity, Appetecchi et al. demonstrated IL-doped polyether-based polymer electrolytes with ionic conductivity exceeding 10$^{-4}$ S cm$^{-1}$ at 20 $^o$C [41] and good performance in a lithium battery prototype [42].

## 1-2. Fluorinated polymers as matrices

### 1-2-1. Fundamental properties of fluorinated polymers

Fluorinated polymers have had a profound effect on all aspects of industry since after discovery during the 1930s. There are two types of fluorinated polymers, *i.e.* perfluorinated- and partially-fluorinated polymers. Fluorinated polymers possess excellent properties such as outstanding chemical resistance, high thermal stability, weather stability, low surface energy, low coefficient of friction, and low dielectric constant (**Table 1-5**). For example, poly(tetrafluoroethylene), most particular fluorinated polymer, has $T_m$ (327$^o$C), high melt viscosity (about 10$^{11}$ poises at 380$^o$C) [43]. These features are a consequence of weak intermolecular forces derived from very strong C-F bond and strong electronegativity of fluorine atoms in the PTFE.

**Table 1-5.** The summary of fluoropolymers with their general properties adapted from ref [44]. ($E$: Tensile Modulus, $E_B$: Break Elongation)

| Unit structure of fluorinated polymers | $T_m$ / °C | $E$ / MPa | $E_B$ / % | Dielectric Strength / kV mm$^{-1}$ | Main Applications |
|---|---|---|---|---|---|
| $-(CF_2CF_2)-$ PTFE | 317–337 | 550 | 300-550 | 19.7 | Chemical processing, wire and cable |
| $-(CF_2CFCl)-$ PCTFE | 210-215 | 60-100 | 100-250 | 19.7 | Barrier film, packaging and sealing |
| $-(CF_2CF_2\text{-}co\text{-}CF_2CF(CF_3))-$ FEP | 260-282 | 345 | ~300 | 19.7 | Cable insulation |
| $-(CH_2CHF)-$ PVF | 190-200 | 2000 | 90-250 | 12–14 | Lamination, film and coating |
| $-(CF_2CH_2)-$ PVDF | 155–192 | 1040-2070 | 50-250 | 63–67 | Coating, wire, cable, electronic |
| $-(CH_2CH_2\text{-}co\text{-}CF_2CFCl)-$ ECTFE | 235–245 | 240 | 250-300 | 80 | Flame resistant insulation |
| $-(CF_2CF_2\text{-}co\text{-}CF_2CF(OC_3F_7))-$ PFA | 302–310 | 276 | ~300 | 19.7 | Chemical resistant components |
| $-(CH_2CH_2\text{-}co\text{-}CF_2CF_2)-$ ETFE | 254–279 | 827 | 150-300 | 14.6 | Wire and cable insulation |

Low surface energy of fluorinated polymers is beneficial for a large number of applications; however, it does raise problems in some applications. It is difficult to incorporate PTFE powders homogeneously into other materials, and vice versa, it is also difficult to prepare composites with small molecular weight. Usually these results in agglomeration of the PTFE particles or bleed out of the combined molecules. Due to these properties, modification of PTFE is proposed for further material design. For examples, these materials are designed by using high-energy irradiation [45], new precursors for radial polymerization [46], alkali metals which arise defluorination [47].

## 1-2-2.   Polymer electrolytes consisting fluorinated polymers

In considering stability of fluorinated polymer, some of them are used to prepare polymer electrolytes. For example, PVDF and PVdF-HFP are applied to polymer matrices for electrochemical actuator, super capacitor, and lithium ion battery. Among latter purposes, fluorinated polymers are used as matrices for electrolyte solutions. For battery purpose, these polymers especially PVdF-HFP are plasticized with carbonate solvents to enhance stability

towards electrodes and improve ionic conductivity. However, after long-time usage, the carbonate can leak form polymer matrix, and it may cause a decrease in ion conductivity and an ignition. Soaking property of PVdF-HFP is important to be controlled. In order to control the bleed out of functional material, some functional moiety are fixed into fluorinated polymers (*e.g.* Nafion ® is used as proton-exchange membrane in fuel-cells). In terms of stability, fixation of functional group onto fluorinated polymers via covalent bond is attractive. However, there are limited possibility to design new fluorinated polymer matrices, since some derivatives of tetrafluoroethylene are not stable. If the fluorinated polymers can interact with functional molecules and design of their composite is possible, a wide variety of novel polymer electrolytes can be designed.

### 1-2-3.   Comparison of polyether- and fluorinated polymer-based electrolytes

Here I compare properties of polyether- and fluorinated polymer-based electrolyte in terms of thermal stability, mechanical strength, and mechanisms of ion conduction, and summarize requirements for further development. For the case of polyether-based electrolyte, systems without molecular solvent can be designed because polyether has ability to dissociate salts into ions. Solvent-free PEO/salt composites can enhance considerable ionic conductivity which range from $10^{-8}$ to $10^{-4}$ S cm$^{-1}$ at a range of temperature from 40 to 100 $^{\circ}$C. Temperature dependence of ionic conductivity is slightly stronger compared to fluorinated polymer-based electrolytes, since PEO tend to crystallize around 60 $^{\circ}$C and this suppress ion conduction. Polyether based electrolytes melts above 60 $^{\circ}$C, and mechanical stability of them are deteriorated above the temperature. However, considerable ionic conductivity are observed in melted phase. Mechanisms of ionic conductivity of polyether based polymer electrolytes based on segmental motion of polymer matrices. Thus, ionic conductivity of the electrolyte are affected from $T_g$ of composites and affinity between polyether and salts. In the view of ion density, larger amount of inorganic salts are needed to be added to polyethers; however, this results in increase of $T_g$ of the composites. For design of polyether based electrolyte, addition of larger amount of salts is important together with maintaining low $T_g$. The morphology of the composites are affected by affinity between inorganic salts and polyether. This study was carried out at condition of "salts in polymer" based on HSAB theory. However, no strategy has been proposed to control affinity between salts and polyethers under condition of "polymer in salts".

On the other hand, fluorinated polymers are known to form homogeneous hybrid films with a lithium salt and carbonate solutions. The biggest advantage of a use of fluorinated polymer is anodically stable property due to the strongly electronegative properties of CF$_2$ unit. Beside the vaporization of carbonate solutions, fluorinated polymer-based electrolytes are intrinsically stable at high temperature. Flammability of carbonate solution can be suppressed by controlling the ratio

of carbonate solution and salts component [48].    The ionic conductivity are enhanced in plasticized polymer phase, thus temperature dependence of ionic conductivity is small compared to the system with polyethers.    Due to these properties, improvement carbonate solution are important as well as adsorption stability are need to be improved.

## 1-3.    Compatibility of ionic liquids and fluorinated materials

### 1-3-1.    Solubility of fluorinated polymers into conventional solvents

As summarized in **Section 1-2-1**, both fully- and partially-fluorinated polymers have high resistivity to dissolve in common solvents.    Only few groups are working on solubilization of fluorinated polymers.    There are two main reports of dissolution of fluorinated polymers; one is about PTFE[49] and the other is FEP[49b, 50].    The dissolution behavior of PTFE resembles that of polyethylene (PE).    Similar to that PE has only H-C-H group, PTFE has F-C-F in polymer structure, and these are incapable to interact with other molecules.    Accordingly, dissolution can be brought out only by entropy increment upon mixing the polymer.    Expecting moderate repulsion between PTFE and molecules, the most obvious candidates as solvent for PTFE are its oligomers.    As preliminary step, dissolution temperature of PTFE in its oligomers are theoretically discussed. **Figure 1-8** shows calculated dissolution temperature of PTFE in its oligomers as a function of the alkyl chain length of oligomers.    The dissolution temperature was calculated based on the Flory-Huggins theory for melting point depression in polymeric system.    For this case, the dissolution temperature was defined as the depressed melting point of PTFE/oligomer mixture.    As shown in **Figure 1-8**, dissolution temperature of PTFE/oligomer composite increase depending on increase carbon number due to a reduced entropy of mixing.    However, for the case of oligomers having alkyl chain shorter than 23, boiling temperature of oligomer is low.    This suggest that PTFE oligomers having more than 22 carbon atoms have potentials to dissolve PTFE at ambient pressure.    Then, solubility of PTFE into $C_{24}F_{50}$ (with a distribution of chain length) was checked by using optical microscope.    A mixture containing 10 % of PTFE was place to microscope slide and slowly heated.    At a temperature of 295 $^oC$ the PTFE particles was found to dissolve to $C_{24}F_{50}$ without boiling of $C_{24}F_{50}$.    The dissolution temperature can be lowered by using cyclic aliphatic fluorinated carbons due to their lower molar volume per molecular weight compared to linear fluorinated alkanes.
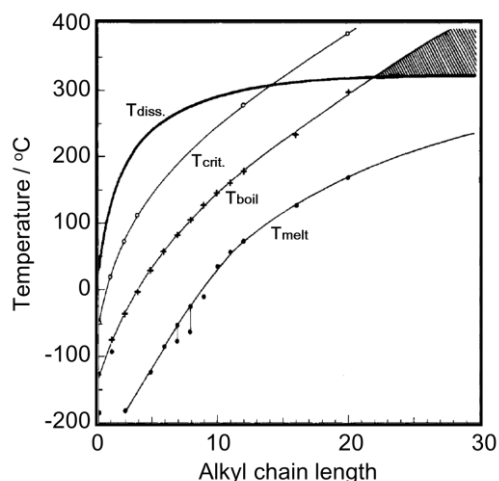
**Figure 1-8.**  Dissolution temperature of PTFE in its oligomers calculated referring to Flory-Huggins theory as a function of the alkyl chain length of oligomers.   The melting, boiling, and critical temperatures of the fluorinated oligomers are also plotted.

Dissolution of FEP to supercritical carbon dioxide as well as halogenated solvent such as $CF_4$, $C_2F_6$, $C_3F_8$, $C_3F_6$, $CClF_3$, and $SF_6$ were also reported.   The solubility of FEP to these supercritical solvents are evaluated by analyzing the cloud-point pressure of polymer/solvent biphase.   Among biphase sample of polymer and supercritical solvents, the pressure decrease $C_3F_8 > C_2F_4 > CF_4$. The pressure of slightly polar $C_3F_6$ and $CClF_3$ was found to be almost similar to nonpolar $C_3F_8$. The highest cloud-point pressure were found in the mixture of $CO_2$ which is attributed to the large quadrupole moment.   This moment may suppress the dissolution of nonpolar FEP to supercritical $CO_2$.   This result suggests that dispersion-type forces are expected to be the dominant type of intermolecular force between fluorinated polymers and solvents.

### 1-3-2.　Distribution of fluoroalkane into ionic liquids

Some ILs are used as the solvent for separation of tetrafluoroethylene (TFE) [51].   TFE is a gas at ambient temperature, and liquefied with sufficient pressure during storage and transport.   TFE is unstable properties that is flammability with air and contact with hot surfaces, as well as, there are fear of decomposition of TFE to $CF_4$ and carbon.   Polymerization of TFE is caused by the presence of oxygen, therefore TFE should be inhibited with contact with $CO_2$.   ILs such as [$C_2$mim][$Tf_2$N], 1-butyl-3-methylimidazolium dicyanamide ([$C_4$mim][DCA]), 1-butyl-4-methylpyridinium $BF_4$ ([$Py_{14}$]$BF_4$), 1-butyl-3-methylimidazolium 1,1,2,3,3,3-hexafluoropropanesulfonate [$C_4$mim]$C_3F_6HSO_3$, 1-octyl-3-methylimidazolium 1,1,2,2-tetrafluoroethanesulfonate [$C_8$mim]$C_2F_4HSO_3$ are soluble the TFE .   The solubility of TFE was larger than ethylene gas due to high hydrogen bond ability of TFE arise from presence of fluorine

atoms in TFE.　Using remarkable solubility of TFE into ILs, TFE was separated from its mixture of $CO_2$.　The purity of the TFE distillate from adsorption column of ILs exceed 99.9%.

　　Solubility of alkanes, alkanols and their fluorinated counterparts in ILs are also studied (**Figure 1-9**) [52].　For the case of fluorinated alkanols, hydroxyl group of alcohols interact strongly with the anions of ILs and also hydrogen atoms on the C-2 position of imidazolium ring.　The solubility decrease with increase of alkyl chain length of imidazolium ring.　Conversely, perfluoroalkanes without both spacer and hydroxyl group, showed large immiscibility with ILs. For fluorinated alcohols, the hydroxyl group will close to polar domain of the ILs, thus increasing the mutual miscibility.　When the hydroxyl group is absent, fluoroalkanes cannot orient to ILs and aggregate.
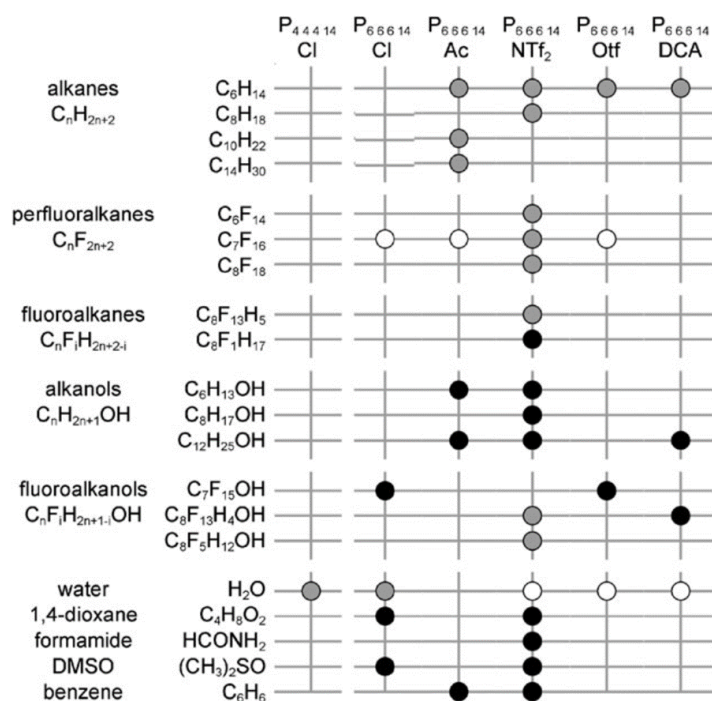


**Figure 1-9.**　Solubility of alkanes, alkanols and their fluorinated counterparts in ILs.　Black dots indicate totally miscible pairs; grey dots indicate partially miscible pairs; and white dots represent immiscible pairs.　In the case of the [$P_{444,14}$]Cl plus water system, the grey dot refers to the existence of a solubility limit which caused by the state of the ILs (that is solid at room temperature).

### 1-3-3.  Wettability of ionic liquids with fluorinated polymers

On the contrary of solubility of fluorinated polymers to their oligomers or super critical solvent, no strategy has yet been proposed to design ILs to dissolve fluorinated polymers.    Some ILs containing fluoroalkyl group has been reported [53], and some of them can disperse perfluorohexane [54] or swell fluorinated polymers [55].    From the view point of fundamental study on interfacial properties of ILs, contact angle of ILs on the PTFE were evaluated [56].    **Figure 1-10** summarizes the effect of ion structure on the contact angle of the ILs with PTFE.    In a series of [DCA] salts, contact angle was decreased in the order of $[C_4mim] > [P_{666,14}] > [P_{8881}] > [(di-h)_2dmG]$.    This suggests that an increase in IL polarity allows higher contact angles of PTFE.    In regard to the effect of the anion, contact angle decreased in a manner of $BF_4 > [DCA] > Cl > [Tf_2N] > [TsO]$.    Among these anions, [TsO] anion which has planarity structure showed lowest contact angle.    This trend also follows that planarity $[(di-h)_2dmG]$ showed lowest contact angle in a series of [DCA] salts.    When alkyl chain of imidazolium-based ILs is changed, contact angle increased by inserting polar oxymethylene group and decreased by inserting methylene group on to C-(2) position of imidazolium ring or longer alkyl chain on to C-(3) position.    Consequently, contact angle of ILs on PTFE surface decrease with increase of alkyl chain length and decrease of polarity of ILs.



| ILs | $\theta$/deg |
|---|---|
| $[C_4mim]BF_4$ | $80.51 \pm 0.79$ |
| $[C_4mim][Tf_2N]$ | $66.25 \pm 0.09$ |
| $[C_4mim][DCA]$ | $81.71 \pm 0.26$ |
| $[C_8mim]Cl$ | $47.11 \pm 0.26$ |
| $[C_8mim][Tf_2N]$ | $49.58 \pm 0.21$ |
| $[C_2OCH_3mim]BF_4$ | $88.19 \pm 0.21$ |
| $[C_4mmim][Tf_2N]$ | $70.62 \pm 0.34$ |
| $[N_{8881}]Cl$ | $56.53 \pm 0.42$ |
| $[N_{8881}][Tf_2N]$ | $46.20 \pm 0.48$ |
| $[N_{8881}][DCA]$ | $63.28 \pm 0.39$ |
| $[P_{666,14}]Cl$ | $64.18 \pm 0.49$ |
| $[P_{666,14}][DCA]$ | $68.95 \pm 0.20$ |
| $[P_{666,14}][p\text{-}TsO]$ | $39.77 \pm 0.14$ |
| $[(di-h)2dmg]Cl$ | $58.96 \pm 0.06$ |
| $[(di-h)2dmg][DCA]$ | $39.66 \pm 0.71$ |
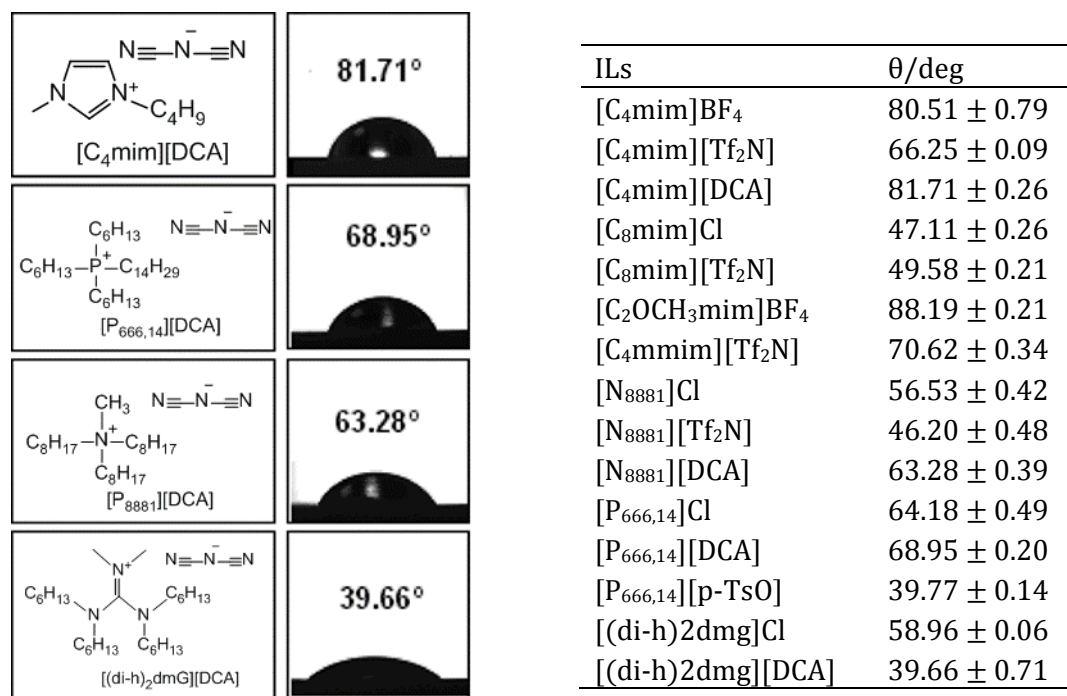
**Figure 1-10.**     Effect of cation structure (left) on the contact angle of the ILs with PTFE.    Table (right) summarize contact angle of ILs on PTFE [56].

On interface of ILs and polymers, there considered to exist three different types of interactions: (1) dispersive interactions, (2) dipolar interactions, and (3) acid-base interactions (including hydrogen bond).   Contact angle are frequently evaluated to two energetic contributions of dispersive interactions and non-dispersive interactions [57].   The total work of adhesion for a solid-liquid interface ($W_{SL}$) can simply be expressed with surface tension ($\gamma_{LV}$), and can be divided into dispersive term ($W_{SL}^d$) and polar term ($W_{SL}^p$) as seen in **Equation 1-1** to **1-3**.

$$W_{SL} = \gamma_{LV}(1 + \cos\theta) \quad \cdots \quad (\textbf{Equation 1-1})$$

$$W_{SL}^d = 2\sqrt{\gamma_{SV}^d \cdot \gamma_{LV}^d} \quad \cdots \quad (\textbf{Equation 1-2})$$

$$W_{SL}^p = W_{SL} - W_{SL}^d \quad \cdots \quad (\textbf{Equation 1-3})$$

To determine $W_{SL}^d$, the dispersive component of the free energy of the solid-vapor interface ($\gamma_{SV}^d$) must be calculated using the Good-Girifalco-Fowkes (GGF) approximation, which relates the total work of adhesion, $\gamma_{LV}$ $(1 + \cos \theta_a)$, to the dispersive components of the surface free energy of the solid ($\gamma_{SV}^d$) and the surface tension of the liquid ($\gamma_{LV}^d$).   Those terms are considered to relate to dispersive interaction for $W_{SL}^d$ and polar interaction for $W_{SL}^p$.   For the case of PTFE, negligible $W_{SL}^p$ and small $W_{SL}^d$ were found.   This indicates that PTFE contribute to only dispersive work. This study also applied to explain contact angle of ILs [58].   The ILs with the longer alkyl substituent in the imidazolium ring, [C$_8$mim]BF$_4$, has the lowest polar contribution, while the presence of the OH group in [C$_2$OHmim]BF$_4$ is responsible for its highest polar contribution on the interface of PTFE.   Consequently, to obtain lower contact angle with PTFE which only have $W_{SL}^d$, [C$_8$mim]BF$_4$ which have lowest polar contribution is favorable.

## 1-4. Issues of fluorinated polymer-based electrolytes and aim of this study

In this section, properties and requirements of polymer electrolytes were summarized. Polymer electrolytes are expected to improve stability and credibility of energy devices. Many polymer electrolytes have been designed with various matrices, and there are two major routes of development of polymer electrolytes: one is based on polyethers and the other is based on fluorinated polymers. Ionic conductivity of polyether-based polymer electrolytes is realized by ion migration based on segmental motion of polymer matrices. Thus, ionic conductivity of the electrolyte is related to low $T_g$ and concentration of dissociated ions. For fluorinated polymer-based electrolytes, the ionic conductivity is enhanced in amorphous phase plasticized with electrolyte solution. Due to the presence of molecular solvents in the electrolyte solution, there are fears of bleed out of molecular solvents from the matrices and ignition of the molecular solvents. On the other hand, ILs have been applied as additive salts for polymer electrolytes due to their thermal stability and ionic conductivity. As their another advantage, ILs possess unlimited possibility of ion structures. This advantage of ILs enables to prepare stable composites with polymers. In this study, ILs will be used as additive salts to design polymer electrolytes based on polyethers and fluorinated polymers. The requirements for ILs to form stable composites with these matrices will be discussed.

In chapter 2, we designed functional materials based on ILs and versatile polymers. Prior to design of IL/polymer composites, the affinity between ILs and the polymers were analyzed. Then, we prepared IL/polymer composites and analyzed some fundamental properties of them. To obtain the proposal for functional design of IL/polymer composites, effect of the affinity between IL and polymers on the properties of their composites are discussed.

In chapter 3, we tried to design functional composites based on fluorinated polymers. As a fundamental study of design of ILs/fluorinated polymer composites, affinity between ILs and the fluorinated polymers were analyzed. Among a series of fluorinated polymers, poly(vinylidene fluoride) (PVdF) were soluble, and poly(ethylene-*co*-chlorotrifluoroethylene) (PECTFE) and Cytop® were slightly soluble in the ILs. Based on these results, copolymer of PVdF and hexafluoropropylene (PVdF-HFP) was proposed to prepare composites with ILs. Thermal and electrochemical properties of the composites were analyzed.

In chapter 4, design of fluorophilic ILs are discussed in order to improve affinity between ILs and fluorinated polymers. In this section fluoroalkanes were used as model compounds of fluorinated polymers, and factors to control the solubility of the fluoroalkanes into ILs were analyzed. Based on these results, requirements for ILs to improve fluorophilicity were summarized.

In chapter 5, polymer composite based on PVdF, poly(ethylene-*co*-tetrafluoroethylene) (ETFE) and poly(tetrafluoroethylene) (PTFE) were designed.   First, two types of [Tf$_2$N] salts were used; one is phosphonium-based ILs and the other is imidazolium-based ILs.   The effect of affinity between these IL groups and fluorinated polymers on properties of their composite are discussed.   Also, fluorophilic ILs containing heptadecafluorooctanesulfonate were applied to prepare composites based on PTFE.   The possibility of design of PTFE-based ion conductive materials are discussed.

In chapter 6, I conclude this dissertation.

## 1-5.   References

[1]     J. A. Kent, *Handbook of Industrial Chemistry and Biotechnology, Vol. 1*, Springer Science & Business Media, **2013**.

[2]     (a) M. S. Hong, S. H. Lee, S. W. Kim, *Electrochem Solid St* **2002**, *5*, A227-A230; (b) V. Khomenko, E. Raymundo-Pinero, F. Beguin, *Journal of Power Sources* **2010**, *195*, 4234-4241.

[3]     (a) S. Hasegawa, N. Imanichi , T. Zhang, J. Xie, A. Hirano, Y. Takeda, O. Tamamoto, *Journal of Power Sources* **2009**, *189*, 371-377; (b) Y. Wang, H. Zhow, *Journal of Power Sources* **2010**, *195*, 358-361; (c) A. Kraytsberg, Y. Ein-Eli, *Journal of Power Sources* **2011**, *196*, 886-893.

[4]     D. Guyomard, J. M. Tarascon, *Journal of Power Sources* **1995**, *54*, 92-98.

[5]     D. Aurbach, *Nonaqueous Electrochemistry*, CRC Press, **1999**.

[6]     (a) U. Heider, R. Oesten, M. Jungnitz, *Journal of Power Sources* **1999**, *81*, 119-122; (b) D. Aurbach, A. Zaban, Y. Ein-Eli, I. Weissman, O. Chusid, B. Markovsky, M. Levi, E. Levi, A. Schechter, E. Granot, *Journal of Power Sources* **1997**, *68*, 91-98.

[7]     T. Kawamura, S. Okada, J.-i. Yamaki, *Journal of Power Sources* **2006**, *156*, 547-554.

[8]     (a) J. Kummer, N. Weber, *Proc. Ann. Power Sources Conf.* **1967**, *19*, 113-115; (b) M. S. Whittingham, R. A. Huggins, *J. Chem. Phys.* **1971**, *54*, 414-416.

[9]     K. Edström, J. O. Thomas, G. C. Farrington, *Acta Cryst.* **1991**, *B47*, 210-216.

[10]    A. D. Robertson, A. R. West, A. G. Ritchie, *Solid State Ionics* **1997**, *104*, 1-11.

[11]    P. V. Wright, *British Polymer Journal* **1975**, *7*, 319-327.

[12]    M. B. Armand, J. M. Chabagno, M. Duclot, *Fast ion Transport in Solids. Electrodes and Electrolytes*, North Holland Publishers, **1979**.

[13]    F. B. Dias, L. Plomp, J. B. J. Veldhuis, *Journal of Power Sources* **2000**, *88*, 169-191.

[14]    (a) J. Y. Song, Y. Y. Wang, C. C. Wan, *Journal of Power Sources* **1999**, *77*, 183-197; (b) W. H. Meyer, *Advanced Materials* **1998**, *10*, 439-448.

[15]    J. M. Tarascon, A. S. Gozdz, C. Schmutz, F. Shokoohi, P. C. Warren, *Solid State Ionics* **1996**,

*86-8*, 49-54.

[16]    (a) H. Tadokoro, *Journal of Polymer Science: Macromolecular Reviews* **1967**, *1*, 119-172; (b) K.-J. Liu, *Macromolecules* **1968**, *1*, 308-311.

[17]    B. L. Papke, *Journal of The Electrochemical Society* **1982**, *129*, 1694-1701.

[18]    B. L. Papke, *Journal of The Electrochemical Society* **1982**, *129*, 1434.

[19]    (a) P. G. Bruce, G. S. MacGlashan, Y. G. Andreev, *Nature* **1999**, *398*, 792-794; (b) C. Zhang, S. Gamble, D. Ainsworth, A. M. Z. Slawin, Y. G. Andreev, P. G. Bruce, *Nature materials* **2009**, *8*, 580-584.

[20]    M. B. Armand, *Annual Review of Materials Science* **1986**, *16*, 245-261.

[21]    R. G. Pearson, *Journal of Chemical Education* **1968**, *45*, 581.

[22]    (a) E. Tsuchida, H. Ohno, N. Kobayashi, *Macromolecules* **1988**, *21*, 96-100; (b) E. Tsuchida, H. Ohno, N. Kobayashi, H. Ishizaka, *Macromolecules* **1989**, *22*, 1771-1775.

[23]    B. Scrosati, F. Croce, G. B. Appetecchi, L. Persi, *Nature* **1998**, *394*, 456-458.

[24]    W. P., *Bull. Acad. Imp. Sci. Saint-Pétersbourg. VI serié* **1914**, *8*, 405-422.

[25]    (a) P. Wasserscheid, T. Welton, *Ionic Liquids in Synthesis*, Wiley-VCH, Weinheim, **2007**; (b) T. Welton, *Chemical Reviews* **1999**, *99*, 2071-2084; (c) P. Wasserscheid, W. Keim, *Angewandte Chemie* **2000**, *39*, 3772-3789.

[26]    (a) K. Bica, C. Rijksen, M. Nieuwenhuyzen, R. D. Rogers, *Physical chemistry chemical physics : PCCP* **2010**, *12*, 2011-2017; (b) J. Stoimenovski, D. R. MacFarlane, K. Bica, R. D. Rogers, *Pharmaceutical research* **2010**, *27*, 521-526; (c) U. Kragl, M. Eckstein, N. Kaftzik, *Current Opinion in Biotechnology* **2002**, *13*, 565-571.

[27]    (a) M. Armand, F. Endres, D. R. MacFarlane, H. Ohno, B. Scrosati, *Nature materials* **2009**, *8*, 621-629; (b) F. Endres, *Chemphyschem : a European journal of chemical physics and physical chemistry* **2002**, *3*, 144-154.

[28]    R. D. Rogers, K. R. Seddon, *Science* **2003**, *302*, 792-793.

[29]    H. Ohno, *Ionic Liquid II-Marvelous Developments and Colorful Near Future-*, CMC Publishing, Tokyo, **2006**.

[30]    Y. Fukaya, H. Ohno, *Physical chemistry chemical physics : PCCP* **2013**, *15*, 4066-4072.

[31]    Y. Zhang, J. M. Shreeve, *Angewandte Chemie* **2011**, *50*, 935-937.

[32]    B. Garcia, S. Lavallée, G. Perron, C. Michot, M. Armand, *Electrochimica Acta* **2004**, *49*, 4583-4588.

[33]    (a) J. Hassoun, A. Fernicola, M. A. Navarra, S. Panero, B. Scrosati, *Journal of Power Sources* **2010**, *195*, 574-579; (b) P. Reale, A. Fernicola, B. Scrosati, *Journal of Power Sources* **2009**, *194*, 182-189.

[34]    K. Tsunashima, A. Kawabata, M. Matsumiya, S. Kodama, R. Enomoto, M. Sugiya, Y. Kunugi, *Electrochemistry Communications* **2011**, *13*.

[35]    H. H. Zheng, K. Jiang, T. Abe, Z. Ogumi, *Carbon* **2006**, *44*.

[36]    A. P. Lewandowski, A. F. Hollenkamp, S. W. Donne, A. S. Best, *Journal of Power Sources* **2010**,

195.

[37]    A. Martinelli, A. Matic, P. Jacobsson, L. Borjesson, A. Fernicola, B. Scrosati, *Journal of Physical Chemistry B* **2009**, *113*.

[38]    L. Larush, V. Borgel, E. Markevich, O. Haik, E. Zinigrad, D. Aurbach, G. Semrau, M. Schmidt, *Journal of Power Sources* **2009**, *189*.

[39]    (a) G. H. Lane, A. S. Best, D. R. MacFarlane, M. Forsyth, P. M. Bayley, A. F. Hollenkamp, *Electrochimica Acta* **2010**, *55*, 8947-8952; (b) A. Lewandowski, A. Swiderska-Mocek, *Journal of Power Sources* **2009**, *194*.

[40]    H. F. Xiang, B. Yin, H. Wang, H. W. Lin, X. W. Ge, S. Xie, C. H. Chen, *Electrochimica Acta* **2010**, *55*.

[41]    G. B. Appetecchi, G. T. Kim, M. Montanino, F. Alessandrini, S. Passerini, *Journal of Power Sources* **2011**, *196*.

[42]    G. T. Kim, S. S. Jeong, M. Z. Xue, A. Balducci, M. Winter, S. Passerini, F. Alessandrini, G. B. Appetecchi, *Journal of Power Sources* **2012**, *199*.

[43]    G. G. Hougham , P. E. Cassidy, K. Johns, T. Davidson, *Fluoropolymers 2: Properties (Topics in Applied Chemistry), Vol. New York*, Springer Science & Business Media, **1999**.

[44]    H. Teng, *Applied Sciences* **2012**, *2*, 496-512.

[45]    (a) K. Lunkwitz, U. Lappan, U. Scheler, *Journal of Fluorine Chemistry* **2004**, *125*, 863-873; (b) M. M. Nasef, *Polymer International* **2001**, *50*, 338-346.

[46]    (a) U. Michel, P. Resnick, B. Kipp, J. M. DeSimone, *Macromolecules* **2003**, *36*, 7107-7113; (b) T. Takayanagi, M. Yamabe, *Progress in Organic Coatings* **2000**, *40*, 185-190.

[47]    J. Jansta, F. P. Dousek, J. Řiha, *Journal of Applied Polymer Science* **1975**, *19*, 3201-3210.

[48]    L. Lombardo, S. Brutti, M. A. Navarra, S. Panero, P. Reale, *Journal of Power Sources* **2013**, *227*, 8-14.

[49]    (a) P. Smith, K. H. Gardner, *Macromolecules* **1985**, *18*, 1222-1228; (b) W. H. Tuminello, G. T. Dee, *Macromolecules* **1994**, *27*, 669-676.

[50]    (a) M. A. McHugh, C. A. Mertdogan, T. P. DiNoia, C. Anolick, W. H. Tuminello, R. Wheland, *Macromolecules* **1998**, *31*, 2252-2254; (b) C. A. Mertdogan, H.-S. Byun, M. A. McHugh, W. H. Tuminello, *Macromolecules* **1996**, *29*, 6548-6555.

[51]    (a) M. B. Shiflett, B. A. Elliott, A. Yokozeki, *Fluid Phase Equilibria* **2012**, *316*, 147-155; (b) M. B. Shiflett, A. D. Shiflett, A. Yokozeki, *Separation and Purification Technology* **2011**, *79*, 357-364; (c) M. B. Shiflett, M. A. Harmer, C. P. Junk, A. Yokozeki, *Fluid Phase Equilibria* **2006**, *242*, 220-232.

[52]    (a) R. Ferreira, M. Blesic, J. Trindade, I. Marrucho, J. N. C. Lopes, L. P. N. Rebelo, *Green Chemistry* **2008**, *10*, 918; (b) M. Blesic, J. N. Lopes, M. F. Gomes, L. P. Rebelo, *Physical chemistry chemical physics : PCCP* **2010**, *12*, 9685-9692.

[53]    (a) A. B. Pereiro, J. M. M. Araújo, S. Martinho, F. Alves, S. Nunes, A. Matias, C. M. M. Duarte, L. P. N. Rebelo, I. M. Marrucho, *ACS Sustainable Chemistry & Engineering* **2013**, *1*, 427-439;

(b) O. Kysilka, M. Rybáčková, M. Skalický, M. Kvíčalová, J. Cvačka, J. Kvíčala, *Journal of Fluorine Chemistry* **2009**, *130*, 629-639; (c) H. B. Alhanash, A. K. Brisdon, *Journal of Fluorine Chemistry* **2013**, *156*, 152-157.

[54]    T. L. Merrigan, E. D. Bates, S. C. Dorman, J. H. Davis Jr, *Chemical communications* **2000**, 2051-2052.

[55]    E. Redel, M. Walter, R. Thomann, C. Vollmer, L. Hussein, H. Scherer, M. Kruger, C. Janiak, *Chemistry* **2009**, *15*, 10047-10059.

[56]    G. a. V. S. M. Carrera, C. A. M. Afonso, L. C. Branco, *Journal of Chemical & Engineering Data* **2010**, *55*, 609-615.

[57]    S. Lee, J. S. Park, T. R. Lee, *Langmuir : the ACS journal of surfaces and colloids* **2008**, *24*, 4817-4826.

[58]    (a) H. Li, R. Sedev, J. Ralston, *Physical chemistry chemical physics : PCCP* **2011**, *13*, 3952-3959; (b) J. Restolho, J. L. Mata, B. Saramago, *Journal of colloid and interface science* **2009**, *340*, 82-86.

# Chapter 2

# Factors to control solubility of polymers

# in ionic liquids and their functional design

## 2-1.　Introduction

　　　　Ionic liquids (ILs), which are molten salts below 100 $^o$C [1], have been proposed as potential candidates as new additives due to their chemical stability, electrochemical stability, low vapor pressure, and high ionic conductivity.　The most important and interesting point of ILs is that they provide many mobile ions in polymer matrices without molecular solvents even at ambient temperature.　On the other hand, polymers are added to liquid materials to form gel resulting in improvement of mechanical stability of liquid components.　Consequently, there are increasing number of studies concerning design of new IL/polymer electrolytes.　There are two major tasks in developing IL/polymer composites: design of both component and considering their combination.　In spite of some new proposal for new polymers and ILs, few systematic studies have been made to discuss their combination.

　　　　As fundamental study of IL/polymer composites, here we discuss effects of affinity between polymers and ILs on the properties of their composites.　In this chapter, factors to control solubility of polymers in ILs have been analyzed, and functional design of IL/polymer composites have been carried out considering the affinity.

## 2-2.　Experimental procedure

## 2-2-1.　Materials

　　　　Structure, abbreviation, and preparation for all ILs are summarized in the Appendix (P. 88).　All ILs were dried under vacuum at 60 $^o$C for at least 3 h.

　　　　Polymers such as poly(ethylene oxide) with average Mw. of 1000 (PEO$_{1000}$), 2000 (PEO$_{2000}$), 4000 (PEO$_{4000}$), 6000 (PEO$_{6000}$), 10,000 (PEO$_{10000}$), and poly(ethylene glycol) dimethyl ether (average Mw. of 1000, dMe-PEO) were purchased from Wako Pure Chemical Industries., Kanto Chemical Co., Inc., or Fluka Chemie GmbH.　Poly(vinylpyrrolidone) (PVP, average Mw. of 25,000, from Sigma-Aldrich Co. LLC.) and poly(acrylic Acid) (PAA, average Mw. of 25,000, from Wako Pure Chemical Industries.) were purchased.

## 2-2-2.　Dissolution of polymers in ionic liquids

　　　　Mixing procedures were carried out in N$_2$ filled glove box.　The vials containing ILs and polymers were tightly closed with PTFE thread seal tape.　Then, these samples were vigorously stirred at ambient atmosphere.

### For polyethers

To 1.0 mL of dry ILs, 10.0 mg of polyethers were added and stirred for 1 h at 25 °C.    After stirring, the solubility of polyethers in ILs was examined visually with naked eyes.    If polyethers proved insoluble, the mixture was then heated at 70 °C for 1 h with vigorous stirring.    The transparency of the mixture was inspected immediately after stirring at 70 °C, then again after leaving the mixtures for 3 h at 25 °C.

### For PVP and PAA

To 300 mg of dry ILs, 3 mg of the polymers were added and stirred for 1h at 25 °C.    Their solubility were inspected visually with naked eyes.    If the mixture provided insoluble, the mixture was heated up to 120 °C and its solubility was inspected every 20 °C.

### 2-2-3.    Evaluation of Kamlet-Taft parameters of ionic liquids

### Fundamentals

Polarity is a useful parameter to determine solvation properties of chemicals.    Polarity for molecular solvents are generally evaluated by using dielectric constant measurements.    Same method cannot be applied for ILs, however, because ILs possess considerable ionic conductivity. In order to evaluate solvation characteristics of ILs, Kamlet-Taft parameters which reflect hydrogen-bonding ability are often used.    These parameter include 3 values: hydrogen bond acidity ($\alpha$), hydrogen bond basicity ($\beta$), and dipolarity/polarizability ($\pi^*$), and these values are evaluated based on solvatochromisms of dye.    For solvatochromic measurement, a set of dyes: *N,N*-diethyl-4-nitroaniline (NN), 4-nitroaniline (4N), and Reichardt' dye 33 (Rei), was chosen in this study (**Figure 2-1**).
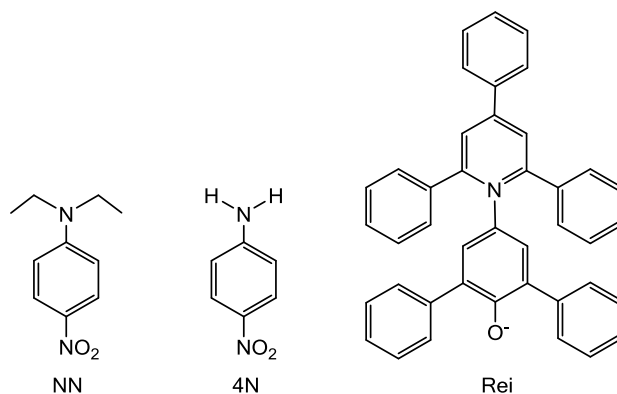


**Figure 2-1.**    Structure of a set of dyes.

## Mechanisms of solvatochromisms

*N,N-Diethyl-4-nitroaniline* (NN)    The NN, a non-hydrogen bond donor solute, is used to estimate $\pi^*$ value and $\beta$ value.    The NN shows a $\pi$-$\pi^*$ transition based on a non-specific interaction with a solvent.    This transition is detected as solvatochromisms of the NN.    As a result, dipolarity/polarizability, $\pi^*$ value, is calculated by using maximal absorption wavelength ($\nu_{NN=}$ $1(/\lambda_{max} \times 10^{-4}$, in kK) of NN (**Equation 2-1**).

$$\pi^* = 0.314(27.52 - \nu_{NN}) \cdots \text{(Equation 2-1)}$$

*4-Nitroaniline* (4N)    The 4N having amine group in C(1) position which contributes to hydrogen bond as donnor.    Interaction between 4N and a solvent with high hydrogen bond basicity results in formation of extended $\pi$-conjugated system on benzene ring.    This causes bathochromical shift of maximal absorption wavelength ($\nu_{4N}$). Accodingly, hydrogen bond bascity, $\beta$ value, is caluculated by using **Equation 2-2**.

$$\beta = (1.035 \, \nu_{NN} + 2.64 - \nu_{4N})/2.80 \cdots \text{(Equation 2-2)}$$

*Reichardt' dye* (Rei)    According to inherent molecular structure, Rei posess 44 $\pi$-electrons and phenolate oxygen which contributes to hydrogen bond as acceptor [2].    In a solvent with high hydrogen bond acidity, ground-state of Rei is more stabilized by solvation.    As a result, intermolecular charge transfer absorption bands is hypsochromically shifted.    Hydrogen bond acidity, $\alpha$ value, is caluculated by using Et(30), molar transition energies of Rei (**Equation 2-3**), and $\pi^*$ value (**Equation 2-4**).

$$E_T(30) = 28592/\lambda_{max \, (Rei)} \cdots \text{(Equation 2-3)}$$
$$\alpha = 0.0649 \, E_T(30) - 2.03 - 0.72\pi^* \cdots \text{(Equation 2-4)}$$

where, $\lambda_{max \, (dye)}$ is the maximum absorption wavelength of the dye.

A set of dye NN (from Wako Pure Chemical Industries.), 4N (from Tokyo Chem. Ind. Co.), and Rei (from Fluka Chemie GmbH) were purchased and used.    The dry methanol solutions, 0.3 mL containing 0.03 g of corresponding dyes, were added to ILs.    Methanol was then removed by vacuum drying at 60 °C for 6 h.    For the solvatochromic measurements, the IL solution containing dyes were placed in quartz cells with light path length of 0.1 mm, and their visible spectra were recorded with Shimadzu UV 2550 (from Shimadzu Corp.).

### 2-2-4.   Estimation of ion hardness based on frontier orbital energy

We focused on the energies of the highest-occupied and lowest-unoccupied Kohn-Sham orbitals (HOMO and LUMO), in order to estimate the hardness of the ion.   According to simple molecular orbital theory, a hard acid is characterized by a high LUMO energy ($E_{LUMO}$), and a hard base is characterized by a low HOMO energy ($E_{HOMO}$)[3].   MO calculations for the isolated ions were determined according to density functional theory (DFT) by using Gaussian 98 with B3LYP parameters and a 6-31G+d basis set.

### 2-2-5.   Evaluation of electrochemical properties of ionic liquid/polymer composites

IL/polymer mixtures for conductivity measurement were prepared by adding 200.0 mg polymer to 1.0 mL ILs. The mixture was then stirred and dried under vacuum at 60 $^o$C for 6 h. Cells with a four-pair-toothed formation with a 0.3 mm distance between electrodes and 7.0 mm length were used.   To this cell, a drop of mixture was added and covered with a square glass with 7 mm per side, then tightly packed with double clips, then overflowed portion was removed.   A signal of amplitude 0.5 V was applied to the cell in the frequency range of $10^3$ to $10^7$ Hz.   Conductivity was calculated according to the amplitude of a semicircle or intersection on the Z′ axis of the Nyquist plot of the impedance.   The measurement was carried out from 0 to 70 $^o$C at a heating or cooling rate of 2 $^o$C min$^{-1}$ in an Ar-filled globe box.
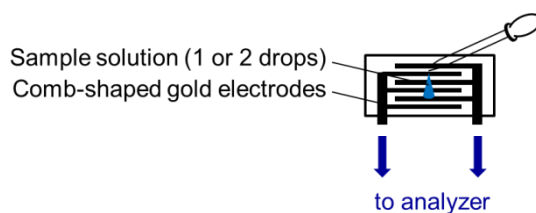


**Figure 2-2.**  Configuration of cells for impedance measurement.

### 2-2-6.   Evaluation of thermal properties of ionic liquid/polymer composites

The same mixtures for impedance or $R$s measurements were used for characterization of thermal properties.   Differential scanning calorimetry (DSC) measurements (DSC-120, from Seiko instrument Inc.) equipped with a liquid $N_2$ cooling system were carried out.   The sample pans were sealed in a $N_2$-filled glove box and the measurements were carried out in an ambient atmosphere.   The samples were heated to 120 $^o$C and cooled to -120 $^o$C with a scan rate of 5 $^o$C

min$^{-1}$, then heated to 120 $^o$C with same scan rate.    For discussion, the data for 2nd heating was used.


## 2-3.    Compatibility of ionic liquids with polyethers

### 2-3-1.    Solubility of polyethers in ionic liquids

First, the solubility of PEO$_{4000}$ in various ILs was investigated.    It is generally believed that PEO is miscible with any IL, provided that there are some interactions between them through the ion-dipole interaction mechanism.    In fact, as seen in **Table 2-1**, the miscibility depended strongly on the ion species.

To 1.0 mL ILs, we added 10.0 mg PEO$_{4000}$ and stirred for 1 h at 25 $^o$C.    In a series of [Tf$_2$N] salts, [P$_{4448}$][Tf$_2$N], [DEME][Tf$_2$N] and [Pyr$_{14}$][Tf$_2$N] showed poor affinity with PEO$_{4000}$.    Heating at 70 $^o$C for 1 h promoted dissolving PEO$_{4000}$ in [DEME][Tf$_2$N] and [Pyr$_{14}$][Tf$_2$N].    However, the [DEME][Tf$_2$N]/PEO$_{4000}$ and [Pyr$_{14}$][Tf$_2$N]/PEO$_{4000}$ mixed solutions turned turbid while being kept

**Table 2-1.**  Solubility of PEO$_{4000}$ in various ILs.

| ILs | [Cation]/[EO][a] ratio | Solubility of PEO$_{4000}$ | | |
| --- | --- | --- | --- | --- |
| | | 1 h stirring at room temp. | 1 h stirring at 70 $^o$C | keeping for 3 h at room temp. |
| **[Tf$_2$N] slats** | | | | |
| [P$_{4448}$] | 8.8 | × | × | × |
| | 21.9[b] | × | ○ | t |
| [DEME] | 14.7 | × | ○ | t |
| [Pyr$_{14}$] | 14.6 | × | ○ | t |
| [AAim] | 14.8 | ○ | | -[c] |
| [C$_4$mmim] | 14.6 | ○ | | -[c] |
| [C$_2$OHmim] | 17.1 | ○ | | -[c] |
| **[C$_4$mim] salts** | | | | |
| [Tf$_2$N] | 15.1 | ○ | | -[c] |
| PF$_6$ | 21.3 | ○ | | -[c] |
| BF$_4$ | 23.5 | ○ | | -[c] |
| CF$_3$SO$_3$ | 19.9 | × | ○ | ○ |
| CF$_3$CO$_2$ | 21.3 | × | ○ | t |
| [Ala] | 21.0 | × | × | × |
| **Other salt** | | | | |
| [P$_{4444}$][Ala] | 12.3 | × | ○ | t |

10.0 mg PEO$_{4000}$ was mixed with 1.0 mL ionic liquids.    ○: soluble, ×: insoluble, and t: turbid.
[a] [EO] = ethylene oxide unit, [b] 4.0 mg PEO$_{4000}$ in 1.0 mL ILs, [c] not measured.

at 25 °C after heating.    The $[P_{4448}][Tf_2N]$/PEO$_{4000}$ mixture was nevertheless obtained as an opaque solution even after heating at 70 °C for 1 hr.    Because of the different formula weight of these ILs, the molar ratio of cation to ether oxygen unit ([cation]/[EO]) was not the same.    In the case of $[P_{4448}][Tf_2N]$, affinity was poor, as seen in the first column of **Table 2-1**.    The mixing ratio of [cation]/[EO] was 8.8, which was afraid not to provide enough cation units for dissolution. Then 4.0 mg PEO$_{4000}$ was added to 1.0 mL $[P_{4448}]$[TFSI], as seen in thesecond column of the **Table 2-1**.    In spite of the larger [cation]/[EO] ratio (= 21.9), affinity remained poor.    These data indicate that the mixing ratio of IL to PEO$_{4000}$ is not the major factor controlling solubility when [cation]/[EO] > 10.

In comparison with these salts, imidazolium-type ILs exhibited a good solubility of PEO$_{4000}$.    [C$_4$mim] cation was used in order to analyze the anion effect.    The [C$_4$mim] salts with $[Tf_2N]$, PF$_6$, or BF$_4$ anions were miscible with PEO$_{4000}$.    Since alkyl imidazolium cations are known to interact with ether oxygens of PEO [4] in addition to ion-dipole interactions, these imidazolium salts are considered to display better affinity with PEO chains.    Despite the ability of the [C$_4$mim] cation to coordinate with PEO, PEO$_{4000}$ was insoluble in [C$_4$mim] salts containing CF$_3$CO$_2$, CF$_3$SO$_3$, or [Ala] anions.    The [C$_4$mim]CF$_3$CO$_2$/PEO$_{4000}$ and [C$_4$mim]CF$_3$SO$_3$/ PEO$_{4000}$ both turned clear after heating at 70 °C for 1 h.    Upon maintaining them at 25 °C for 3 h, the former was clear, but the latter became opaque.    No clear solution of the [C$_4$mim][Ala]/PEO$_{4000}$ mixture was obtained even after heating at 70 °C for 1 hr.    Interestingly, $[P_{4444}]$[Ala], which is expected to show poor solubility due to cation structure, showed better solubility compared to [C$_4$mim][Ala].    These results show that the affinity of PEO and ILs is strongly influenced by the component ion species and their combinations.

## 2-3-2.    Effect of molecular weight and terminal structure of polyethers on the solubility

Then, effects of molecular weight and terminal structure of PEO on their solubility into ILs were analyzed.    There were negligible changes of the solubility depending on terminal structure.    The change was observed only for the mixture with [C$_4$mim][Ala] (**Table 2-2**).    For the mixture with [C$_4$mim][Ala], the solubility decreased by changing terminal structure of PEO from hydroxyl to methyl group.    Insertions of methyl group are considered to change not only hydrogen-bond ability but also polarity and cohesive energy of PEO, and these somehow affected the solubility of dMe-PEO in [C$_4$mim][Ala].    Considering the ratio of terminal structure is small (*e.g.* terminal group : ether oxygen = 1 : 22 for dMe-PEO used in this study) and this number decrease depending on the Mw. of PEO, the effects of terminal structures on the solubility are considered to be negligible.    **Table 2-2** also shows the changes of the solubility depending on molecular weight of PEO, and the solubility into H$_2$O is shown as reference.    A trend of the solubility depending on IL species was almost same for a series of PEO with Mw. from 2000 to 10000.    The mixtures of

**Table 2-2.** Changes of the solubility depending on Mw. of PEO.

| ILs | Solubility | | | | | |
|---|---|---|---|---|---|---|
| | dMe-PEO | $PEO_{1000}$ | $PEO_{2000}$ | $PEO_{4000}$ | $PEO_{6000}$ | $PEO_{10000}$ |
| $[P_{4448}][Tf_2N]$ | ○*t | ○*t | × | × | × | × |
| $[C_4mmim][Tf_2N]$ | - | ○ | ○ | ○ | ○* | ○* |
| $[C_4mim][Tf_2N]$ | ○ | ○ | ○ | ○ | ○ | ○ |
| $[C_4mim]PF_6$ | ○ | ○ | ○ | ○ | ○ | ○ |
| $[C_4mim]CF_3CO_2$ | ○ | ○ | ○*t | ○*t | ○*t | ○*t |
| $[C_4mim][Ala]$ | ○*t | ○ | × | × | × | × |
| $H_2O$ | ○ | ○ | ○ | ○* | ○* | ○* |

○: soluble (*: under heating and t: turbid after 1hr keeping at room temperature) and ×: insoluble even after heating

$[C_4mim][Tf_2N]$/PEO and $[C_4mim]PF_6$/PEO were soluble under any condition, and vice versa $[P_{4448}][Tf_2N]$/PEO and $[C_4mim][Ala]$/PEO were always insoluble regardless of heating. For the case of $[C_4mmim][Tf_2N]$/PEO mixture, as well as $H_2O$/PEO mixture, the solubility decreased depending on increment of Mw. of PEO. This change is due to increase of cohesive energy as a function of Mw. of PEO, and might also be affected by a number of terminal hydroxyl groups in PEO. Considering these results, ILs can be classified to three groups in terms of affinity of PEO: one having moderate affinity with PEO equivalent to $H_2O$, another having high affinity such as $[C_4mim][Tf_2N]$, and the other having poor affinity such as $[P_{4448}][Tf_2N]$.

### 2-3-3. Effect of hydrogen bond ability of ionic liquids on the solubility

In order to clarify the discussion, the solubility of $PEO_{4000}$ in ILs are only focused in the following section. Taking the hydrogen-bonding ability of PEO into account, the Kamlet-Taft parameters of the ILs were measured. **Figure 2-3** shows the effect of the polarity of the ILs on miscibility with $PEO_{4000}$. The solubility in a series of $[C_4mim]$ salts and $[Tf_2N]$ salts were examined here. Open circles denote IL/$PEO_{4000}$ mixtures that were obtained as a clear solution after stirring at 25 °C for 1h or by keeping them at 25 °C for 3 h after stirring at 70 °C for 1hr.

Since PEO has a simple unit structure, we expected to find an unambiguous relation between the Kamlet-Taft parameters and solubility of the $PEO_{4000}$ in the ILs. **Figure 2-3** does not show any clear relation, however. The affinity of $PEO_{4000}$ and ILs is not simply correlated with the hydrogen-bonding ability of the ILs. This result pushed us to analyze the affinity between PEO and ILs with other parameters.

33
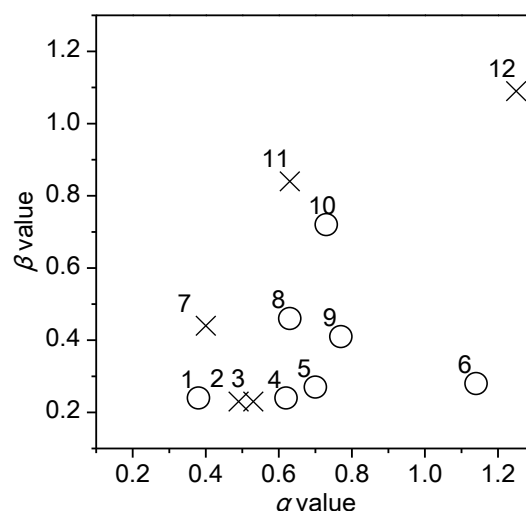
**Figure 2-3.** Effect of $\alpha$ and $\beta$ values on the solubility of $PEO_{4000}$ in various ILs after 1h stirring at 70 °C and 3 h keeping at room temperature.    Each number of besides plot corresponds to 1: [$C_4$mmim][$Tf_2$N], 2: [$Pyr_{14}$][$Tf_2$N], 3: [DEME][$Tf_2$N], 4: [$C_4$mim][$Tf_2$N], 5: [AAim][$Tf_2$N], 6: [$C_2$OHmim][$Tf_2$N], 7: [$P_{4448}$][$Tf_2$N], 8: [$C_4$mim]$CF_3SO_3$, 9: [$C_4$mim]$PF_6$, 10: [$C_4$mim]$BF_4$, 11: [$C_4$mim]$CF_3CO_2$, and 12: [$C_4$mim][Ala]. ○: soluble, ×: insoluble or turbid (=× and t in **Table 2-1**).

### 2-3-4.    Relation between ion hardness and the solubility

To analyze the interaction between PEO and salts, we used HSAB theory.    The hardness of inorganic salts is determinable from atomic energy levels such as the ionization potential and electron affinity.    No statistical study of the hardness of ILs exists, however, and we estimated the hardness of the component ions of the ILs from the $E_{HOMO}$ and $E_{LUMO}$.    These hardness data for ILs is valuable in considering their properties.    **Table 2-3** shows the relation between ion hardness solubility of $PEO_{4000}$ in various ILs.    We first estimated the hardness of cations from their $E_{LUMO}$. The hardness of cations was in the order: [$C_2$OHmim] > [$C_4$mim] > [$C_4$mmim] > [AAim] >> [$Pyr_{14}$] > [DEME] > [$P_{4448}$] (**Table 2-3**, a).    This trend agrees well with the miscibility of $PEO_{4000}$ and [$Tf_2$N] salts.    PEO, as a hard base, prefers harder acids, as shown in **Table 2-3**.

We next investigated the correlation between the hardness of anions, and the miscibility of $PEO_{4000}$ and [$C_4$mim] salts.    Anion hardness was estimated from their value of $E_{HOMO}$.    The hardness of anions was in the order [Ala] > $CF_3CO_2$ >> $CF_3SO_3$ > [$Tf_2$N] > $BF_4$ > $PF_6$ (**Table 2-3**, b).    In a series of [$C_4$mim] salts, lower hardness improved the miscibility of $PEO_{4000}$ and ILs. This is may be because that hard anions are more favorable to interact with hard cation, [$C_4$mim]. This assumption is also valid to explain better affinity of dMe-PEO with [$P_{4444}$][Ala] than [$C_4$mim][Ala] (shown in **Table 2-1**).    There was a competition between cation-PEO interaction and cation-anion interaction.    The hard anion, [Ala], are considered to interact strongly with [$C_4$mim] cation rather than [$P_{4444}$] cation ($E_{LUMO}$ was -0.124).    This may conduce better solubility

34

**Table 2-3.** Relation between ion hardness and solubility of $PEO_{4000}$
in (a) [Tf$_2$N] salts and (b) [C$_4$mim] salts.

(a)

| Cations for [Tf$_2$N] | Solubility of PEO$_{4000}$ | E$_{LUMO}$ of Cations | Hardness |
|---|---|---|---|
| [C$_2$OHmim] | ○ | -0.193 | Harder |
| [C$_4$mim] | ○ | -0.186 | |
| [C$_4$mmim] | ○* | -0.174 | |
| [AAim] | ○* | -0.168 | |
| [Pyr$_{14}$] | ○*t | -0.137 | |
| [DEME] | ○*t | -0.135 | |
| [P$_{4448}$] | × | -0.122 | Softer |

(b)

| Anions for [C$_4$mim] | Solubility of PEO$_{4000}$ | E$_{HOMO}$ of Anions | Hardness |
|---|---|---|---|
| [Ala] | × | -0.043 | Harder |
| CF$_3$CO$_2$ | ○*t | -0.081 | |
| CF$_3$SO$_3$ | ○ | -0.107 | |
| [Tf$_2$N] | ○ | -0.160 | |
| BF$_4$ | ○ | -0.166 | |
| PF$_6$ | ○ | -0.198 | Softer |

○: soluble (*: under heating and t: turbid after 1hr keeping at room temperature) and ×: insoluble even after heating

of dMe-PEO in [P$_{4444}$][Ala] compared to [C$_4$mim][Ala].

These results suggest that the hardness of both cations and anions exert their effects in different manners.   Harder cations were more compatible with PEO$_{4000}$ because of the direct interaction of PEO and cations.   Anions, in contrast, are fairly free from PEO.   In summary, we successfully applied HSAB theory to consider the affinity of PEO and ILs under excess salt conditions.

### 2-3-5.   Properties of ionic liquid/polyether composites

Since ILs are salts having very low glass transition temperature ($T_g$), they should act as excellent additive salts for polymer electrolytes.   Similarly, liquid salts enable homogeneous mixing with polymers even under salt excess conditions if they show moderate affinity.   We designed PEO-based polymer electrolytes containing excess salts.   The results may facilitate the creation of new gel type polymer electrolytes with small amount of polymers.

We concluded that the HSAB theory can be used to consider the affinity of PEO and ILs even under polymer in salt conditions.   We then looked at the effect of affinity on the properties of PEO$_{4000}$/IL polymer electrolytes.   **Figure 2-4** is the picture of PEO$_{4000}$ mixture containing

[AAim][Tf$_2$N], [DEME][Tf$_2$N], and [P$_{4448}$][Tf$_2$N], from left to right. The composite containing [P$_{4448}$][Tf$_2$N], showing poor affinity with PEO$_{4000}$, resulted in phase separation of solid components and liquid components. The mixture containing [DEME][Tf$_2$N], showing moderate affinity with PEO$_{4000}$, resulted in homogeneous solid and the mixture containing [AAim][Tf$_2$N], showing good affinity with PEO$_{4000}$, resulted in homogeneous liquid.
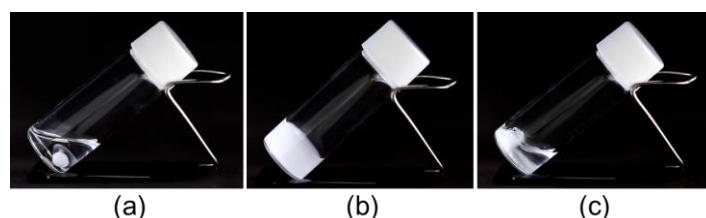


**Figure 2-4.** Pictures of the PEO mixture with (a) [AAim][Tf$_2$N], (b) [DEME][Tf$_2$N], and (c) [P$_{4448}$][Tf$_2$N] (PEO$_{4000}$:IL = 200.0 : 1.0 mg/mL) at room temperature.

Then mixture (a) and (b) shown in **Figure 2-4** were used for ionic conductivity measurement. **Figure 2-5** shows the DSC trace and ionic conductivity of [AAim][Tf$_2$N], PEO$_{4000}$ and their mixture. For these mixing conditions, the [cation]/[EO] ratio was approximately 0.7, a value unattainable with inorganic salts. The mixture was obtained as a clear solution. The $T_g$ of [AAim][Tf$_2$N] ionic conductivity decreased upon adding PEO$_{4000}$ (○ to ● in **Figure 2-5**), as well as the mixture showed $T_g$ higher than the pure IL. The same trend was observed in other
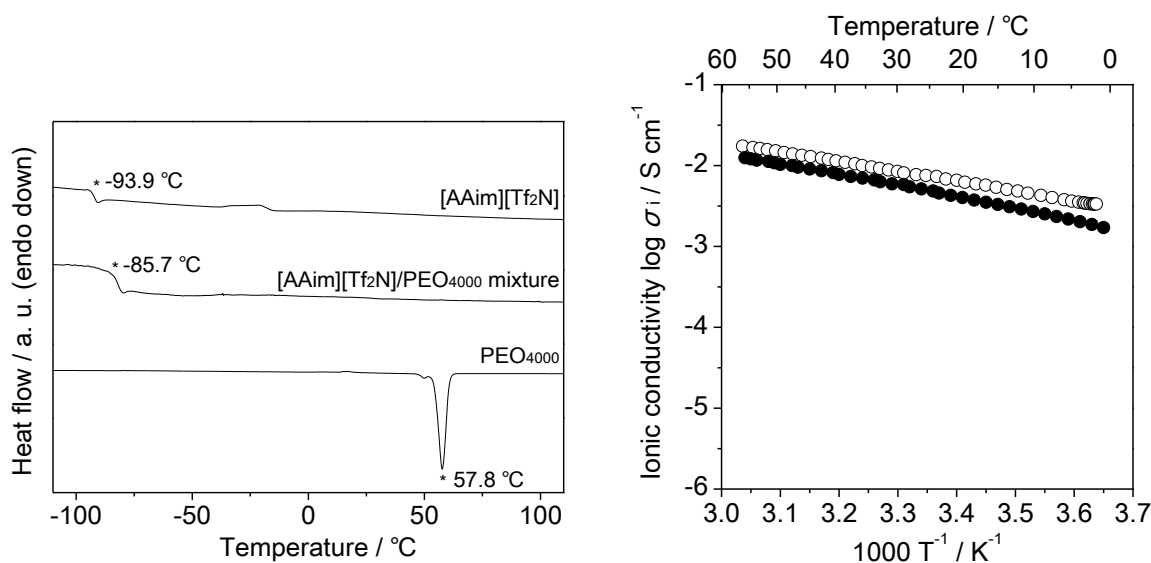


**Figure 2-5.** (left) DSC trace of [AAim][Tf$_2$N], [AAim][Tf$_2$N]/PEO$_{4000}$ composite, and PEO$_{4000}$. (right) Ionic conductivity of [AAim][Tf$_2$N]-PEO$_{4000}$ composite (●) and [AAim][Tf$_2$N] (○).

ILs which dissolved PEO$_{4000}$ well.    This is due to both decrease in the number of carrier ions and increase in the solution viscosity as a result of interaction with PEO.

**Figure 2-6** shows the ionic conductivity of the mixture of [DEME][Tf$_2$N]/PEO$_{4000}$.    The mixture was prepared by the same procedure as for the [AAim][Tf$_2$N]/PEO$_{4000}$ mixture.    The mixture retained low $T_g$ which is comparable to neat [DEME][Tf$_2$N] and showed melting temperature around 33.7 and 40.3 °C.    The ionic conductivity dropped at 20 °C by cooling, then increased at 40 °C by heating this sample.    There was a hysteresis in the ionic conductivity suggesting formation of a thermotropic gel as seen in **Figure 2-6**, right.    The mixture maintained its gel state below 20 °C.    This gel formation is the reason of the drop of ionic conductivity at lower temperatures was about 100 times less than that of [DEME][Tf$_2$N].    Above 40 °C, however, the mixture became a clear solution, and its conductivity reached that of pure [DEME][Tf$_2$N].    The negligible change of the ionic conductivity before and after addition PEO$_{4000}$ are considered to be attributed to weak interaction between PEO and ILs.    We also checked the effect of the affinity on viscosity of the PEO/IL mixtures.    Smaller increase of viscosity was found for the mixture which having ILs showing less affinity with PEO (for this measurement PEO$_{400}$ was used, see Appendix P. 95).    There are two significant characteristics of the [DEME][Tf$_2$N]/PEO$_{4000}$ mixture.    The first is the almost identical ionic conductivity to pure [DEME][Tf$_2$N] at higher temperature, and the second is the reduced but relatively high ionic conductivity of the SOLID sample at lower temperatures.    The ionic conductivity below 20 °C should be attributed to the migration of component ions of ILs in solid PEO$_{4000}$ network.
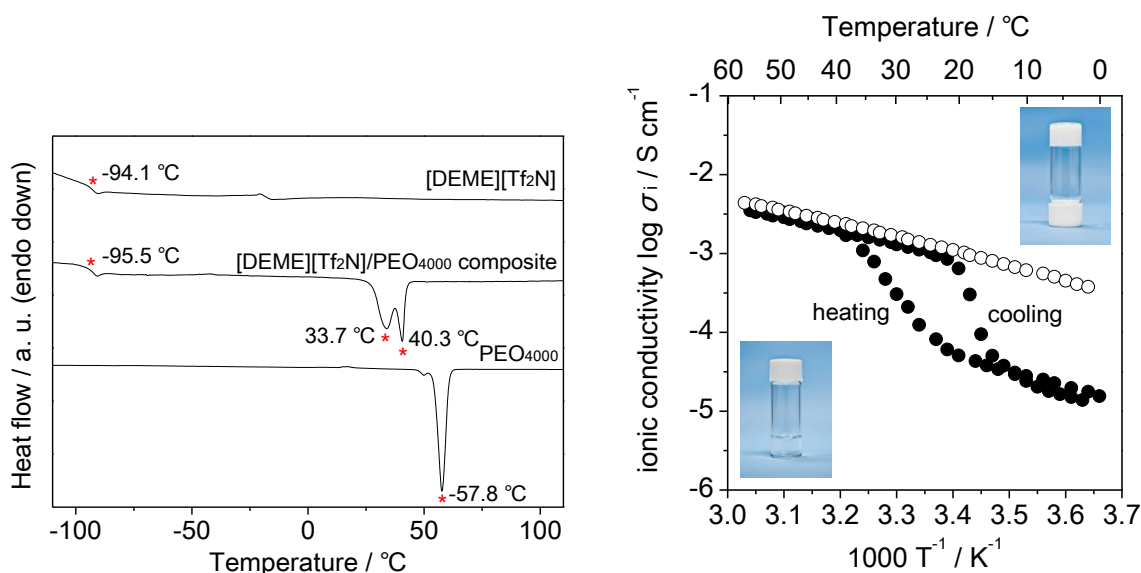


**Figure 2-6.**  (left) DSC trace of [DEME][Tf$_2$N], [DEME][Tf$_2$N]/PEO$_{4000}$ composite, and PEO$_{4000}$.
(right) Ionic conductivity of [DEME][Tf$_2$N]/PEO$_{4000}$ composite (●) and [DEME][Tf$_2$N] (○).

Segmental motion of the polymer is not a primary factor determining the ionic conductivity when ILs were used to prepare polymer electrolytes.　Consequently, ILs promise a new opportunity to create novel polymer electrolytes without PEO.　We conclude that salt-rich polymer electrolytes can be designed with ILs, and that many polymers have the capability to act as matrixes for ILs when they show moderate affinity with ILs.

## 2-4.　Functional design of ionic liquid/polymer composites by tuning affinity

　　　　For polymer composites containing inorganic salts, salts are dissociated into ions via interaction with polymer matrices and migrate along with segmental motions of matrices.　For this reason, low $T_g$ of polymer matrices is a key factor to enhance ionic conductivity.　On the other hand, the composites of polymers and ILs enhance ionic conductivity derived from intrinsic conductivity of ILs.　Throughout the design of IL/PEO composites in former section, we came to the conclusion that the moderate affinity between ILs and PEO is important to design the composites showing desirable ionic conductivity.　Here we designed the composites based on other polymers and ILs by controlling their affinity.

　　　　We designed the composites based on PVP and PAA.　Both polymers are hydrophilic and expected to dissolve ILs via interaction concerned by polarity.　By considering Lewis basicity of PVP, solubility to a series of [Tf$_2$N] salts was investigated.　As seen in **Table 2-4**, PVP easily dissolved to ILs at 70°C excepting [P$_{4448}$][Tf$_2$N].　This may be due to the low polarity of [P$_{4448}$] cations.　Then, ionic conductivity of [C$_4$mim][Tf$_2$N]/PVP having good affinity pair and [P$_{4448}$][Tf$_2$N]/PVP having low affinity pair were measured.　For the case of [C$_4$mim][Tf$_2$N], ionic conductivity decreased after addition of PVP suggesting there exist strong interaction between [C$_4$mim][Tf$_2$N] and PVP (**Figure 2-7**, left).　On the other hand, the ionic conductivity comparable to pure [P$_{4448}$][Tf$_2$N] was found for the [P$_{4448}$][Tf$_2$N]/PVP composite (**Figure 2-7**, right).　Same trend was observed for PAA composites. For the case of PAA, PAA hardly dissolved to ILs, and only [C$_4$mim]CF$_3$CO$_2$ having high hydrogen bond basicity dissolved PAA.　Ionic conductivity of PAA/[C$_4$mim]CF$_3$CO$_2$ composite was found ten times smaller compared to pure [C$_4$mim]CF$_3$CO$_2$ (**Figure 2-8**).　This data follows that moderate affinity between polymers and ILs is important to retain ionic conductivity of ILs after addition of polymers.

**Table 2-4.**　Solubility of polymers to ILs when samples are mixed at 70°C (left) and after keeping one night at room temperature (right). (○: soluble, ×: insoluble, and t: turbid)

| | Molecular weight | [Tf$_2$N] salts | | | | CF$_3$CO$_2$ |
|---|---|---|---|---|---|---|
| | | [C$_4$mim] | [C$_4$mmim] | [Pyr$_{14}$] | [P$_{4448}$] | [C$_4$mim] |
| PVP | 40,000 | ○/○ | ○/○ | ○/○ | t / t | ○/○ |
| PAA | 25,000 | t /× | t / t | t /× | t /× | ○/○ |

$[C_4mim][Tf_2N]$             $[P_{4448}][Tf_2N]$
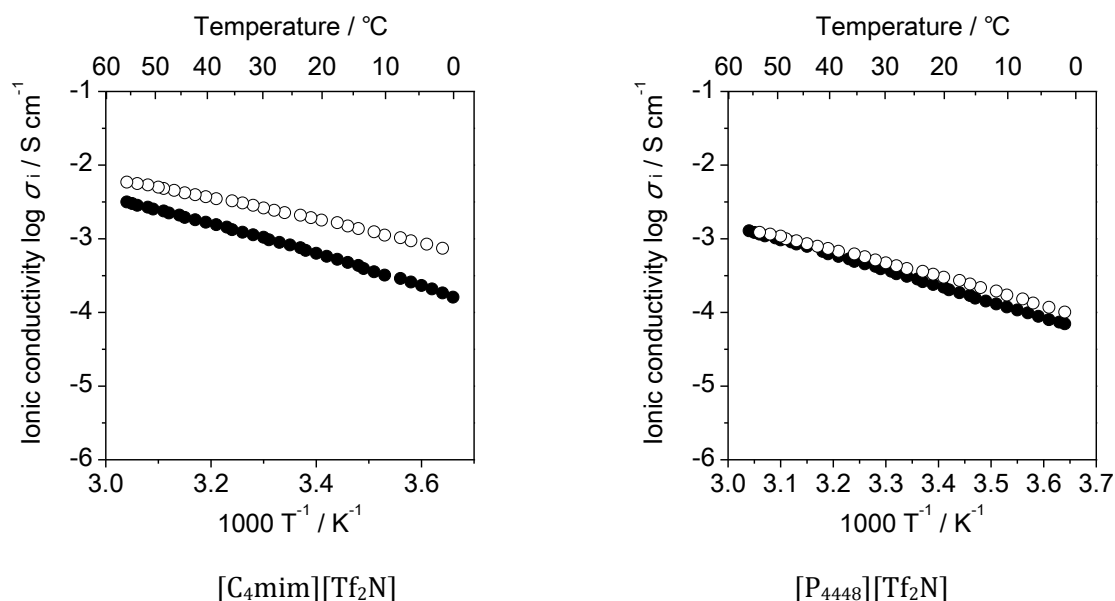
**Figure 2-7.** Ionic conductivity of $[C_4mim][Tf_2N]$ and $[P_{4448}][Tf_2N]$ with (●) and without (○) PVP.
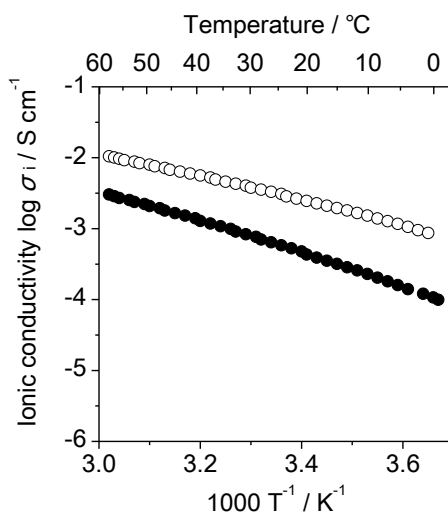


**Figure 2-8.** Ionic conductivity of $[C_4mim]CF_3CO_2$/PAA composite (●) and $[C_4mim]CF_3CO_2$ (○).

## 2-5. Summary

First, solubility of PEO in ILs was checked to evaluate affinity between them.   HSAB theory was found to be applicable to discuss the affinity between ILs and PEO.   ILs composed of relatively hard acids such as imidazolium cations and soft bases such as $[Tf_2N]$ anions showed good miscibility with $PEO_{4000}$ at all mixing ratios.   Choice of the hardness of component ions is effective in controlling the dispersion state of $PEO_{4000}$ in ILs.   When $[P_{4448}][Tf_2N]$ containing soft cation

was added to PEO$_{4000}$, PEO$_{4000}$ precipitated in ILs.   The stable composite cannot be obtained when ILs with poor affinity with PEO$_{4000}$ were added.   The mixture containing [AAim][Tf$_2$N], showing good affinity with PEO$_{4000}$, resulted in homogeneous liquid, and [DEME][Tf$_2$N], showing moderate affinity with PEO$_{4000}$, resulted in homogeneous solid.   For [AAim][Tf$_2$N]/PEO$_{4000}$ composites, its ionic conductivity was always lower than that of pure [AAim][Tf$_2$N].   On the other hand, the comparable ionic conductivity were found between the [DEME][Tf$_2$N]/PEO$_{4000}$ composites and pure [DEME][Tf$_2$N] above phase transition temperature of the composites.   The ionic conductivity of the IL/PEO composites were differentiated depending on affinity between ILs and PEO.

Then, we tried functional design of IL/polymer composites by controlling the affinity. For IL/PVP and IL/PAA composites, ionic conductivity was retained even after adding polymers when the ILs showing moderate affinity with polymers.   Consequently, we concluded polymer electrolytes can be designed with ILs, and many polymers have the capability to act as matrixes for ILs as long as they show moderate affinity with ILs.

## 2-6.   References

[1]      J. S. Wilkes, *Green Chemistry* **2002**, *4*, 73-80.

[2]      C. Reichardt, *Green Chemistry* **2005**, *7*, 339-351.

[3]      G. Klopman, *Journal of the American Chemical Society* **1968**, *90*, 223-234.

[4]      S. Luo, S. Zhang, Y. Wang, A. Xia, G. Zhang, X. Du, D. Xu, *The Journal of organic chemistry* **2010**, *75*, 1888-1891.

# Chapter 3
# Compatibility of fluorinated polymers
# into ionic liquids and design of their composites

## 3-1.  Introduction

Fluorinated polymers are desirable polymers in terms of stability and credibility.   They possess high chemical inertness, electrochemical stability, and thermal stability.   The materials based on fluorinated polymers should enhance incredible stability which is supported by inertness of polymers; however, the functional design of fluorinated polymers are difficult due to their extremely low surface free energy.   Many functional materials based on fluorinated polymers have been designed by inserting functional groups onto polymer structure via covalent bond. Only limited fluorinated polymers have been applied to design composite with small molecules.

In the former section, the effect of affinity between ionic liquids (ILs) and polymers have been discussed and functional design of their composites were carried out by controlling the affinity.   By mixing components which show poor affinity, polymers precipitate in ILs and stable composites cannot be obtained.   In order to obtain stable composites, components of the composites are required to show suitable affinity to suppress phase separation of components. Among the stable composites, enhanced ionic conductivity was found with the mixture consisting components which show moderate affinity, since high affinity between the components suppresses the conductivity of ILs.   In this section, compatibility between fluorinated polymers and ILs were evaluated.   Similar to former section, the effect of the compatibility on the properties of their composites were analyzed.

## 3-2.  Experimental procedure – dissolution of polymer

### 3-2-1.  Materials

Structure, abbreviation, and preparation for all ILs are summarized in the Appendix (P. 88).   All IL were dried under vacuum at 60 °C for at least 3 h.

Structures of fluorinated polymers are summarized in **Figure 3-1**.   Partially-fluorinated polymers, such as poly(vinylidene fluoride) (PVdF, average Mw. of ~534,000), Poly(chlorotrifluoroethylene) (PCTFE), poly(ethylene-*co*-chlorotrifluoroethylene) (PECTFE), and poly(vinyl fluoride) (PVF) were purchased from Sigma-Aldrich or Scientific Polymer Products, Inc. Poly(ethylene-*co*-tetrafluoroethylene), Fluon® ETFE Z-8820X (ETFE) was kindly donated from Asahi Glass Co.   Fully-fluorinated polymer such as poly(tetrafluoroethylene) (PTFE, average Mw. of 5,000 ~ 20,000, from Wako Pure chemical Industries, Ltd.) was purchased. Poly(perfluorobutenylvinyl ether), CTL-810S (Cytop) was kindly donated from Asahi Glass Co.
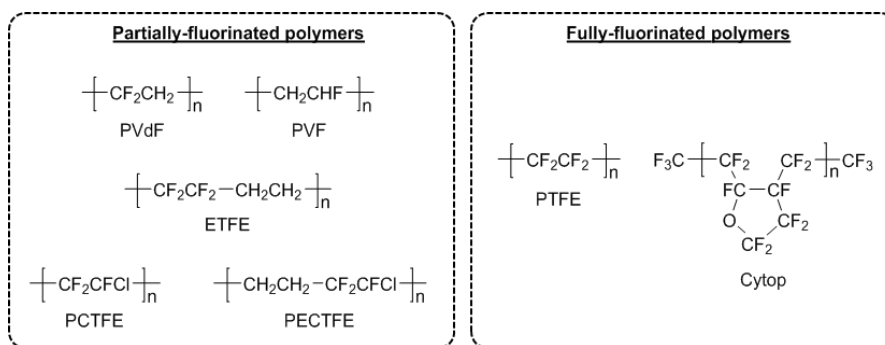
**Figure 3-1.** Structure of partially- and fully-fluorinated polymers.

### 3-2-2. Evaluation of solubility

#### Mixing condition

For PVdF, ETFE, PVF, PECTFE, PCTFE, PTFE

To 300 mg of dry ILs, 3 mg of the polymers were added in $N_2$ filled glove box. The vials containing samples were tightly closed with PTFE thread seal tape and stirred for 1 h at ambient atmosphere. Their solubility were inspected visually with naked eyes. If the mixture provided insoluble, the mixture was heated up to 120 °C and solubility was inspected every 20 °C.

For Cytop

Cytop diluted tenfold with fluoroalkane was donated. First, 30 μl of Cytop solution was taken with a micropipette. Each samples were dried under vacuum at 80 °C to remove fluoroalkane. To dried samples, 300 mg of dried ILs was added and tightly closed with PTFE thread seal tape in $N_2$ filled glove box. The mixture was stirred for 1 h at ambient atmosphere. Their solubility were inspected visually with naked eyes. If the mixture provided insoluble, the mixture was heated up to 120 °C and solubility was inspected every 20 °C.

#### Investigation of solubility

Solubility of fluorinated polymers to ILs was firstly investigated visually with naked eyes. Turbidity differed depending on the combination of fluorinated polymers and ILs. There is a fear that some ILs dissolved small amount of fluorinated polymers in which are not detectable with naked eyes. Samples having potential of the dissolution were proposed for further test.

Thermogravimetric analysis (TGA)

To confirm the possibility of polymer dissolution, TGA was carried out for some samples. Prior to the measurement, the samples were filtrated with PTFE filter having 0.20 μm pore. The samples were heated up to 450 °C with a heating rate of 15 °C min⁻¹ and held for 15 min. The

ratio of leftover was compared to that of pure ILs after thermolysis in a same condition.


Nuclear magnetic resonance (NMR) measurement

^{19}F NMR were also carried out to check the dissolution of fluorinated polymers in ILs.　Same samples of solubility measurement were used with or without filtration.　The samples were placed in outer tube and hexafluorobenzene diluted to $CDCl_3$ as standard for chemical shift was placed in inner tube.　These were analyzed by ^{19}F NMR with the accumulation of 1000 scans at room temperature.


## 3-3.　Solubility of partially-fluorinated polymers


### 3-3-1.　Poly(vinylidene fluoride)


PVdF are known as important materials due to their stability comparable to other fluorinated polymers, as well as moderate solubility to organic solvents.　For this reason, PVdF are used in electronics field especially as binder for electrode materials to produce thin electrodes.

　　　Temperature when PVdF dissolved in ILs are summarized in **Table 3-1**.　Among [$Tf_2N$] salts, phosphonium and sulfonium-type ILs showed poor solubility of PVdF compared to other ILs containing such cation as imidazolium, piperidinium, pyrrolidinium, and pyridinium. Imidazolium cation has been reported to interact with -$CF_2$- [1]; however, not only imidazolium salts but also piperidinium, pyrrolidinium, and pyridinium salts showed similar solubility od PVdF. Then, the solubility of PVdF to a series of imidazolium salts and phosphonium salts were compared. All imidazolium salts used in this study showed solubility of PVdF (**Table 3-1**, b).　For the case of [$C_4$mim][FAP], the solubility was once observed under heating condition; however, the mixture got turbid after keeping the sample at room temperature.　A similar ILs comprising longer alkyl chain on imidazolium, 1-methyl-3-octadecylimidazolium [FAP] ([$C_{18}$mim][FAP]), are known to form high-entropy bulk structures at high temperature and ordered structures at lower temperature [2].　This is due to the separation of layer consisting [FAP] anion and imidazolium ring from alkyl chain of cations which is induced by van der Waals interaction.　Since the alkyl chain length of [$C_4$mim] cation is shorter than [$C_{18}$mim] cation, the effect of van der Waals interaction are diluted but somehow effected the temperature dependence of dissolution of PVdF. In contrast to considerable affinity between imidazolium salts and PVdF, phosphonium salts were confirmed to have poor affinity with PVdF even if these cations were combined with $PF_6$, $CF_3SO_3$, and SCN.　When these anions replaced to ones containing high fluorine content such as $BF_4$ (F, 87.6), $C_8F_{17}SO_3$ (F, 64.7), [$Nf_2N$] (F, 58.9), and $C_4F_9SO_3$ (F, 57.2), the phosphonium salts dissolved PVdF.　For the case of [$P_{666,14}$]$C_8F_{17}SO_3$, the IL dissolved PVdF at room temperature.　Throughout this study, we saw that cation structure strongly affect to dissolution of PVdF.　Although the

change of solubility of PVdF with different anionic structures was not remarkable.　　Consequently, we concluded that cation structures play an important role to solubilize PVdF.

**Table 3-1.**　Temperature when PVdF dissolved in the (a) [$Tf_2N$], (b) imidazolium, and (c) phosphonium salts. (×: insoluble up to 120 °C and $^t$: turbid after keeping at room temperature)

| Dissolution temperature / °C | | | | | |
|---|---|---|---|---|---|
| (a) [$Tf_2N$] salts | | (b-1) [$C_4mim$] salts | | (c-1) [$P_{444,12}$] salts | |
| [$C_4mim$] | 80 | $PF_6$ | 60 | $PF_6$ | × |
| [$Pyr_{14}$] | 80 | $CF_3SO_3$ | 80 | $CF_3SO_3$ | × |
| [$C_2OHmim$] | 100 | $BF_4$ | 80 | $BF_4$ | 100 |
| [$C_4py$] | 100 | [FAP] | 100$^t$ | SCN | × |
| [$Pip_{14}$] | 100 | | | | |
| [$N_{4441}$] | 100 | (b-2) [$C_2mim$] salts | | (c-2) [$P_{666,14}$] salts | |
| [$P_{4441}$] | 100 | $C_4F_9SO_3$ | 60$^t$ | $C_8F_{17}SO_3$ | 25 |
| [$S_{111}$] | × | FSI | 80 | [$Nf_2N$] | 80$^t$ |
| [$P_{444,12}$] | × | $(CH_3O)(H)PO_2$ | 100 | | |
| [$P_{8888}$] | × | | | (c-3) [$P_{4446}$] salts | |
| [$P_{666,14}$] | × | | | $C_4F_9SO_3$ | 80 |

### 3-3-2.　Poly(ethylene-*co*-tetrafluoroethylene)

ETFE consist of same constituent as PVdF, *i.e.* -$CH_2$- and -$CF_2$-.　　These constituents are sequenced one by one for PVdF.　　In contrast to this, the sequence is two by two for ETFE, and their solubility to solvents are very poor.　　In this study, solubility of ETFE to 24 different ILs were investigated; however, no ILs fully dissolved 1 wt% of ETFE.　　Then, we investigated transparency of the IL/ETFE mixtures (**Table 3-2**).　　The transparency of the mixture was roughly investigated with naked eye by comparing the mixture and a standard.　　The standard was prepared based on a sheet of polypropylene with a thickness of 0.5 mm and adhesive Teflon tape.　　Transparency of the samples classified based on a number of Teflon tape.　　According to UV-vis spectroscopy, the transparency of the polypropylene sheet is equal to -21%, and that with Teflon tape is equal to -33 % for one layer, and decrease -41, -48, and -56 % with increase of layer.　　The mixture with [$Tf_2N$] salts containing such cation as [$C_4mim$], [$Pyr_{14}$], [$S_{111}$], [$Pip_{14}$], and [$N_{4441}$] showed transparent phase comparable to the propylene sheet; however, many mixtures were turbid more than layered Teflon tape.　　Since turbidity of the mixture should be affected by formula weight of the ILs, reflective index, and affinity between ETFE and ILs, evaluation of the affinity based on the turbidity of the mixture was quite complicated.　　For only the mixture with [$C_2mim$]$CH_3O(H)PO_2$, noticeably low affinity which is accounted by separation of ETFE from the IL was found.

**Table 3-2.**   Transparency of the mixture evaluated by comparing the sample and polypropylene sheet with adhesive Teflon tape. (Character $n$ is number of layer of Teflon tape)

| Transparent | Turbid | | Separate |
|---|---|---|---|
| [Tf$_2$N] | [Tf$_2$N] | Other ILs | Other ILs |
| [C$_4$mim] | $n = 1$ | $n = 1$ | [C$_2$mim](CH$_3$O)(H)PO$_2$ |
| [Pyr$_{14}$] | [P$_{4441}$] | [P$_{8888}$]SCN | |
| [S$_{111}$] | [P$_{8888}$] | [P$_{8888}$][Pf$_2$N] | |
| [Pip$_{14}$] | [C$_2$OHmim] | [S$_{111}$][Nf$_2$N] | |
| [N$_{4441}$] | [AAim] | [P$_{666,14}$]C$_8$F$_{17}$SO$_3$ | |
| | [C$_4$py] | $n = 2$ | |
| | $n = 2$ | [P$_{444,12}$]SCN | |
| | [C$_2$mim] | [P$_{444,12}$]BF$_4$ | |
| | [P$_{444,12}$] | $n = 3$ | |
| | $n = 3$ | [P$_{444,12}$]PF$_6$ | |
| | [P$_{666,14}$] | [P$_{666,14}$]CF$_3$SO$_3$ | |
| | | $n = 4$ | |
| | | [P$_{8888}$]CF$_3$SO$_3$ | |

### 3-3-3.   Poly(vinyl fluoride)

PVF consists of one fluorine in one ethylene unit: *i.e.* -CH$_2$CHF-.   First, we intended to analyze solubility of poly(trifluoroethylene) (PTE, -CF$_2$CFH-) to ILs; however, PTE is unstable due to the presence of acidic proton.   The acidic proton are easily pulled from the polymer opening it to oxidation or dehydrofluorination, and PTE degrade easily.   Considering this, we used PVF for solubility measurement instead of PTE.   We expected that PVF easily dissolve to ILs due to presence of acidic proton.   On the contrary, PVF was found to be insoluble to any ILs.   This may be due to the diluted acidity of proton.   Since there exists only one fluorine in one polymer unit, electronegativity of one fluorine was not enough to generate acidity of three protons.

### 3-3-4.   Poly(chlorotrifluoroethylene) and poly(ethylene-*co*-chlorotrifluoroethylene)

The fluorinated polymers containing chloride were also used for solubility measurement.   PCTFE containing one chloride on one polymer unites (-CF$_2$CFCl-) and its copolymer with polyethylene named PECTFE (-CH$_2$CH$_2$-co-CF$_2$CFCl-) were used.   To a series of ILs shown in **Table 3-3**, 1wt% of PCTFE was added, and solubility was inspected visually.   PCTFE was found to be insoluble to the ILs.   Since there is a possibility that small portion of added PCTFE was dissolved to the ILs, the ratio of leftover after thermolysis was compared before and after PCTFE addition.   For this

measurement, the mixture was filtered and heated up to 450 °C.   All ILs decompose and only polymers remain at this temperature.   As seen in **Table 3-3**, the leftover of the mixture after filtration was almost equal to that of ILs.   We concluded that PCTFE is difficult to dissolve to ILs.   Then, we analyzed the solubility of PECTFE into ILs.   PECTFE is also known to insoluble to any organic solvent, however, it is slightly compatible with nonpolar solvent such as cyclohexane.   With respect to this, $[P_{666,14}][Tf_2N]$, $[C_2mim][Nf_2N]$, $[P_{666,14}]C_8F_{17}SO_3$ were chosen to analyze the effect of polarity.    Among these three mixtures, transparent mixture was obtained with $[P_{666,14}][Tf_2N]$.    Since there is a fear, that $[P_{666,14}][Tf_2N]$ has refractive index similar to PECTFE resulted in transparent mixture, the solubility of PECTFE in $[P_{666,14}][Tf_2N]$ was

**Table 3-3.**  Comparison of leftover ratio after thermolysis of
ILs and PCTFE mixture, and pure ILs.

|  | Ratio of leftover / % | |
| --- | --- | --- |
|  | IL + PCTFE* | IL |
| $[C_2mim][Tf_2N]$ | 6.9 | 6.4 |
| $[C_2mim]C_4F_9SO_3$ | 4.5 | - |
| $[C_2mim](CH_3O)(H)PO_2$ | 26.9 | 26.0 |
| $[P_{666,14}]C_8F_{17}SO_3$ | 0.6 | 3.6 |
| $[C_2mim][FSI]$ | 11.1 | - |
| $[C_2OHmim][Tf_2N]$ | 8.8 | 9.4 |
| $[C_2mim][FAP]$ | 9.7 | 9.9 |

* after filtration of the mixtures
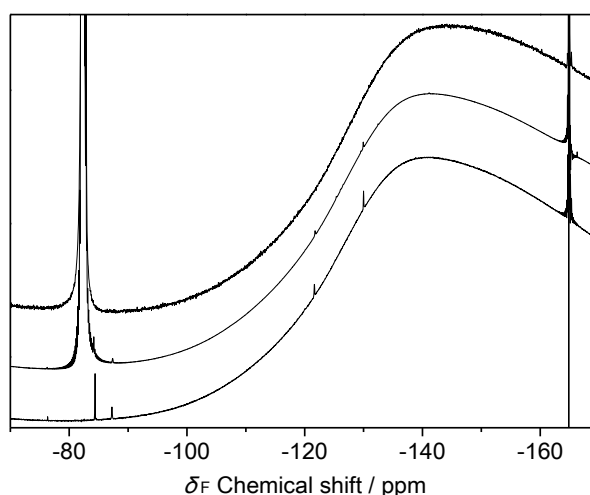


**Figure 3-2.** $^{19}F$ NMR spectra of $[P_{666,14}][Tf_2N]$, PECTFE in $[P_{666,14}][Tf_2N]$, and PECTFE in cyclohexane (top to bottom).

47

analyzed by using ^{19}F NMR.　**Figure 3-2** shows ^{19}F NMR trace of pure $[P_{666,14}][Tf_2N]$, PECTFE in $[P_{666,14}][Tf_2N]$, and PECTFE in cyclohexane as reference.　The peaks attributed to PECTFE were observed around -76.3, -84.4, -87.3, -121.6, and -130.1 ppm.　These peaks were not detected with mixture containing other ILs.　Aside the amount of PECTFE dissolved into ILs was very small, we successfully detected solubilized PECTFE in $[P_{666,14}][Tf_2N]$ by ^{19}F NMR.

## 3-4.　Solubility of fully-fluorinated polymers

### 3-4-1.　Poly(tetrafluoroethylene)

Among fluorinated polymers, PTFE is known to have strongest inertness to chemicals.　No ILs could dissolve PTFE for 1 wt%; however, difference in terms of dispersion state was observed. **Figure 3-3** shows optical microscope image of the sample containing 1 wt% of PTFE in $[C_2mim][Tf_2N]$ and $[P_{8888}][Pf_2N]$.　PTFE dispersed as small particle in $[P_{8888}][Pf_2N]$, nevertheless aggregation of PTFE was observed in $[C_2mim][Tf_2N]$.　This suggest the compatibility of PTFE with $[P_{8888}][Pf_2N]$ is slightly better than that with $[C_2mim][Tf_2N]$.　This difference was also distinguishable with naked eyes.



(a) $[C_2mim][Tf_2N]$　　　　　(b) $[P_{8888}][Pf_2N]$
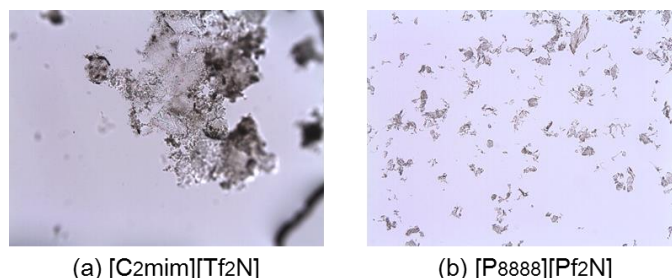
**Figure 3-3.** Optical microscope images of PTFE in (a) $[C_2mim][Tf_2N]$ and (b) $[P_{8888}][Pf_2N]$.

### 3-4-2.　Cytop®

Cytop was kindly donated from Asahi Glass Co.　This polymer containing oxygens in main chain of polymers and these classified as perfluorinated polymers.　First, the solubility of Cytop was analyzed in same procedure of PCTFE.　Among eight ILs shown in **Table 3-4**, change of leftover ratio was found for $[C_2mim][Tf_2N]$.　The subtraction of leftover ratio between IL+Cytop and IL was larger than additive amount of Cytop.　This is may be due to the change of decomposition temperature of ILs with the presence of small amount of polymers.　Then, we checked the solubility of Cytop to $[C_2mim][Tf_2N]$ by using ^{19}F NMR.　To confirm the particular solubility of the

Cytop to [C$_2$mim][Tf$_2$N], same measurement was also carried out for [C$_2$mim]C$_4$F$_9$SO$_3$.    As shown in **Figure 3-4**, peaks of Cytop® was found at -87.8, -122.2, and -130.4 ppm in [C$_2$mim][Tf$_2$N], nonetheless no peaks was found in [C$_2$mim]C$_4$F$_9$SO$_3$.    Aside the amount of Cytop which can be dissolved into ILs was very small, we confirmed that Cytop is possible to be dissolved in designed ILs.

**Table 3-4.**    Comparison of leftover ratio after thermolysis of ILs and Cytop mixture, and pure ILs.

|  | Ratio of leftover / % | |
| --- | --- | --- |
|  | IL + Cytop | IL |
| [C$_2$mim][Tf$_2$N] | 29.2 | 6.4 |
| [C$_2$mim]C$_4$F$_9$SO$_3$ | 4.2 | - |
| [C$_2$mim]CH$_3$O(H)PO$_2$ | 24.9 | 26.0 |
| [P$_{666,14}$]C$_8$F$_{17}$SO$_3$ | 1.8 | 3.6 |
| [C$_2$mim](FSO$_2$)$_2$N | 10.8 | - |
| [C$_2$OHmim][Tf$_2$N] | 10.6 | 9.4 |
| [C$_2$mim][Nf$_2$N] | 7.7 | 7.0 |
| [C$_2$mim][FAP] | 9.8 | 9.9 |
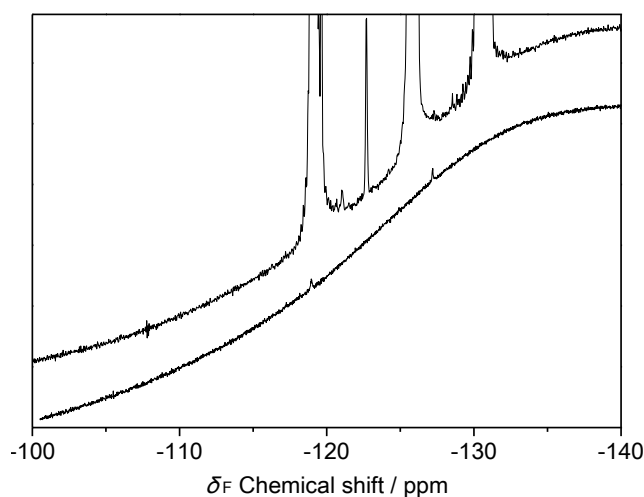


**Figure 3-4.** $^{19}$F NMR spectrum of Cytop in [C$_2$mim]C$_4$F$_9$SO$_3$ (top) and [C$_2$mim][Tf$_2$N] (bottom).

### 3-4-3. Effect of fluorine content of the polymers on the solubility

Throughout solubility measurement, many fluorinated polymers were hard to dissolve.   Slight solubility was observed with PECTFE in $[P_{666,14}][Tf_2N]$ and Cytop in $[C_2mim][Tf_2N]$.   Only PVdF showed considerable change of the solubility depending on IL species.   Both PVdF and ETFE are composed from same unit of $-CH_2-$ and $-CF_2-$, and only the sequence of these unit is different.   The difference of solubility can be explained by different sequence of these unit [3].   For the case of ETFE, they consists of two by two structure of these units, which give dipolar moment that lie along the polymer backbone and compensate each other.   On the other hand, PVdF has alternating units of $-CH_2-$ and $-CF_2-$, and this sequence enhance surface dipole moment along with direction of C-F bond.   The different solubility of ETFE and PVdF is considered to be affected by surface dipole moment.   Considering this, we checked the contribution of polar interaction between ILs and PVdF on their solubility by using Kamlet-Taft parameter (hydrogen bond acidity; $\alpha$ and basicity; $\beta$, see **Section 2-2-3**) of ILs.   **Figure 3-5** shows relation between Kamlet-Taft parameters and solubility of PVdF into the ILs.   ILs which dissolved PVdF were found to possess high $\alpha$ value and low $\beta$ value.   Data in red denote the solubility of PVdF in to $[Tf_2N]$ salts.   Among $[Tf_2N]$ salts, only phosphonium salts showed poor solubility of PVdF (see **Section 3-3-1**), and these were found to have $\beta$ value lower than 0.4.   This suggests that contribution of polar interaction of phosphonium cation are weak, and result in poor solubility of PVdF.   We concluded that PVdF has considerable affinity between ILs, and these can be controlled by changing polarity of cation.
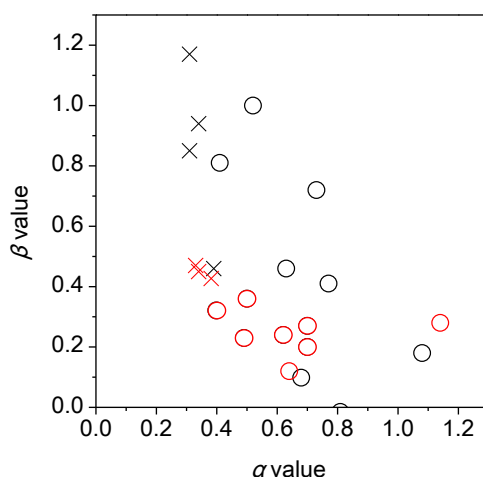


**Figure 3-5.**  Relation between Kamlet-Taft parameters and solubility of PVdF into the ILs. Cations in red were coupled with $[Tf_2N]$ anions.   ($\times$: insoluble, $\circ$: soluble)

## 3-5. Experimental procedure –preparation of polymer electrolytes

Then we prepared polymer electrolyte based on fluorinated polymers. As we discussed in former section, fluorinated polymers were hard to interact with molecules and difficult to make composite of them. Among these fluorinated polymers, only PVdF has considerable affinity with other molecules or ions. Considering this, PVdF-based polymers named PVdF-HFP has been proposed to prepare polymer electrolytes. As additive salts, [Pyr$_{14}$] salts was chosen due to its moderate affinity with PVdF as well as electrochemical stability. As anion to combine with [Pyr$_{14}$] cation, PF$_6$ anion was chosen. Because PF$_6$ salts is acknowledged as one of potential salts for lithium ion batteries because it has a unique set of properties that include sufficient ionic conductivity and negligible reactivity toward aluminum current collectors [4]. With respect to these discussion, we prepared PVdF-HFP based electrolytes with [Pyr$_{14}$]PF$_6$ and electrolyte solution containing LiPF$_6$.

### 3-5-1. Materials

**Figure 3-6** shows structure of the component for polymer electrolytes investigated. Battery grade electrolytes, namely LP 30 (from Merck KGaA) was purchased. This electrolyte consists 1M LiPF$_6$ in ethylene carbonate (EC)/dimethyl carbonate (DMC) 1:1 wt/wt mixture. PVdF-HFP, Kynar Flex® 2801 (PVdF-HFP, from Atofina Chemicals, Inc.) and [Pyr$_{14}$]PF$_6$ (from Solvionic) were purchased. These polymer and salts were dried under vacuum at 120 ºC for 12 h prior to use.
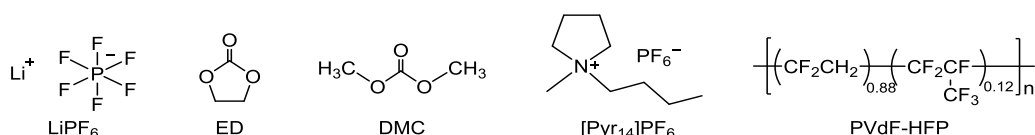


**Figure 3-6.** Structure of the electrolyte components.

### 3-5-2. Preparation of electrolyte solution for lithium ion batteries

A series of solutions was prepared by varying the [Pyr$_{14}$]PF$_6$ content in LP 30 from **5** to **30** wt%. **Table 3-5** shows the compositions and acronyms of the resulting solutions. The water content of all solutions prepared was less than 20 ppm according to a standard Karl Fischer titration method (831 KF Coulometer, from Metrohm). All procedures were carried out in an Ar-filled glove box.

**Table 3-5.** Composition of the solutions used in this study.

| Sample name | Component ratio / wt% | |
| --- | --- | --- |
| | LP-30 | $[Pyr_{14}]PF_6$ |
| LP 30 | 100 | 0 |
| sol-**5** | 95 | 5 |
| sol-**15** | 85 | 15 |
| sol-**20** | 80 | 20 |
| sol-**25** | 75 | 25 |
| sol-**30** | 70 | 30 |

### 3-5-3. Polymer films containing the electrolytes

PVdF-HFP based polymer membranes were prepared by a solution casting procedure.   We selected DMC as a diluting solvent, since EC/DMC cosolvent is the solvent of LP 30, and DMC evaporates at lower temperature than EC in the cosolvent [5].   Initially, 0.3 g of PVdF-HFP was dissolved in 5.0 g of DMC.   Sol-**30** was selected as the electrolyte solution, and 0.7 g of it was added to the PVdF-HFP-DMC solution.   The resulting solution was stirred vigorously at room temperature overnight, then for 10 min at 70 °C.   The mixture was cast on a 5 cm diameter Petri dish at 70 °C.   To evaporate the DMC, the Petri dish was heated for 1 h at 70 °C and quenched to room temperature for 1 h.   The heating-quenching procedures were repeated 4 times, and additional shorter cycles until a weight loss of ca. 5.0 g had occurred, corresponding to removal of the DMC solvent.   The polymer membrane we obtained had thickness of 200 ± 10 µm and was stored in immersion in the electrolyte solution (*i.e.*, sol-**30**) prior to use.   All procedures and handling of materials were carried out in an Ar-filled glove box.

### 3-5-4. Measurement of electrochemical properties

#### Thermal properties

We carried out differential scanning calorimetry (DSC) measurements using a DSC 821 (from Mettler-Toledo) equipped with a liquid nitrogen cooling system.   The sample pans were sealed in an Ar-filled glove box and measurements were carried out in ambient atmosphere.   The samples were cooled to -95 °C with a rate of -10 °C min$^{-1}$ and held for 7 min, then DSC scans were taken from -90 to 90 °C with a scan rate of 3 °C min$^{-1}$.   TGA were carried out using a TGA/SDTA 851 (from Mettler-Toledo) in ambient atmosphere from room temperature to 600 °C with a scan rate of 5 °C min$^{-1}$.

## Ionic conductivity

Ionic conductivity was measured by electrochemical impedance spectroscopy, using a frequency response analyzer (FRA 1260, from Solatron).   A cell consisted of two platinum electrodes immersed in the electrolyte solution, with a nominal cell constant of 0.98 cm$^{-1}$ (**Figure 3-7**).   In the case of the polymer electrolyte, cells were fabricated by sandwiching a disk of a membrane with two stainless steel electrodes.   The cells were tightly sealed in an Ar-filled glove box and measurements were carried out in ambient atmosphere.   A signal of amplitude 5 mV was applied to the cell in the frequency range of 100 kHz to 1 Hz.   Conductivity was measured every 5 $^o$C from -30 to 30 $^o$C after equilibration for ca. 8 h at each temperature.
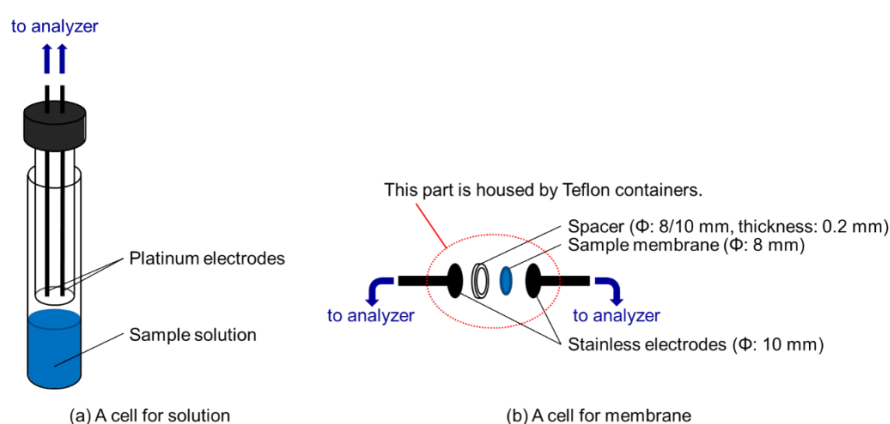


**Figure 3-7.**  Structures of impedance cells (a) with platinum electrodes for electrolyte solution and (b) with Teflon containers for membrane.

## Interfacial resistivity

The interfacial resistance between electrolyte and Li metal electrode was determined by impedance spectroscopy analysis, using a FRA 1260.   We used cells formed by symmetrical Li metal electrodes and three disks of electrolyte-soaked WhatmanTM GF/A separators between them, and applied a 5 mV amplitude signal to the cell in the frequency range of 150 kHz to 10 Hz. Impedance measurement was carried out every day for nearly two months, and spectrum was fitted according to an equivalent circuit using a ZSimp-Win 3.21 program.   All procedures were carried out in an Ar-filled glove box at room temperature.

## Electrochemical stability

The electrochemical stability window was determined by linear sweep and cyclic voltammetry, using a multichannel potentiostat/galvanostat/impedance analyzer (VersaSTAT MC, from Princeton Applied Research).   Cells were fabricated by sandwiching three disks of glass fiber

separators (WhatmanTM GF/A separator) with two electrodes (**Figure 3-8**).   Super P carbon-coated Al or Cu plate was used as the working electrode, and Li foil was used as the counter electrode.   The cells were tightly sealed in an Ar-filled glove box and measurements were carried out in ambient atmosphere.   Voltammetry was performed with a scan rate of 0.2 mV s$^{-1}$.
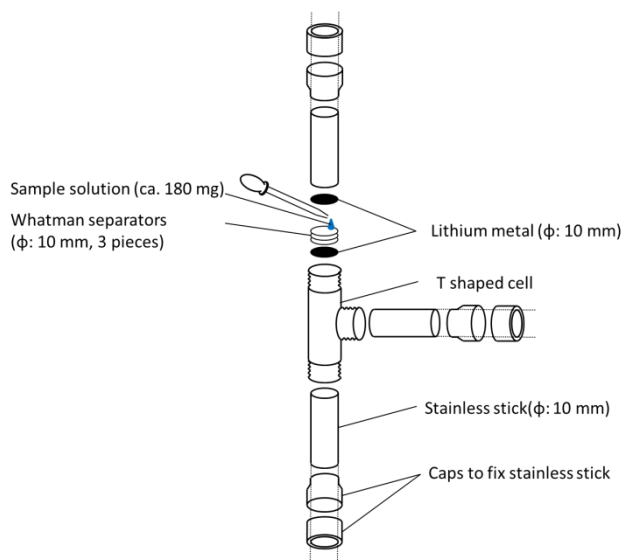


**Figure 3-8.** Structures of the cells for lithium interfacial stability measurement.

### Galvanostatic charge-discharge measurement

Galvanostatic charge-discharge behavior was tested using a battery test system (Series 4000, from Maccor) as the driving and controlling instrument.   Cells were fabricated by sandwiching two disks of electrolyte-soaked WhatmanTM GF/A separators with Li metal and Li$_4$Ti$_5$O$_{12}$ (LTO) or LiFePO$_4$ (LFP).   The cells were tightly sealed in an Ar-filled glove box and measurements were carried out in ambient atmosphere.   The cell was cycled galvanostatically at C/5 (1C current is equivalent to 0.473 mA cm$^{-2}$) using LTO, and at C/3 (1C is equivalent to 0.650 mA cm$^{-2}$) using LFP.

## 3-6.   Composites of partially fluorinated polymers and ionic liquids

### 3-6-1.   Optimization of ionic liquid-based electrolyte solution for lithium ion batteries

### Ionic conductivity

**Figure 3-9** shows the impedance response of six independent cells consisting two platinum electrodes immersed in the electrolyte solution.   Ionic conductivity of LP 30 was improved by the addition of [Pyr$_{14}$]PF$_6$.   The highest ionic conductivity was found for sol-**15**, and comparable

value to this was found for sol-**20** and sol-**25**.　Compared to these value, smaller ionic conductivity was observed with sol-**5** and sol-**30**.　The smaller conductivity of sol-**5** can be explained by lower concentration of ions which contribute to conduction.　Quite identical conductivity of sol-**30** to sol-**5** are attributed to enhancement of ion-ion interaction among condensed salt solution.　These data suggest optimization of the component ratio of the electrolyte solution is required.
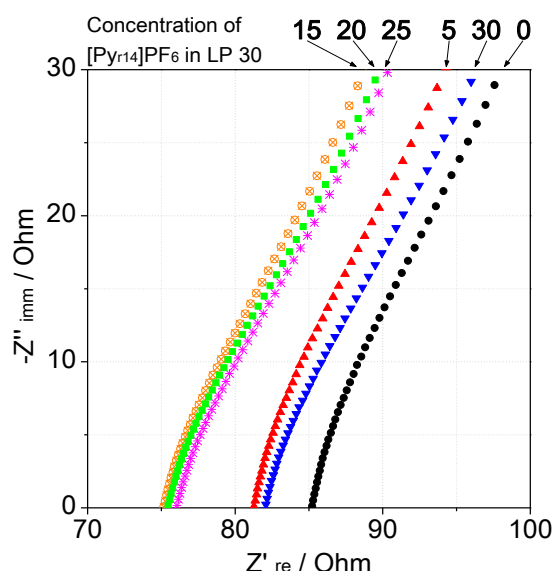


**Figure 3-9.** Impedance spectra of the electrolyte solutions at room temperature.

**Thermal properties**

To investigate the effect of adding ILs, we analyzed thermal properties and ionic conductivities over a wide range of temperatures.　**Figure 3-10** shows the DSC traces of [Pyr$_{14}$]PF$_6$, LP 30, and their hybrid electrolytes.　With [Pyr$_{14}$]PF$_6$, a main endothermic transition is observed at 86 $^o$C, corresponding to the expected melting behavior of the IL.　This phase transition, together with two minor features at around -80 and 46 $^o$C, is not observed after mixing IL with LP 30, confirming the existence of strong ionic and molecular interactions among components of the resulting solutions.　New peaks are observed below 0 $^o$C in the hybrid electrolytes, deriving from the thermal transitions that typically relate to LP 30 and are affected in our experiment by the IL component.　With LP 30 and its mixture with IL, two exothermic peaks are observed, corresponding to solid-solid transitions or cold crystallizations of LP 30 [6].　Also, a typical endothermic response appears around -23 $^o$C and is due to the main melting of LP 30.　This melting feature is followed by less-pronounced endothermic phenomenon around -5 $^o$C, which is often observed in such composite electrolytes [7], and can be ascribed to the heterogeneity of the system, including potential salt segregation/dissolution.　All these features are strongly smoothed by the addition of IL and the temperatures of both endothermic phenomena shift

55

downward.    To simplify the experiment selected mixtures sol-**5**, sol-**20**, and so-**30** proposed next investigation.
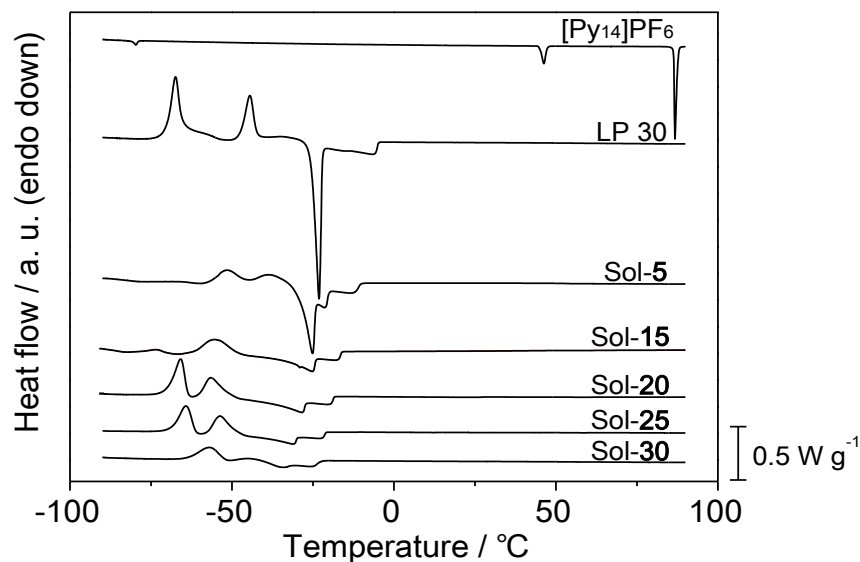


**Figure 3-10.**  DSC curves of [Pyr$_{14}$]PF$_6$, LP 30, and their mixture.


### Ionic conductivity as a function of temperature

**Figure 3-11** shows the Arrhenius plots of ionic conductivity versus temperature from -30 to 30 $^{\circ}$C. The ion conduction of LP 30 is known to be suppressed at temperatures below its crystallization point [6].    The ionic conductivity of crystalized sol-**5** and sol-**20** increases dramatically near the melting temperatures.    The ionic conductivity of sol-**30** exhibits only a smooth change, and the Arrhenius plots obey a Vogel-Fulcher-Tammann behavior.    This may be because [Pyr$_{14}$]PF$_6$ has a plastic crystal phase, as reported previously [8], and the adequate addition of [Pyr$_{14}$]PF$_6$ causes hybrid electrolytes to become amorphous at low temperature.    As a result, the desired ionic conductivity ( > 10$^{-3}$ S cm$^{-1}$) prevails even at -27 $^{\circ}$C with sol-**30**, and its ionic conductivity is 16 times greater than that of sol-**5**, containing 5 wt% IL.    We confirm that the addition of [Pyr$_{14}$]PF$_6$ suppresses the crystallization of LP 30, and allows ion conduction sufficient enough for applications over a wide temperature range.
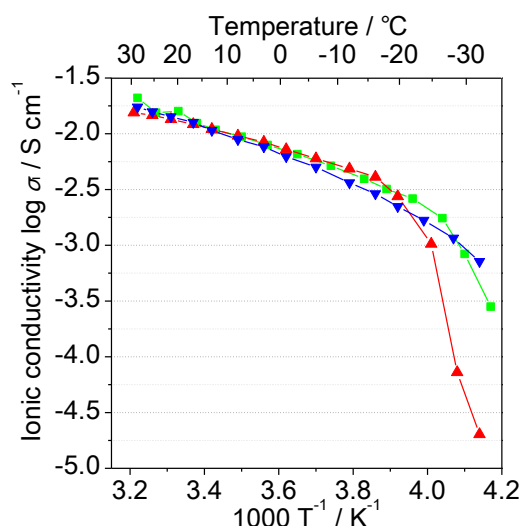
**Figure 3-11.** Arrhenius plots of ionic conductivity versus temperature
for sol-**5** (▲), sol-**20** (■), and sol-**30** (▼).

### Electrochemical stability

With a view to applying LP 30-[Pyr$_{14}$]PF$_6$ hybrid electrolytes in lithium batteries, electrochemical stability was analyzed in terms of the electrochemical potential window and interfacial resistance with Li metal; an effective component ratio of the electrolytes was determined from among those investigated.    **Figure 3-12** shows the electrochemical stability window for the electrolytes.    The linear anodic scan in **Figure 3-12 (A)** shows that the onset of small currents occurs at around 4 V, after which they settle down and remain less than 0.1 mA cm$^{-2}$ up to 4.6 V for the electrolytes containing ILs.    Anodic stability is slightly affected by the presence of the IL.    By taking into account the identical structure of the LP 30 and IL anions, the differences observed among the various solutions toward oxidation can be related to differing mobility of the electrolyte components.    **Figure 3-12 (B)** shows the cyclic voltammetry of the electrolyte solution, and all cathodic scans show three clear stages.    The first current drift appears below 1.5 V, followed by a clear peak around 0.5 V and another current response at ca. 0 V.    The peak at around 0.5 V shifts to the lower potential side upon adding IL, and disappears in the second cathodic scans (see **Figure 3-12**, C).    It relates to an irreversible initial decomposition of the electrolyte components, which lead to the formation of a protective passivation layer on the electrode surface.    Current responses below 1.5 V and at ca. 0 V are almost reproducible after the second cycle, and are related to typical lithium insertion into carbon; this is confirmed by the presence of the corresponding oxidation features in the reverse scan.    The electrochemical stability window is expanded, by the addition of the IL, as a result of specific ionic and/or dipole interactions.
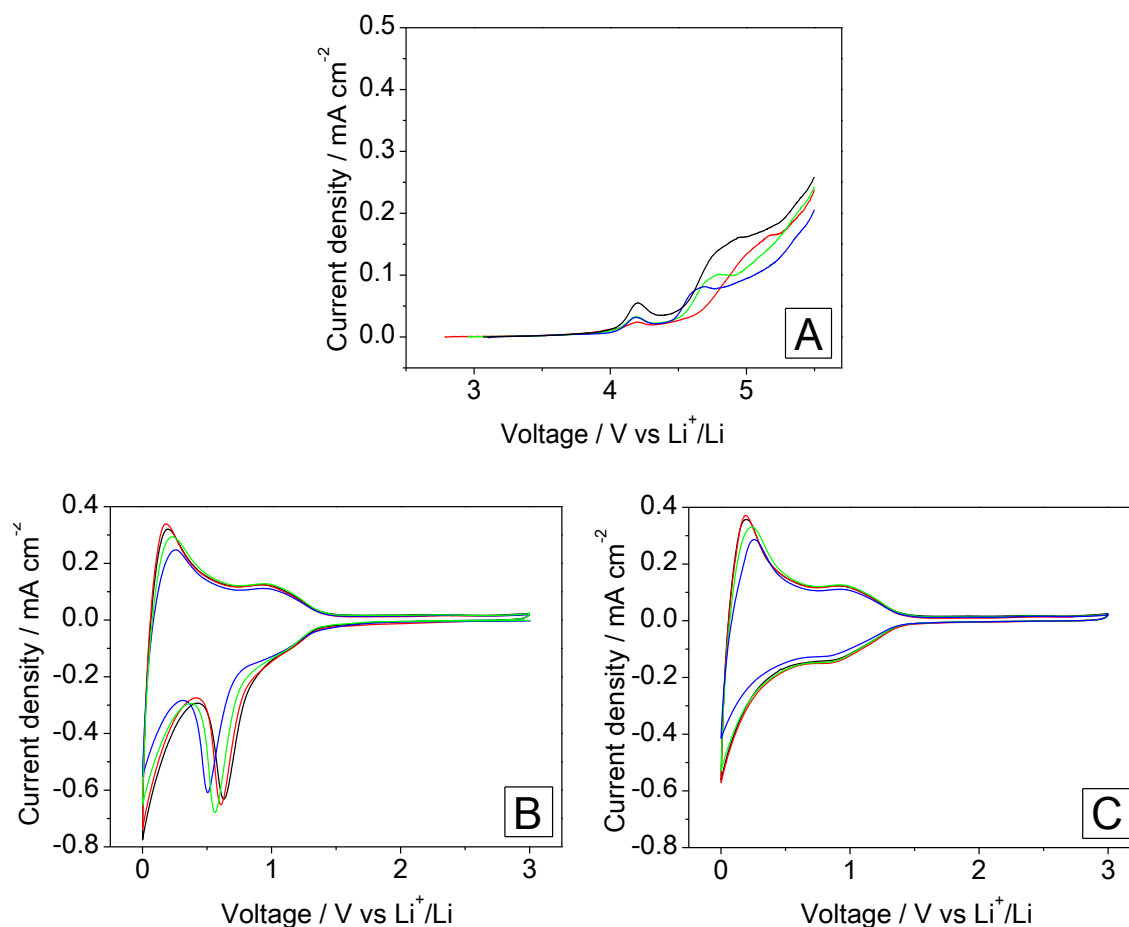
**Figure 3-12.** Electrochemical stability window of the LP-30 (black), sol-**5** (red), sol-**20** (green), and sol-**30** (blue).　(A) Anodic scan with Super P carbon-coated Al working electrode, (B) 1st cycle, and (C) 2nd cycle of cathodic scan with Super P carbon-coated Cu working electrode.

**Surface resistivity**

To analyze the interfacial resistance, cells formed by sandwiching each of the four electrolytes investigated here with two Li metal electrodes were prepared, and their impedance was measured (**Figure 3-13**).

　　　**Figure 3-14** shows the interfacial resistance change over a 2 month period.　The each point is derived by evaluation of the amplitude of a semicircle from the impedance spectrum in the Nyquist plot with increasing times of storage.　Throughout the experiments, measurements were carried out at room temperature.　Accordingly, the changes in the same manner should be attributed to the different daily temperature.　In the first period, the interfacial resistances increase as a result of the formation of a solid electrolyte interface (SEI) film.　In the mid-term, around 15 days, the interfacial resistances are found to decrease slightly.　This may be due to the change in the morphology of SEI.　For LP 30, sol-**5**, and sol-**20**, interfacial resistance begins
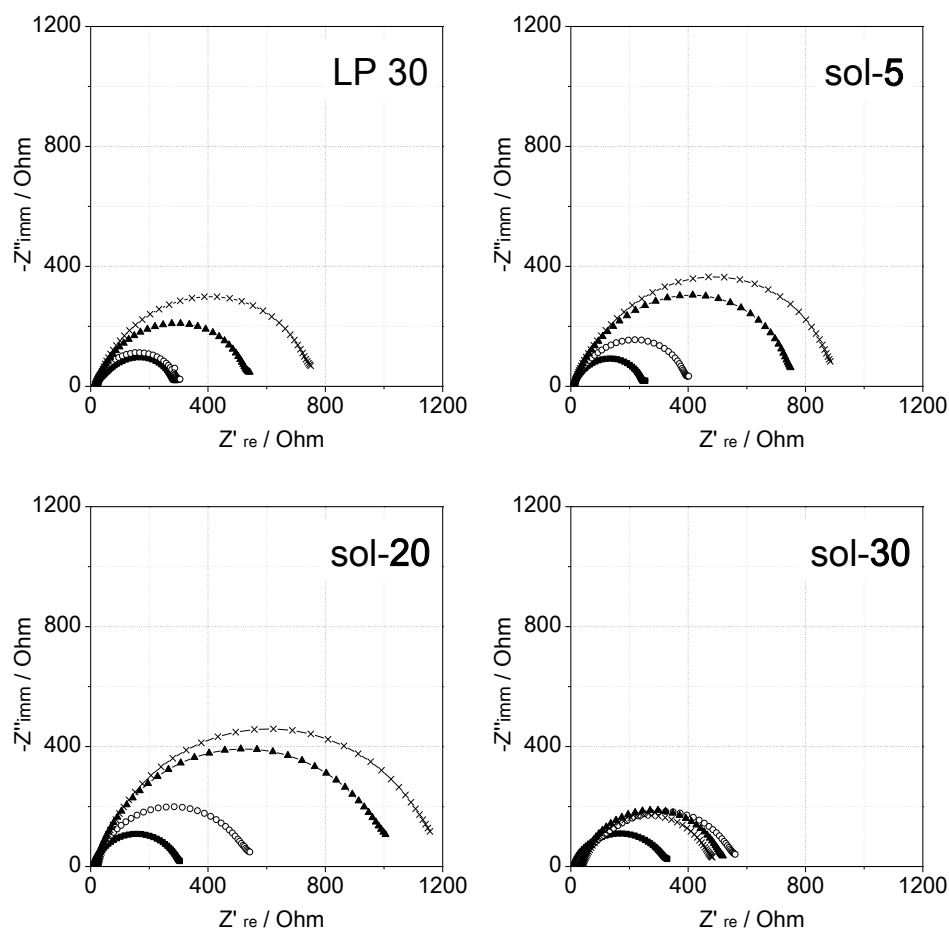
**Figure 3-13.** Nyquist plots of impedance spectra of the cell formed by symmetrical Li metal electrodes and electrolyte-soaked separators (■: 1st, ○: 16th, ▲: 31st, and ×:46th days).

to increase again and reaches a virtually constant value after 30 days.    Sol-**30** exhibits a stable and well controlled interfacial behavior with constant resistances from 15 days onward.    It is well known that the formation of SEI is affected by the environment of the electrolytes, involving such factors as the salt concentration, electrolyte composition, and salt solvation [9].    For the case of sol-**30**, a larger number of [Pyr$_{14}$]PF$_6$ species exists in LP 30 electrolyte than for the other solutions investigated, probably resulting in qualitatively different and more effective solvation of carbonate compounds to ions.    Addition of an adequate amount of [Pyr$_{14}$]PF$_6$ improves the properties of the composite electrolyte, leading to enhanced low-temperature conductivity and electrochemical stability.    Based on these results, sol-**30** is the most suitable composition of those investigated.

59
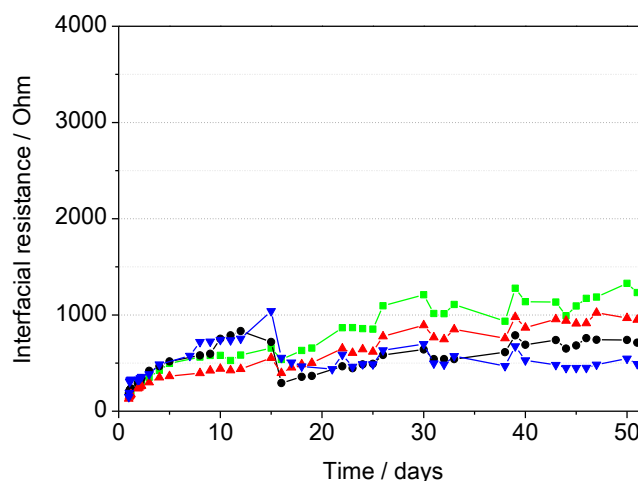
**Figure 3-14.** Resistances at the interface electrolyte/Li metal.
(●: LP-30, ▲: sol-**5**, ■: sol-**20**, and ▼: sol-**30**)

**Charge-discharge measurement**

**Figure 3-15** shows the charge-discharge profiles during the cycle for the cell comprising sol-**30** sandwiched with Li metal and LTO or LFP, respectively.  A fairly high coulombic efficiency is observed in both cells.  For the cell with LTO (**Figure 3-15**, A), the specific capacity reaches 168 mAh g$^{-1}$ at C/5, which is 96% of the theoretical value.  Although there is a slight decrease in capacity with increasing cycle number, the reversible capacity retains over 92% of the theoretical value.  The cell with LFP gives flat voltage profiles (**Figure 3-15**, B) and high specific capacity of at least 164 mAh g$^{-1}$ at C/3, which is 96% of the theoretical value, from 1 to 10 cycles.  These data all show that sol-**30** (i.e., LP 30 with 30 wt% [Pyr$_{14}$]PF$_6$) is confirmed to be effective as electrolyte solution for lithium batteries.
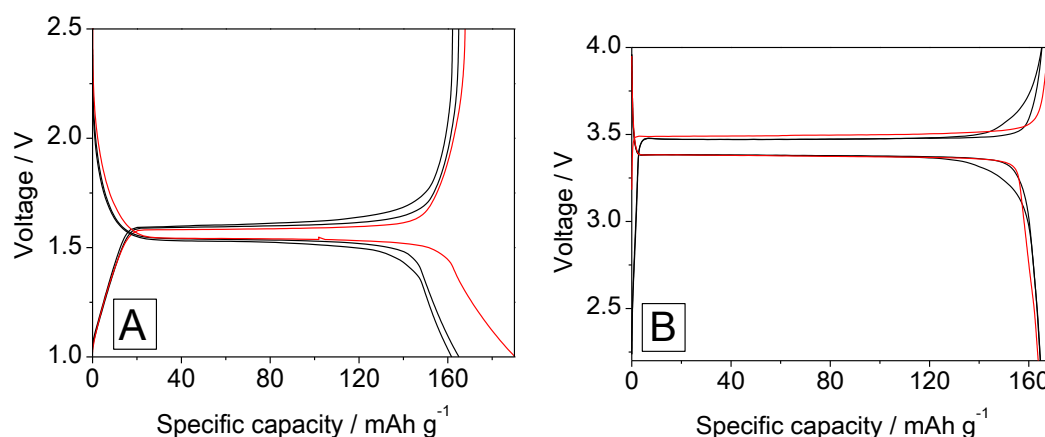


**Figure 3-15.** Charge-discharge behaviors of (A) Li / Sol-**30** / LTO and (B) Li / Sol **30** / LFP at C/5 and C/3 rate, respectively (1st cycle in red, 5th and 10th cycles in black).

60

### 3-6-2.   Preparation of fluorinated polymer films containing the electrolytes

We found that sol-**30** is an excellent electrolyte solution suitable for deployment the preparation of polymer electrolytes.   We successfully prepared PVdF-HFP based membranes.   In this work, acetonitrile, which is typically used as a solution for polymer electrolyte mixture, is replaced with the volatile DMC (a component of LP 30), which is expected to act as both a dispersing and plasticizing agent.   This allows us to manage the removal of the solvent during the preparation of the membrane (see experimental section).   The polymer electrolyte membranes are prepared by a solution casting procedure.   **Figure 3-16** (right) shows a picture of the membrane prepared in this work.   The resulting polymer electrolytes are immersed in sol-**30** so as store the membrane without risk of segregation or lithium salt decomposition.

TG analysis, shown in **Figure 3-16** (left), provides information on composition and on thermal properties of the polymer electrolyte after immersing to sol-**30**.   Weight loss up to 150 $^o$C is due to the removal of the carbonate-based electrolyte components; the weight loss above 300ºC is due to the decomposition of [Pyr$_{14}$]PF$_6$, and the third sequence of weight loss is related to the decomposition of the PVdF-HFP matrix.   The leftover weight at the end of the temperature scan can be assigned to carbonaceous residuals.   **Figure 3-16** shows that about 30 wt% of IL remained in the membrane, suggesting flame retardation.   According to previous work, the concentration of IL we used in sol-**30** is high enough to control or strongly reduce the flammability of the resulting electrolyte [10].
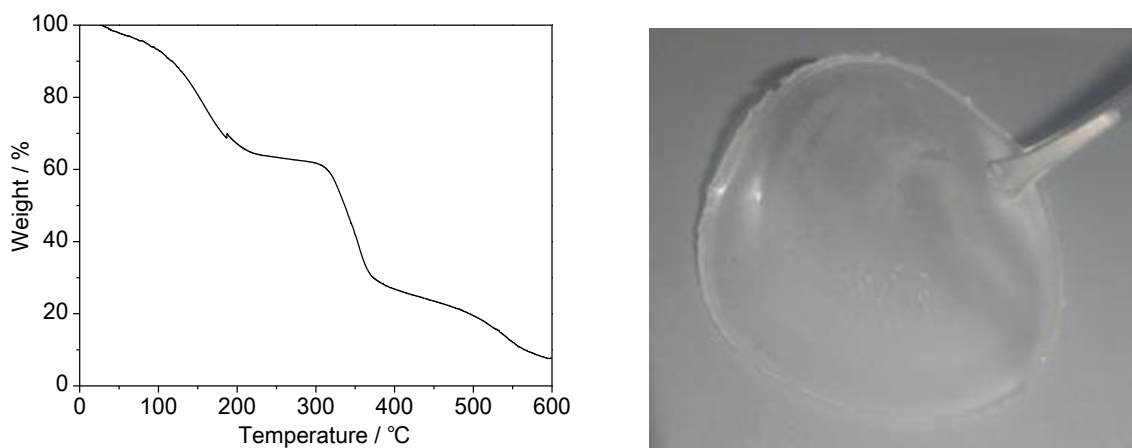


**Figure 3-16.** TGA response of the polymer electrolyte membrane prepared in this work and photo of the membrane.

### 3-6-3.   Electrochemical properties of the polymer electrolyte

### Electrochemical stability

Then, electrochemical properties of the polymer electrolyte was analyzed in terms of the electrochemical stability against oxidation and changes of ionic conductivity with duration of time. **Figure 3-17** shows the electrochemical stability window for the polymer electrolyte containing sol-**30**, and pure sol-**30** and LP 30 as reference.   The linear anodic scan for all samples show that the onset of small currents occurs at around 4 V.   For the polymer electrolyte, current density was smaller compared to sol-**30** and LP 30 in a range of the anodic scan.   The current density of 0.1 mA cm$^{-2}$ was found around 5.4 V.   Anodic stability was affected by the presence of the polymer. As a results, anodic stability window was expanded, by the addition of the polymer.
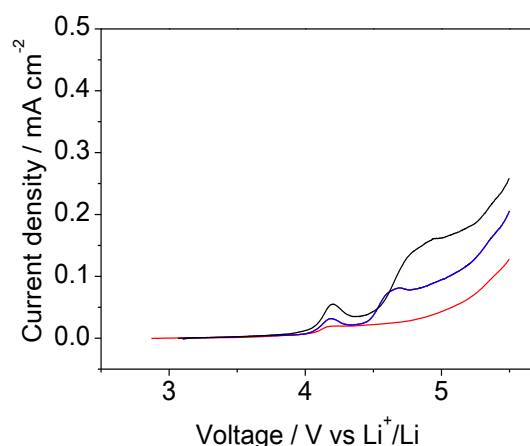


**Figure 3-17.**  Linear voltammogram trace of anodic scan of the polymer electrolyte (red), sol-**30** (blue), and LP 30 (black).

### Ionic conductivity

Ionic conductivity with duration of time up to 120 min was investigated (**Figure 3-18**).   The polymer electrolytes prepared here showed conductivity of $3.5 \times 10^{-4}$ S cm$^{-1}$ at room temperature, suggesting suitability for polymer electrolytes.   There was negligible change of ionic conductivity up to 120 min.   For pure LP 30, the organic components tend to evaporate easily, and ionic conductivity gradually decrease with the time of storage.   In this case, decrease of ionic conductivity was suppressed by adding ILs and polymers.   By combining PVdF-HFP with electrolyte solution having moderate affinity with the matrix, electrolyte retained in polymer matrices regardless of the storage.   Consequently, stable polymer electrolytes containing ILs was prepared.
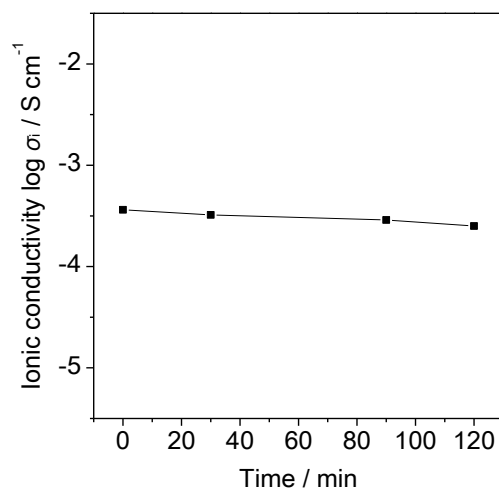
**Figure 3-18.** Change of ionic conductivity with duration of time.

## 3-7.  Summary

In this section, solubility of fluorinated polymers to ILs was analyzed.   Throughout solubility measurement, many fluorinated polymers were hard to dissolve.   Solubility was observed with PECTFE, Cytop, and PVdF.   For former two, solubility was undetectable with naked eyes because only small portion of added polymers were dissolved to ILs.   Thus, solubility of PECTFE in $[P_{666,14}][Tf_2N]$ and Cytop in $[C_2mim][Tf_2N]$ were confirmed by $^{19}F$ NMR.   Solubility of PVdF into ILs was investigated visually and difference of solubility depending on ion structures was found. These solubility was discussed by using Kamlet-Taft parameter of ILs.   ILs having high $\alpha$ value (hydrogen bond acidity) and low $\beta$ value (hydrogen bond basicity) was found to be compatible with PVdF.   This suggests that there is contribution of polar interaction to dissolve PVdF into ILs.

Then we prepared polymer electrolyte based on PVdF.   As we discussed, fluorinated polymers were hard to interact with molecules and difficult to make their composites.   PVdF-based polymers have been proposed to prepare polymer electrolytes expecting moderate affinity with ILs.   As additive electrolyte and ILs, LP 30 and $[Pyr_{14}]PF_6$ were chosen due to their excellent electrochemical properties.   Prior to design of polymer electrolytes, component ratio of LP 30 and $[Pyr_{14}]PF_6$ was optimized.   Considering enhanced ionic conductivity followed by suppressed crystallization of the mixture, stability toward to lithium electrodes, wide electrochemical stability window, LP 30 containing 30 wt% of $[Pyr_{14}]PF_6$ (sol-**30**) was proposed to prepare polymer electrolytes.   By using a solution casting procedure, PVdF-HFP film containing sol-**30** was prepared.   This polymer electrolytes was found to possess high electrochemical stability and stable ionic conductivity against a duration of storage.   Consequently, stable polymer electrolytes containing ILs was prepared by combining PVdF-HFP with electrolyte solution having moderate affinity with the matrix.

63

## 3-8. References

[1]     C. Xing, M. Zhao, L. Zhao, J. You, X. Cao, Y. Li, *Polymer Chemistry* **2013**, *4*, 5726-5734.

[2]     M. Mezger, B. M. Ocko, H. Reichert, M. Deutsch, *Proceedings of the National Academy of Sciences of the United States of America* **2013**, *110*, 3733-3737.

[3]     S. Lee, J. S. Park, T. R. Lee, *Langmuir : the ACS journal of surfaces and colloids* **2008**, *24*, 4817-4826.

[4]     (a) M. Dahbi, F. Ghamouss, F. Tran-Van, D. Lemordant, M. Anouti, *Journal of Power Sources* **2011**, *196*, 9743-9750; (b) M. Morita, T. Shibata, N. Yoshimoto, M. Ishikawa, *Electrochimica Acta* **2002**, *47*, 2787-2793.

[5]     A. Ponrouch, E. Marchante, M. Courty, J.-M. Tarascon, M. R. Palacín, *Energy & Environmental Science* **2012**, *5*, 8572-8583.

[6]     P. E. Stallworth, J. J. Fontanella, M. C. Wintersgill, C. D. Scheidler, J. J. Immel, S. G. Greenbaum, A. S. Gozdz, *Journal of Power Sources* **1999**, *81*, 739-747.

[7]     A. Ponrouch, E. Marchante, M. Courty, J.-M. Tarascon, M. R. Palacín, *Energy & Environmental Science* **2012**, *5*, 8572-8583.

[8]     J. Golding, N. Hamid, D. R. MacFarlane, M. Forsyth, C. Forsyth, C. Collins, J. Huang, *Chemistry of Materials* **2001**, *13*, 558-564.

[9]     (a) D. Fauteux, *Journal of The Electrochemical Society* **1988**, *135*, 2231-2237; (b) S. K. Jeong, M. Inaba, Y. Iriyama, T. Abe, Z. Ogumi, *Electrochimica Acta* **2002**, *47*, 1975-1982; (c) R. Naejus, R. Coudert, P. Willmann, D. Lemordant, *Electrochimica Acta* **1998**, *43*, 275-284.

[10]    (a) A. Guerfi, M. Dontigny, P. Charest, M. Petitclerc, M. Lagacé, A. Vijh, K. Zaghib, *Journal of Power Sources* **2010**, *195*, 845-852; (b) C. Arbizzani, G. Gabrielli, M. Mastragostino, *Journal of Power Sources* **2011**, *196*, 4801-4805.

# Chapter 4
# Design of fluorophilic ionic liquids

## 4-1.  Introduction

In order to prepare composites based on fluorinated polymers and ILs, these components should have considerable affinity to suppress phase separation.   To analyze the affinity between fluorinated polymers and ILs, solubility of fluorinated polymers to ILs was analyzed in Chapter 3. For the case of poly(vinylidenefluoride) (PVdF), solubility changed depending on polarity of ILs. On the other hand, other fluorinated polymers showed poor affinity with ILs, and solubility was not detectable visually.    In order to obtain stable composites, affinity between ILs and fluorinated polymers is needed to be improved.    To apply ILs to fluorinated polymers as additives, design of fluorophilic ILs is important.    In this section fluoroalkanes were used as model compounds of fluorinated polymers, and their solubility into ILs were analyzed to determine fluorophilicity of ILs.    Based on these results, ILs which are expected to show good affinity with fluorinated polymers have been proposed.

## 4-2.  Experimental procedure

### 4-2-1.  Materials

Structure, abbreviation, and preparation for all ILs are summarized in the Appendix (P. 88).    All ILs were dried under vacuum at 60 $^{\circ}$C for at least 3 h.    A series of fluoroalkanes such as eicosafluorononane (20N), tetradecafluorohexane (14H), 1H-tridecafluorohexane (13H), and 1,6-dihydroxy-2,2,3,3,4,4,5,5-octafluorohexane (8H) was purchased from Tokyo Chemical Industry Co., Ltd.    1H,6H-Perfluorohexane (12H) was purchased from Fluorochem Ltd.    Abbreviations represent the number of fluorine atom and an initial letter of alkanes.

$$R_1{-}C_4F_8{-}R_2$$

**20N :** $C_9F_{20}$   **13H :** $R_1$=$CF_3$, $C_2$=$CHF_2$
**14H :** $C_6F_{14}$   **12H :** $R_1$=$R_2$=$CHF_2$
  **8H   :** $R_1$=$R_2$=$CH_2OH$

(a) Fully-fluorinated       (b) Partially-fluorinated
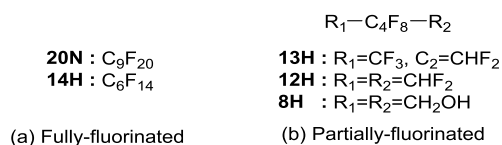
**Figure 4-1.** Structure of fully- and partially- fluorinated fluoroalkanes.

### 4-2-2.  Evaluation of phase behavior of ionic liquids and fluoroalkanes

Fluoroalkanes and ILs were mixed 150:150 (μl/μl) under semi-dry condition (RH < 20 %) and shaken until they form turbid monophase using a vortex mixer.    These mixtures were kept 1 day to 1 week until they separate into fluoroalkane- and IL-rich transparent phase.    Solubility of

fluoroalkanes in ILs were quantified with thermogravimetric analysis (TGA).   The samples were heated by 10 °C min$^{-1}$ upon 10 °C higher than boiling temperatures ($T_b$) of fluoroalkanes: 125 °C for 20N, 80 °C for 14H, 91 °C for 13H, and 105 °C for 12H, and hold for 1 h.   The weight after heating was compared to original value, and the weight loss was used for calculation of mole fraction fluoroalkanes in ILs.   Water content of each samples were confirmed to be less than 0.1 % by using Karl-Fischer titration (MKC-510N, from Metrohm AG).

## 4-3.   Solubility of fluoroalkanes in ionic liquids

### 4-3-1.   Impact of ion structure of ionic liquids on dissolution of fluoroalkanes

In this study, 20N and 14H were used as model components of fluorinated polymers, and dissolution of these compounds to ILs was compared to that of 13H and 12H (solubility of 8H is not discussed here).   All data are shown in Appendix.   First, we focused on the concentration of fluoroalkanes dissolved in [Tf$_2$N] salts with various cation.   **Table 4-1** summarizes mole fraction of 14H and 12H dissolved in a series of [Tf$_2$N] salts.   Slightly larger amount of 14H was dissolved in phosphonium-based IL compared to imidazolium-based ones.   When we focus on cation structure of the [Tf$_2$N] salts, we see that concentration of 14H in ILs having double bond in cation structure is less than 7.8 while that in ILs having only saturated bond in cation structure is larger than 7.8.   Theoretically, $\pi$-electron is known to reduce fluorophilicity [1].   Lowering fluorophilicity is considered to affect lowering solubility of 14H into [Tf$_2$N] salts.   The solubility of 12H to the [Tf$_2$N] salts were also analyzed.   Some [Tf$_2$N] salts combined with [C$_4$py], [C$_2$mim], [AAim], [Pip$_{14}$], [Pyr$_{14}$], and [N$_{4441}$] dissolved 12H at room temperature.   On the other hand, low solubility of 12H was found for [C$_2$OHmim][Tf$_2$N] and [P$_{666,14}$][Tf$_2$N].   For the case of

**Table 4-1.** Concentration of 14H and 12H dissolved in a series of [Tf$_2$N] salts.

| ILs | Mole fraction / mmol mol$^{-1}$ | |
|---|---|---|
| | 14H | 12H |
| [C$_2$OHmim] | 5.2 | 176.5 |
| [C$_4$py] | 5.3 | soluble |
| [C$_2$mim] | 6.0 | soluble |
| [AAim] | 7.7 | soluble |
| [C$_4$mmim] | 7.8 | - |
| [Pip$_{14}$] | 7.8 | soluble |
| [Pyr$_{14}$] | 10.8 | soluble |
| [N$_{4441}$] | 12.2 | soluble |
| [P$_{666,14}$] | 24.92 | 520.7 |

[P$_{666,14}$][Tf$_2$N]/12H mixture, concentration of 12H was found to be 520.7 mmol mol$^{-1}$.　This means that this mixture separate to [P$_{666,14}$][Tf$_2$N]-phase saturated with 12H and 12H- phase. This suggests that [P$_{666,14}$][Tf$_2$N] has a potential to dissolve 12H, and the phase separation was caused by small ion density of the ILs.

　　　Then we analyzed the effect of anion structure to dissolve fluoroalkanes to ILs. Solubility of fluoroalkanes was improved with decrease of length of fluoroalkanes and insertion
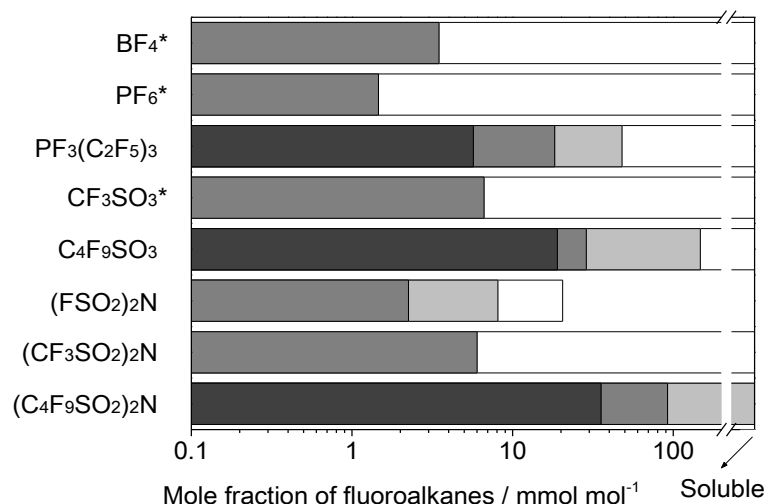


(a) [C$_2$mim] salts
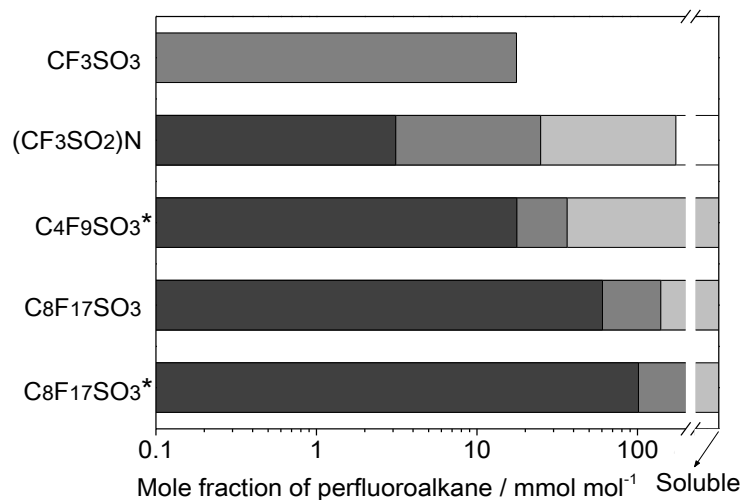


(b) [P$_{666,14}$] salts

**Figure 4-2.** Solubility of 20N (black bar), 14H (dark gray bar), 13H (gray bar), and 12H (white bar) into (a) a series of [C$_2$mim] salts and (b) [P$_{666,14}$] salts.　Asterisk in figure means that the anion was combined with cation having different alkyl length.　Anion structures are shown in this figure, and abbreviation of these anion is (FSO$_2$)$_2$N ([FSI]), (CF$_3$SO$_2$)$_2$N ([Tf$_2$N]), (C$_4$F$_9$SO$_2$)$_2$N ([Nf$_2$N]), and PF$_3$(C$_2$F$_5$)$_3$ ([FAP]).

of hydrogen atoms to terminals of fluoroalkanes.    For the case of imidazolium salts, mole fraction of 14H increased in order of $PF_6 \sim$ [FSI] < $BF_4$ < [$Tf_2N$] ~ $CF_3SO_3$ < [FAP] < $C_4F_9SO_3$ < [$Nf_2N$] (**Figure 4-2**, a).    There were considerable changes of solubility of 14H depending on the anion structure in contrast that cation structure had small effect on the solubility.    When we focus on anion structures, we see that spherical anion is not favorable to dissolve fluoroalkanes.    The mixture of [$C_2$mim][FAP]/14H showed mole fraction of 18.3 mmol mol$^{-1}$.    This value is not high even if fluorine content of [FAP] anion is quite high.    For the case of imide anion and sulfonate anion, mole fraction increased depending on length of fluoroalkyl chain in the anion structure.    Higher mole fraction for [$C_2$mim][$Nf_2N$] compared to [$C_2$mim]$C_4F_9SO_3$ suggests number of fluoroalkyl chain in anion structures also affect to the dissolution of fluoroalkanes.    Same trend was also observed for 20N and 13H.    For the case of 12H, this fluoroalkane dissolved to almost all ILs.

The mole fraction of fluoroalkanes in phosphonium salts were also evaluated (**Figure 4-2**, b).    The mole fraction of 14H increased as a function of length of fluoroalkyl chain.    The mole fraction increased when [$P_{666,14}$] cation was replaced with [$P_{4446}$] cation, and highest mole fraction of 208.6 mmol mol$^{-1}$ was found for [$P_{4446}$]$C_8F_{17}SO_3$.    This is considered to be realized from that fluoroalkyl chain in the anion structure was longer than normal alkyl chain in the phosphonium cation.    With respect to structural difference of $C_8F_{17}SO_3$ anion and small [$C_2$mim] cation, the IL consisting these ions was prepared; however, the IL was obtained as solid at room temperature and solubility of 14H to the ILs was not determined.    For the case of 13H, this fluoroalkanes dissolved to the phosphonium salts having [$Nf_2N$], $C_4F_9SO_3$, and $C_8F_{17}SO_3$.    Presence of hydrogen atoms in 13H are considered to improve solubility of 13H to the phosphonium salts.    Throughout this study, ILs with longer fluoroalkyl chain in anion structures were found to be important to improve fluorophilicity of ILs.

### 4-3-2.    Factors to affect the solubility of fluoroalkanes in ionic liquids

Here we discuss the correlation between properties of ILs and their solubility of fluoroalkanes. In former section, we found that ILs with longer fluoroalkyl chain in anion is favorable to dissolve fluoroalkanes.    Then we calculated fluorine content of the ILs by using Chem Draw, and analyzed their effect on the solubility of fluoroalkanes.    Also, with respect to that interaction between ILs and some organic compound can be discussed based on Kamlet-Taft parameters ($\alpha$: hydrogen bond acidity, $\beta$: hydrogen bond basicity, and $\pi^*$: polarity/polarizability) [2], the effect of these parameters are also discussed.    These parameters are useful to understand interaction derived from polarity, thus we used 8H which having two hydroxyl groups on terminal structures in addition to 20N, 14H, 13H, and 12H.    Kamlet-Taft parameters were evaluated by using the same method mentioned in Section 2-2-3.    **Figure 4-3** summarizes the mole fraction of 20N, 14H, and 13H in ILs as a function of fluorine content of the ILs.    Similar trend was observed for solubility of 20N and 14H, and phosphonium salts having higher fluorine content was confirmed to be

favorable to dissolve 20N and 14H (see square point).   However, strong correlation was not observed for imidazolium or ammonium salts (see circle and triangular points).   Dissolution of fluoroalkanes to ILs may be suppressed by the polar property of these cations.   For the case of 13H, strong deviation was observed with phosphonium salts in contrast to the results of 20N and 14H, and correlation between fluorine content and solubility was found for the system with imidazolium salts.   One point which deviate from the correlation is data for [C₂mim][FAP].   For this case, small surface free energy of [FAP] anion are considered to suppress the dissolution of 13H.
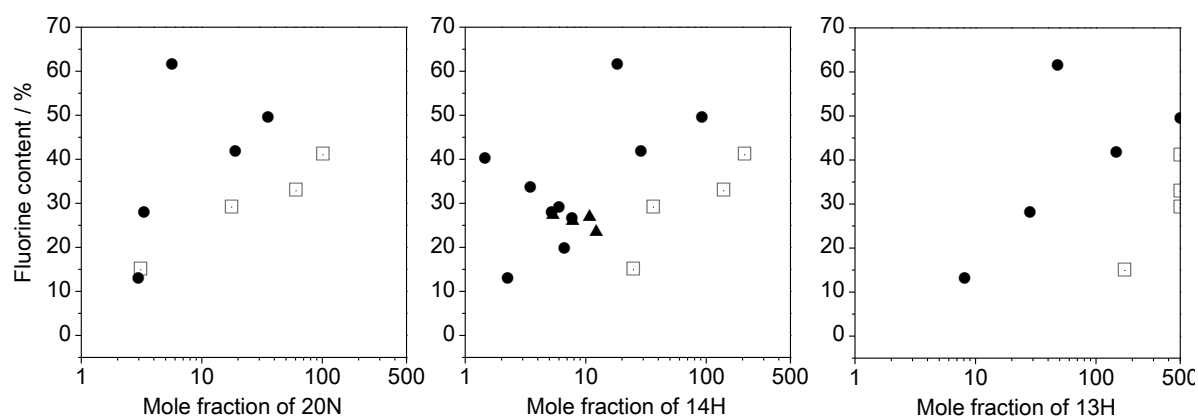


**Figure 4-3.** Mole fraction of 20N, 14H, and 13H dissolved in ILs as a function of fluorine content of the phosphonium salts (□), imidazolium salts (●), and ammonium salts including pyrrolidinium, piperidinium, pyrinidnium salts (▲).

Since 13H has a proton in a terminal structure, this may contribute to hydrogen bond. Then, we checked the effect of Kamlet-Taft parameter of ILs on the solubility of 20N, 14H, 13H, 12H, and 8H.   Not unexpectedly, no correlation between Kamlet-Taft parameter and the solubility of perfluoroalkanes such as 20N and 14H was found.   For the case of 13H, we expected that there should be a correlation between $\beta$ value of Kamlet-Taft parameter and the solubility.   As shown in **Figure 4-4** (far left), ILs having high $\beta$ value seem to have high affinity with 13H; however, strong correlation between $\beta$ value and solubility of 13H was not found.   When another terminal fluorine are replaced to hydrogen; *i.e.* 12H, the solubility of fluoroalkanes was improved.   For this case, only two ILs such as [C₂OHmim][Tf₂N] ($\alpha$: 1.14, $\beta$: 0.28) and [C₂mim][FSI] ($\alpha$: 0.65, $\beta$: 0.21) showed poor solubility of 12H.   The strong correlation between hydrogen bond ability and the solubility was not observed.   Solubility of the fluoroalkanes such as 13H and 12H was not strongly affected by fluorine content neither hydrogen bond ability of ILs.   On the other hand, solubility of 8H, having two hydroxyl groups in terminal structures in the fluoroalkane, strongly correlated with Kamlet-Taft parameters of the ILs.   The effect of fluorine content of ILs was not

observed for 8H dissolution.　　This suggests that effect of hydrogen bond ability of 8H pronounced stronger than the effect of fluorine content of ILs.　　Consequently, we concluded that discussion based on fluorine content of ILs are applicable for the solubility of perfluoroalkanes, and discussion based on Kamlet-Taft parameters are applicable for the solubility of fluoroalkanes containing hydroxyl groups.



|        |        |        |
|--------|--------|--------|
| 13H    | 12H    | 8H     |
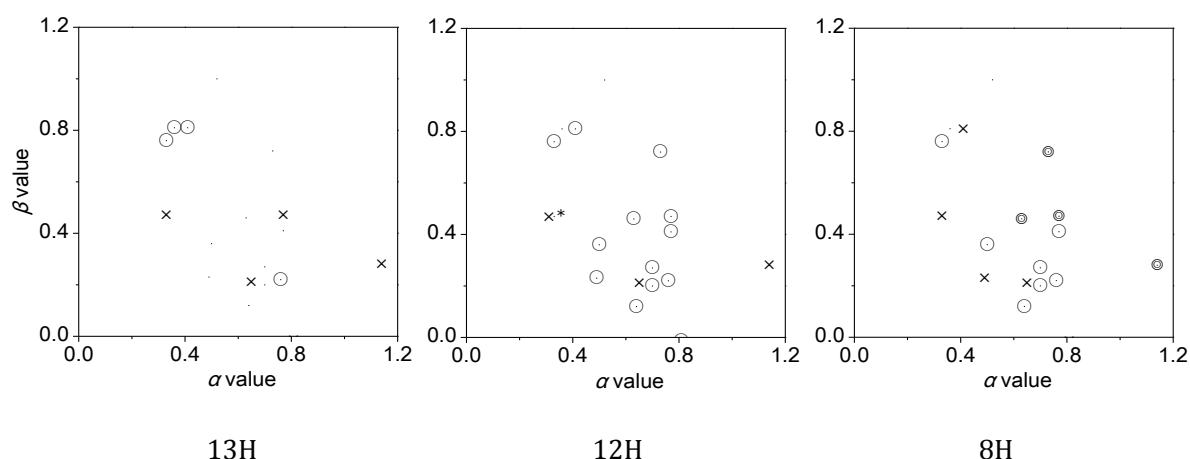
**Figure 4-4.** Effect of Kamlet-Taft parameter ($\alpha$: hydrogen bond acidity, $\beta$: hydrogen bond basicity) on the solubility of 13H, 12H, and 8H.　　○: soluble, ×: insoluble, and ×*: mole fraction was 520.7 mmol mol$^{-1}$ for 13H and 12H, and　◎: soluble at 70 $^{o}$C, ○: soluble at 70 $^{o}$C and crystalize after cooling and ×: insoluble at 70 $^{o}$C for 8H

## 4-4.　　Design of ionic liquids containing long fluoroalkyl chain

Considering that 20N as model of PTFE showed high affinity with phosphonium salts having fluorous anion, here we propose insertion of fluoroalkyl chain onto cation structure.　　As nucleophile, amine was used instead of phosphine due to their stability.　　As electrophile, a series of fluorinated iodoalkane was applied for synthesis of ILs; *i.e.* I(CH$_2$)$_n$(CF$_2$)$_m$CF$_3$ ($n$ = 0, 2, or 3, $m$ = 3 or 7).　　To optimize a reaction, length of hydrocarbon spacer between reaction center and fluorine tail ($n$) was screened.

　　　　A series of reactions were carried out between triethylamine and fluorinated iodoalkane without solvents but with excess triethylamine.　　First, the perfluoroiodoalkanes, such as I(CF$_2$)$_3$CF$_3$ and I(CF$_2$)$_7$CF$_3$, were used.　　To these electrophile, two times of triethylamine was added and stirred at 120 $^{o}$C in reflux filled with Ar.　　Not unexpectedly the mixture did not form any quaternary salts.　　Presence of fluorine atom next to electrophile moiety are considered to suppress the eliminative property of iodide.　　To control this, fluorinated iodoalkane having ethylene spacer, *i.e.* I(CH$_2$)$_2$(CF$_2$)$_3$CF$_3$, was used instead of perfluoroiodoalkane.　　This mixture

resulted in yellow solid.    Then this solid was recrystallized from ethyl acetate/acetonitrile.    The ^{1}H NMR spectra of the crystal showed signals for the ethyl groups of amine (1.17 and 3.10 ppm) shifted from those of the starting amine (0.93 and 2.43 ppm) suggesting that quaternary salts was obtained; however, no signals were observed for the ethylene spacer of the fluorinated iodoalkane but broad peak was observed around 8.8 ppm.    The ^{19}F NMR spectra of the mixture of crystal/LiTf$_2$N 1:1(v/v) which washed with water is shown in **Figure 4-5**.    Compared to the signal of CF$_3$ groups of [Tf$_2$N] anion at -81.86 ppm, very small signals of inserted fluorinated tail were found at -83.96, -116.89, -126.7, and -129.0 ppm.    This suggests protonation of triethylamine was occurred instead of the expected quaternization.    This reaction is explained as Menshutkin reaction according to previous reference [3].
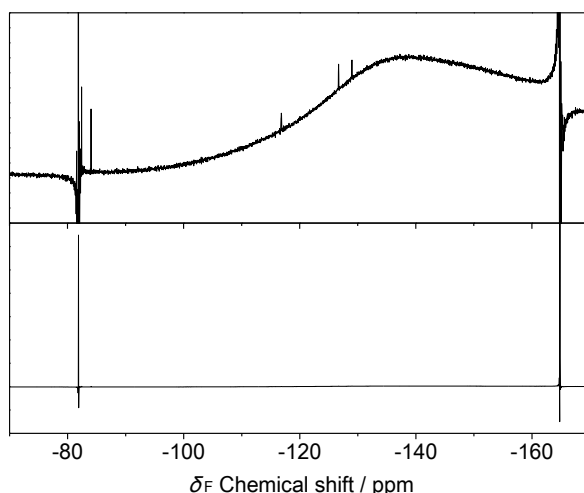


**Figure 4-5.** The ^{19}F NMR spectra of the mixture of crystal obtained from quaternization of triethylamine and I(CH$_2$)$_2$(CF$_2$)$_3$CF$_3$, and LiTf$_2$N.    Enlarged spectrum is shown upper.

Then, we prepared quaternary salts with triethylamine and I(CH$_2$)$_3$(CF$_2$)$_7$CF$_3$ (**Figure 4-6**).    Similar to the reaction with I(CH$_2$)$_2$(CF$_2$)$_3$CF$_3$, yellow solid was obtained.    Then the solid
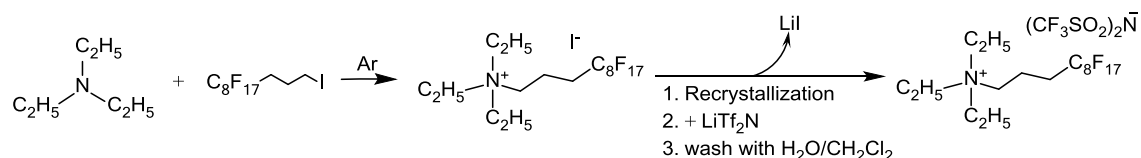


**Figure 4-6.** The reaction of amines with fluorinated iodoalkane and subsequent anion exchange reaction.

72

was washed with acetonitrile to form white solid.   **Figure 4-7** shows $^1$H NMR and $^{19}$F NMR spectra of the obtained solid.   The $^1$H NMR spectra shows signals for the ethyl groups (1.45 and 3.54 ppm) shifted from those of the starting amine (0.93 and 2.43 ppm).   The signals for propylene spacer were found at 2.15, 2.43, and 3.66 ppm.   The signals for perfluorooctyl chain were observed in $^{19}$F NMR spectrum.   From these results, we confirmed that quaternization has successfully been carried out with $I(CH_2)_3(CF_2)_7CF_3$ and triethylamine.   Then anions of iodide salts were exchanged to [Tf$_2$N] anion as showen in **Figure 4-6**.   The salts was obtained as solid state at room temperature and its melting point was found around 100 $^o$C.
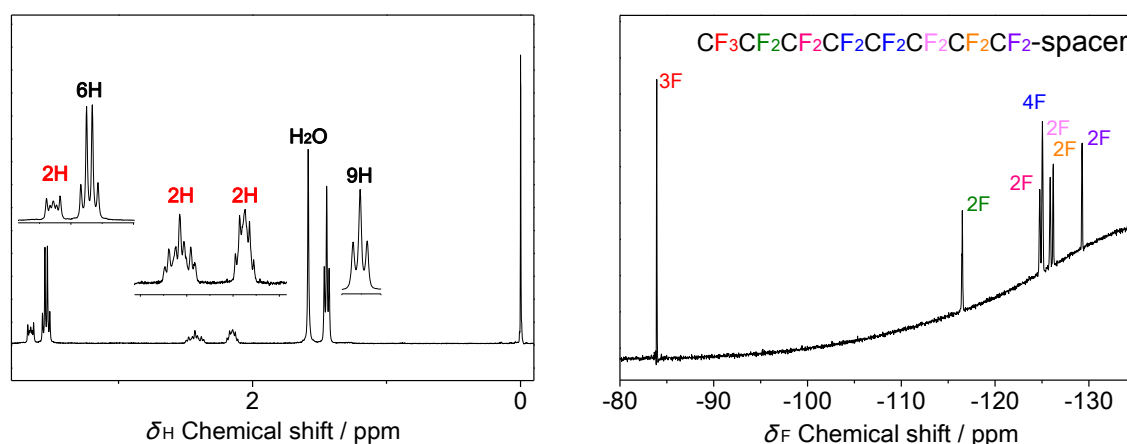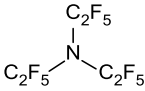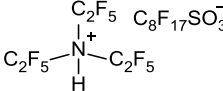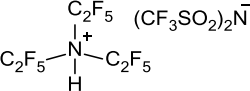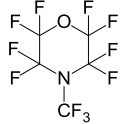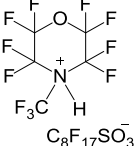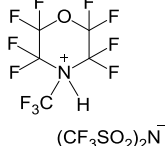
**Figure 4-7.** $^1$H NMR and $^{19}$F NMR spectra of the solid obtained from quaternization of triethylamine and $I(CH_2)_3(CF_2)_7CF_3$.

ILs were also prepared by mixing equimolar of Lewis acid and Lewis bases as shown in **Table 4-2**.   However, all combination resulted in insoluble mixture.   This may be due to that Lewis basicity of amine or morpholine were suppressed by the presence of fluorine atom having strong electron withdrawing ability.

**Table 4-2.** Supposed structure of ILs and miscibility of fluorinated Lewis acids and Lewis bases.

| | $C_8F_{17}SO_3H$ | $(CF_3SO_2)_2NH$ |
|---|---|---|
| Tripentafluoroethylamine | Insoluble | Insoluble |
| Perfluoro(4-methylmorpholine) | Insoluble | Insoluble |

## 4-5.  Summary

In this chapter, fluoroalkanes such as 20N, 14H, 13H, 12H, and 8H were used as model compounds of fluorinated polymers, and solubility of those fluoroalkanes in ILs was analyzed.    For the case of perfluoroalkanes such as 20N and 14H, solubility of these compound was related to fluorine content of ILs.    On the other hand, for fluoroalkanes containing hydrogens or hydroxyl groups in the terminal structures, deviation from the correlation between the solubility and the fluorine content was found.    For the case of 8H, stronger effect of hydrogen bond ability of ILs on the solubility of 8H was observed.    We concluded that discussion based on fluorine content of ILs are applicable for the solubility of perfluoroalkanes, and discussion based on Kamlet-Taft parameter are applicable for the solubility of fluoroalkanes containing terminal hydroxyl groups.    Also, we saw that the presence of fluorinated tail in the structure of ILs is important to improve affinity of the ILs with perfluoroalkanes.    Then, quaternization of triethylamine and fluorinated iodoalkane was carried out.    However, ILs containing fluorinated tail on cation structures resulted in solid state at room temperature.    From these results, we concluded that ILs containing anions with high fluorine content ($e.g.$ [$P_{4446}$]$C_8F_{17}SO_3$) is favorable to dissolve perfluoroalkanes.    These ILs are expected to be also compatible with fluorinated polymers.

## 4-6.  References

[1]      F. T. T. Huque, K. Jones, R. A. Saunders, J. A. Platts, *Journal of Fluorine Chemistry* **2002**, *115*, 119-128.

[2]      (a) Y. Fukaya, K. Hayashi, M. Wada, H. Ohno, *Green Chemistry* **2008**, *10*, 44-46; (b) J. Palgunadi, S. Y. Hong, J. K. Lee, H. Lee, S. D. Lee, M. Cheong, H. S. Kim, *The journal of physical chemistry. B* **2011**, *115*, 1067-1074.

[3]      H. B. Alhanash, A. K. Brisdon, *Journal of Fluorine Chemistry* **2013**, *156*, 152-157.

# Chapter 5

## Functional design
## of fluorinated polymer/ionic liquid composites

## 5-1.　Introduction

In chapter 3, compatibility of ionic liquids (ILs) and fluorinated polymers was evaluated.　Further discussion on the compatibility was carried out in Chapter 4 by using fluoroalkanes as model compounds of fluorinated polymers.　From these results, ILs were classified based on the compatibility with fluorinated polymers.　These ILs were added to fluorinated polymers to prepare the composites in this chapter.　Here we discuss the effect of the compatibility on properties of the composites in terms of form and ionic conductivity.

## 5-2.　Experimental procedure

Structure, abbreviation, and preparation for all ILs are summarized in the Appendix (P. 88).　All ILs were dried under vacuum at 60 $^o$C for at least 3 h.　Material information for fluorinated polymers such as PVdF, ETFE, and PTFE are mentioned in **Section 3-2-1**.

## 5-2-1.　Preparation of the composites

ILs and fluorinated polymers were mixed in ratio of 3:7, 4:6 and 5:5 (w/w) at room temperature.　These were mixed with spatula until they form homogenous phase.　All procedures were carried out in a $N_2$ filled glove box.

## 5-2-2.　Evaluation of electrochemical properties

Prior to measurements, all samples were dried under vacuum at 60 $^o$C at least 3 h. Impedance measurement was carried out with the ILs/fluorinated composites.　Cells were fabricated by sandwiching the composites with two ITO-glass electrodes.　As a spacer to keep the electrode gap distance constant, a 0.38 mm thickness tape based on fluorinated resin stamped out 5 mm circle was used.　The spacer layered to a ITP-glass electrode, and powder samples were filled to the hole.　Then, the samples were covered with another ITP-glass electrode and tightly packed with double clips.　A signal of amplitude 0.5 V was applied to the cell in the frequency range of $10^3$ to $10^7$ Hz.　Conductivity was calculated according to the amplitude of a semicircle or intersection on the Z′ axis of the Nyquist plot of the impedance.　The measurement was carried out from room temperature to 90 $^o$C at a heating or cooling rate of 2 $^o$C min$^{-1}$.　All these procedure was carried out in an Ar-filled glove box.

## 5-3.   Properties of the mixture of the polymer and ionic liquids

The composites of ILs and fluorinated polymers were designed and their form were checked visually with naked eyes.   Depending on the mixing ratio of the composites, they changed their form.   When polymer ratio is larger in the composites, the composites become powder (**Figure 5-1**, far left).   As adding ILs, the composites started to agglomerate and became fragile solid. Among these samples, some composites formed one large chunk (we defined this form as solid as shown in **Figure 5-1**, center).   Further addition of ILs resulted in the composites of waxy solid. Some composites get fluidity upon IL addition (we defined this form as wax as shown in **Figure 5-1**, far right).



| Powder | Fragile Solid | Solid | Waxy Solid | Wax |
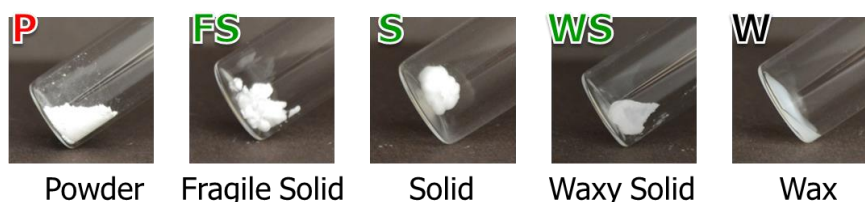
**Figure 5-1.**   Definition of forms of the IL/fluorinated polymer composites.

**Table 5-1** summarize the form of IL/fluorinated polymer composites.   In a series of PVdF composites, the composites changed their states from powder to wax by varying mixing ratios from 4:6 to 5:5 for imidazolium salts which have good solubility of PVdF, and from 3:7 to 4:6 for phosphonium salts which have poor solubility of PVdF.   Similar trend was observed for ETFE composites.   The ETFE composites containing imidazolium salts changed their state from powder to waxy solid by varying mixing ratio from 3:7 to 4:6; however, the ETFE composites containing $[P_{444,12}][Tf_2N]$ and $[P_{8888}][Tf_2N]$ became waxy solid even at mixing ratio of 3:7.   The difference of form may be attributed from the difference of compatibility between polymer matrices and ILs.

For the case of PTFE, PTFE composites in mixing ratio of 3:7 resulted in fragile solid. While the PTFE composites in mixing ratio of 4:6 formed fragile solid or solid accompanied by bleed out of ILs.   This is due that affinity between ILs and PTFE was quite poor.   The composites with phosphonium salts became solid accompanied by bleed out of smaller amounts of ILs compared to imidazolium salts.   This suggests that phosphonium salts have a potential to give higher compatibility with PTFE compared to imidazolium salts, and this follows the results in chapter 3.   On the other hand, among imidazolium salts, $[C_2mim][Tf_2N]$ was separated from PTFE suggesting this is the most poor combination in terms of affinity.

**Table 5-1.** Sample states of [Tf$_2$N]-type IL/fluorinated polymer composites.

| Ratio of ILs : polymer | PVdF | | | ETFE | | | PTFE | | |
|---|---|---|---|---|---|---|---|---|---|
| (w/w) | 3:7 | 4:6 | 5:5 | 3:7 | 4:6 | 5:5 | 3:7 | 4:6 | 5:5 |
| Imidazolium-type | | | | | | | | | |
| [C$_2$mim] | P | P | W | P | WS | W | FS | FS* | separated |
| [C$_4$mim] | P | WS | W | P | WS | W | FS | FS* | FS* |
| [C$_2$OHmim] | P | P | W | P | WS(W) | W | FS | FS* | FS* |
| Phosphonium-type | | | | | | | | | |
| [P$_{4441}$] | P | W | W | P | WS(W) | W | FS | S* | S* |
| [P$_{444,12}$] | P | W | W | WS | W | W | FS | S* | S* |
| [P$_{8888}$] | P | W | W | WS | W | W | FS | S* | S* |

*small amount of ILs remained on glass surface

In order to obtain homogeneous composites based on PTFE, fluorophilic ILs prepared in Chapter 4 have been applied for the preparation of the PTFE composites.   **Figure 5-2** compares the form of the PTFE composites containing [C$_2$mim][Tf$_2$N], [C$_2$mim]C$_8$F$_{17}$SO$_3$, [P$_{666,14}$][Tf$_2$N], and [P$_{4446}$]C$_8$F$_{17}$SO$_3$ in mixing ratio of 5:5.   The pictures in first line display the form of the composites in vial.   The pictures in second and third line were taken in following procedure.   To a glass plate with 0.1 mm spacer, 5 mg of the composites were placed and then sandwiched with another glass plate.

As we expected, homogeneous composite was not obtained with the addition of [C$_2$mim][Tf$_2$N] which shows poor compatibility with PTFE.   By changing anion structure to C$_8$F$_{17}$SO$_3$, which shows better affinity with PTFE than [Tf$_2$N], homogeneous composite was obtained.   However, bleed out of the ILs was observed for this composite.   Same trend was observed by changing cation of [C$_2$mim][Tf$_2$N] to [P$_{666,14}$][Tf$_2$N].   When the [P$_{4446}$]C$_8$F$_{17}$SO$_3$ was used as additive salts, homogeneous composite was obtained.   This composite retained ILs in the PTFE matrices even after sandwiching the composite with a pair of glass plates.   [P$_{4446}$]C$_8$F$_{17}$SO$_3$ successfully provided homogeneous composites with PTFE without bleed out of the IL.   This was attributed by high affinity between [P$_{4446}$]C$_8$F$_{17}$SO$_3$ and PTFE.   Then, ionic conductivity of the composite based on PTFE and [P$_{4446}$]C$_8$F$_{17}$SO$_3$ in a mixing ratio of 5:5 was measured.   As shown in **Figure 5-3**, the composite showed ionic conductivity comparable with pure [P$_{4446}$]C$_8$F$_{17}$SO$_3$. Throughout these experiments, we concluded that design of polymer electrolytes based on fluorinated polymer are possible by designing ILs.   Even if we chose PTFE as matrix polymer, designed ILs enables to facilitate formation of homogeneous composite with PTFE.
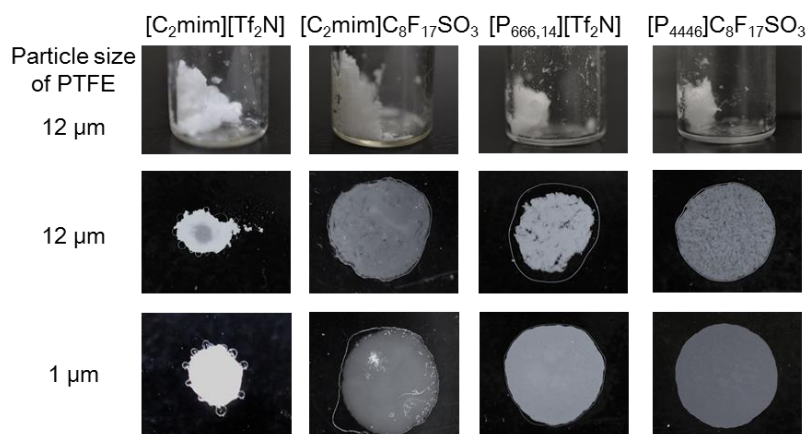
**Figure 5-2.** Composites based on PTFE and ILs in a ratio of 5:5 (w/w).
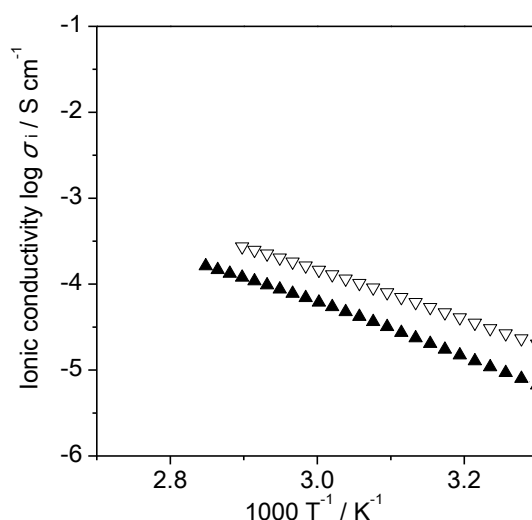


**Figure 5-3.** Arrhenius plot of ionic conductivity of $[P_{4446}]C_8F_{17}SO_3$ ($\triangledown$) and its composited with PTFE in ratio of 1:1 (▲).

## 5-4. Summary

The effect of affinity between fluorinated polymers and ILs on the properties of their composites was analyzed. When the ILs and PVdF were mixed in ratio of 4:6 (w/w), the composites having high affinity among the components became powder state. On the other hand, the PVdF composite having poor affinity among the components resulted in fluid composites. Similar trend was found for the composites of ETFE. For the case of PTFE, some composites were accompanied with bleed out of ILs. For the case of the PTFE/[C2mim][Tf2N] composite mixed in ratio of 5:5, [C2mim][Tf2N] was separated from PTFE. In order to obtain homogeneous

79

composites with PTFE, $[P_{4446}]C_8F_{17}SO_3$, fluorophilic ILs prepared in chapter 4, was added to PTFE. This ILs facilitated formation of homogeneous composites without of bleed out of the ILs. This composite was confirmed to show ionic conductivity comparable with pure $[P_{4446}]C_8F_{17}SO_3$. Throughout these experiment, we concluded that design of polymer electrolyte based on fluorinated polymer are possible by designing ILs.

# Chapter 6
# Conclusion and future prospect

## Chapter 6. Conclusion and future prospect

In "**Polymer composites containing ionic liquids** (chapter 1)", properties of fluorinated polymers as matrices and ionic liquids (ILs) as additives were summarized. Among various kind of electrolytes, polymer based electrolytes gathered much attention due to their thermal stability and considerable electrochemical properties. In the development of polymer electrolytes, two major polymers have been used; *i.e.* polyethers (*e.g.* poly(ethylene oxide) (PEO)) and fluorinated polymers (*e.g.* poly(vinylidene fluoride-*co*-hexafluoropropylene) (PVdF-HFP)). For PEO-based electrolytes, salts are dissociated into ions and enhance ionic conductivity via segmental motion of PEO. In order to improve their conductivity, large amount of salts are need to be dissociated into free ions in PEO matrix. As a trade of, addition of inorganic salts suppresses segmental motion of PEO due to their high glass transition temperature. For the case of fluorinated polymer-based electrolytes, ionic conductivity are enhanced in amorphous polymer phase plasticized with carbonate solution. Thus, there are fears that carbonate solution bleed out from polymer matrices and cause ignition. On the other hand, ILs have been applied as additive salts for polymer electrolytes due to their thermal stability and ionic conductivity. Considering the properties of ILs, ILs seem to be useful additive salts for polymer electrolytes to overcome the issues which are stated above. As a view point of design of additive salts, ILs (organic salts) have advantages because there are numerous combinations of cation and anions. Focusing on these properties, in this dissertation, ILs were suitably designed as additive salts for polymers considering compatibility between ILs and polymers.

In "**Factors to control solubility of polymers in ionic liquids and their functional design** (Chapter 2)", effect of affinity between polymers and ILs on the properties of their composites have been analyzed. For the case of PEO, we found that Hard and Soft Acids and Bases (HSAB) theory is applicable to consider the affinity of PEO and ILs. Then we extended this study to design IL/PEO composites. The composite having poor affinity among components resulted in phase separation of PEO and ILs. The mixture containing ILs, showing moderate affinity with PEO, resulted in homogeneous solid and the mixture containing ILs, showing good affinity with PEO, resulted in homogeneous liquid. The latter liquid resulted in high viscosity and lower ionic conductivity compared to pure ILs. On the other hand, the former solid resulted in a thermotropic gel. Above transition temperature, the composite changed their state to liquid and showed ionic conductivity comparable to pure ILs. Below transition temperature, the ionic conductivity decreased hundred times, however, considerable ionic conductivity was found even if they were solid state. From these results we concluded that moderate affinity is important to retain ionic conductivity of ILs after mixing with polymers. Consequently, we concluded that properties of IL/polymer composites can be designed by changing affinity between ILs and polymers.

In "**Compatibility of fluorinated polymers into ionic liquids and design of their composites** (Chapter 3)", solubility of fluorinated polymers into ILs was investigated. Poly(vinylidenefluoride) (PVdF) was capable to dissolve in ILs having high polarity. Slight solubility of poly(ethylene-*co*-chlorotrifluoroethylene) (PECTFE) in $[P_{666,14}][Tf_2N]$ and Cytop® in $[C_2mim][Tf_2N]$ were confirmed by ^{19}F NMR. Perfluorinated polymers such as poly(tetra-fluoroethylene) (PTFE) was difficult to dissolve to ILs. Then, by using PVdF which showed moderate affinity with ILs, polymer electrolytes for lithium ion batteries were designed. The composite film containing PVdF-based polymer, electrolyte solution, and ILs was found to possess ionic conductivity of $10^{-4}$ S $cm^{-1}$ at room temperature. This number was retained even after a storage of the films. We successfully obtained stable polymer electrolytes based on fluorinated polymers and ILs. This suggest that composite of ILs and fluorinated polymer can be designed if they show moderate affinity. However, to obtain wide variety of these composites, ILs having improved affinity with fluorinated polymers are required to be designed.

In "**Design of fluorophilic ionic liquids** (Chapter 4)", firstly fluoroalkanes were used as model compounds of fluorinated polymers, and solubility of fluoroalkanes in ILs was analyzed. For the case of perfluoroalkanes such as eicosafluorononane (20N) and tetradecafluorohexane (14H), solubility of these compounds was related to fluorine content of ILs. We concluded that the presence of fluoroalkyl chain in the structure of ILs is important in order to improve affinity of the ILs with perfluoroalkanes. Among ILs prepared in Chapter 4, tributyl(hexyl)phosphonium heptadecafluorooctanesulfonate ($[P_{4446}]C_8F_{17}SO_3$) showed highest mole fraction of perfluoroalkanes dissolved in the ILs. From this result, $[P_{4446}]C_8F_{17}SO_3$ is considered to show good affinity with fluorinated polymers.

In **Functional design of fluorinated polymer/ionic liquid composites** (chapter 5)**,** we analyzed the effect of affinity between fluorinated polymers and ILs on the properties of their composites. As polymer matrices, PVdF, Poly(ethylene-*co*-tetrafluoroethylene) (ETFE) and poly(tetrafluoro-ethylene) (PTFE) were applied for preparation of composites. For the case of PVdF and ETFE, homogeneous composites were obtained by using normal ILs. On the other hand, for the case of PTFE, normal ILs bled out from polymer matrices. One ILs, $[P_{4446}]C_8F_{17}SO_3$, which showed highest compatibility with perfluoroalkane in Chapter 4, enabled to produce homogenous composites with PTFE without bleed out of ILs. The composites were confirmed to show suitable ionic conductivity. From these results, the possibility of PTFE-based ion conductive materials has been firstly discussed with designing ILs.

In "**Conclusion and future prospect** (Chapter 6)"**,** I summarized my dissertation. Throughout this study, we discussed how to design polymer/IL composites and control their property. Many polymers have been concluded to have the capability to act as potential matrices

for ILs when they show moderate affinity with ILs.    For the case of fluorinated polymers, since these have low affinity with ILs, only designed ILs were possible to facilitate the composites.    In order to design fluorophilic ILs, we also discussed what is a key factor to control affinity between fluorinated polymers and ILs.    This study will widen the possibility of fluorinated polymers as matrices for polymer electrolytes.

# Bibliography

## Bibliography

### Original papers

(1) <u>Akiko Tsurumaki</u>, Junko Kagimoto, and Hiroyuki Ohno, Properties of polymer electrolytes composed of poly(ethylene oxide) and ionic liquids according to hard and soft acids and bases theory, *Polym. Adv. Technol.*, **2011**, *22*, 1223-1228.   (Chapter 2)

(2) <u>Akiko Tsurumaki</u>, Saori Tajima, Takuya Iwata, and Hiroyuki Ohno, Antistatic effects of ionic liquids for polyether-based polyurethanes, *Electrochim. Acta*, in press. (Chapter 2)

(3) <u>Akiko Tsurumaki</u>, Maria Assunta Navarra, Stefania Panero, Bruno Scrosati, and Hiroyuki Ohno, *N*-n-Butyl-*N*-methylpyrrolidinium hexafluorophosphate-added electrolyte solutions and membranes for lithium-secondary batteries, *J. Power Sources*, **2013**, *233*, 104-109. (Chapter 3)

(4) <u>Akiko Tsurumaki</u> and Hiroyuki Ohno, Novel composites of poly(tetrafluoroethylene) with ionic liquids, *Chem. Commun.,* in preparation. (Chapter 4,5)

### Author is also contributed to following papers, report and review.

(5) Takuya Iwata, <u>Akiko Tsurumaki</u>, Saori Tajima, and Hiroyuki Ohno, Bis(trifluoromethane-sulfonyl)imide-type ionic liquids as excellent antistatic agents for polyurethanes, *Macromol. Mat. Eng.*, **2014**, *299*, 794-798.

(6) Takuya Iwata, <u>Akiko Tsurumaki</u>, Saori Tajima, and Hiroyuki Ohno, Fixation of ionic liquids into polyether-based polyurethane films to maintain long-term antistatic properties, *Polymer*, **2014**, *55*, 2501-2504.

(Report) <u>Akiko Tsurumaki</u>
A report of the ILED-2014 (written in Japanese)
*Circular Journal of Ionic Liquids research Association, Japan*, **2014**, *3*, 14.

(Review) Takuro Matsumoto, Kosuke Kuroda, Shohei Saita, <u>Akiko Tsurumaki</u>, Mitsurua Abe, Satomi Taguchi, Kyoko Fujita, Naomi Nishimura, Nobuhumi Nakamura and Hiroyuki Ohno
Abbreviation list of ionic liquids (written in Japanese)
*Circular Journal of Ionic Liquids research Association, Japan*, **2014**, *1*, 2-10.

# Appendix

## Structure of ILs

**Cation structure**

[C₂mim]: R₂=C₂H₅
[C₄mim]: R₂=C₄H₉ — written as $[C_2mim]: R_2=C_2H_5$ / $[C_4mim]: R_2=C_4H_9$

$[C_2mim]$: $R_2=C_2H_5$
$[C_4mim]$: $R_2=C_4H_9$
1-alkyl-3-methylimidazolium

$[C_2OHmim]$
1-(2-hydroxyethyl)-3-methylimidazolium

$[C_4mmim]$
1-butyl-2,3-dimethylimidazolium

$[AAim]$
1,3-diallylimidazolium

$[P_{4441}]$: $R_2=CH_3$
$[P_{4444}]$: $R_2=C_4H_9$
$[P_{4446}]$: $R_2=C_6H_{13}$
$[P_{4448}]$: $R_2=C_8H_{17}$
$[P_{444,12}]$: $R_2=C_{12}H_{25}$
tributyl(alkyl)phosphonium

$[P_{666,14}]$
trihexyl(tetradecyl)phosphonium

$[P_{8888}]$
tetraoctylphosphonium

$[N_{4441}]$
tributyl(methyl)ammonium

$[DEME]$
*N,N*-diethyl-*N*-methyl-
*N*-(2-ethoxyethyl)ammonium

$[S_{111}]$
trimethylsulfonium

$[Pyr_{14}]$
1-butyl-1-methylpyrrolidinium

$[Pip_{14}]$
1-butyl-1-methylpiperidinium

$[C_4py]$
1-butylpyridinium

**Anion structure**

$[FSI]$
bis(fluorosulfonyl)imide

$[Tf_2N]$
bis(trifluoromethanesulfonyl)imide

$[Pf_2N]$
bis(nonafluorobutanesulfonyl)imide

$[Nf_2N]$
bis(nonafluorobutanesulfonyl)imide

$Cl^-$   $CF_3SO_3^-$   $CF_3CO_2^-$

$BF_4^-$   $C_4F_9SO_3^-$   $N\equiv C-S^-$

$PF_6^-$   $C_8F_{17}SO_3^-$   $(CH_3O)(H)PO_2^-$

$[Ala]$
alanine

$[FAP]$
tris(pentafluoroethyl)trifluorophosphate

$[DCA]$
dicyanamide

Figure A1.   Structure and abbreviation of ionic liquids (ILs) used in this study.

# Appendix

## Materials

Precursors of ILs such as 1-ethylimidazole (>98.0%), 2-bromoethanol (>95.0%), dimethyl phosphite (min. 98.0 %), $CF_3SO_3H$ (≥98.0%), $C_4F_9SO_3H$ (≥98.0%), and $C_8F_{17}SO_3H$ (>98.0%) were purchased from Tokyo Chemical Industry Co., Ltd.   $CF_3CO_2H$ (min. 98.0 %), Li[$Nf_2N$] (97.0+%) and L-alanine (99.0+%) were purchased from Wako Pure Chemical Industries, Ltd. 1-Bromobutane (min. 98%, from Kanto Chemical Co., Inc.), 1-methylimidazole (99%, from Sigma Aldrich Co. LLC.), and 1,2-dimethylimidazole (98%, from Acros Organics) were purchased from each companies.   Li[$Tf_2N$] (98%) and Li[FSI] were kindly donated from Sumitomo 3M. Co. and Dai-Ichi Kogyo Seiyaku Co. Ltd., respectively.

ILs such as [DEME][$Tf_2N$] (min. 99%), [$C_4mim$]$BF_4$ (min. 95%), [$C_4mim$]$PF_6$ (min. 97%), [AAim][$Tf_2N$] (min. 97%), [$P_{666,14}$]Cl (>95%), and [AAim]Cl (min. 97%) were purchased from Kanto Chemical Co., Inc. and used without further purification.   [$S_{111}$]I (>98.0%), [$N_{4441}$][$Tf_2N$] (> 98%), [$P_{4441}$][$Tf_2N$] (> 98%), and [$Pip_{14}$][$Tf_2N$] (> 98%) were purchased from Tokyo Chemical Industry Co., Ltd. and used without further purification.   [$P_{4448}$]Br (97.0+%) and [$C_4py$][$Tf_2N$] were purchased from Wako Pure Chemical Industries, Ltd. and used without further purification. [$Pyr_{14}$]Br (≥99.0%, from Sigma Aldrich Co. LLC.), [$C_4mim$]Br (99%, from IoLiTec GmbH), and [$C_2mim$]Cl (≥98.0%, from Merck Ltd.) were purchased from each companies and used without further purification.   [$P_{4444}$]OH solution, [$P_{4446}$]Br, [$P_{444,12}$][$Tf_2N$], [$P_{444,12}$]$BF_4$, [$P_{444,12}$]$PF_6$, [$P_{444,12}$]$CF_3SO_3$, [$P_{444,12}$]SCN, [$P_{8888}$][$Tf_2N$], [$P_{8888}$][$Pf_2N$], [$P_{8888}$][FSI], [$P_{8888}$]$CF_3SO_3$, [$P_{8888}$]SCN, and [$C_2mim$][$Tf_2N$] were kindly donated from Hokko Chemical Industry Co., Ltd.   [$C_4mim$][FAP], [$C_2mim$][FAP], and [$Pyr_{14}$][FAP] were kindly donated from Merck Ltd.   Other ILs such as [$C_4mim$][$Tf_2N$], [$P_{4448}$][$Tf_2N$], [$Pyr_{14}$][$Tf_2N$], [$C_4mmim$][$Tf_2N$], [$C_2OHmim$][$Tf_2N$], [$C_2mim$][FSI], [$C_2mim$][$Nf_2N$], [$S_{111}$][$Tf_2N$], [$C_4mim$]$CF_3SO_3$, [$C_4mim$]$CF_3CO_2$, [$C_4mim$][Ala], [$P_{4444}$][Ala], [$C_2mim$]$(CH_3O)(H)PO_2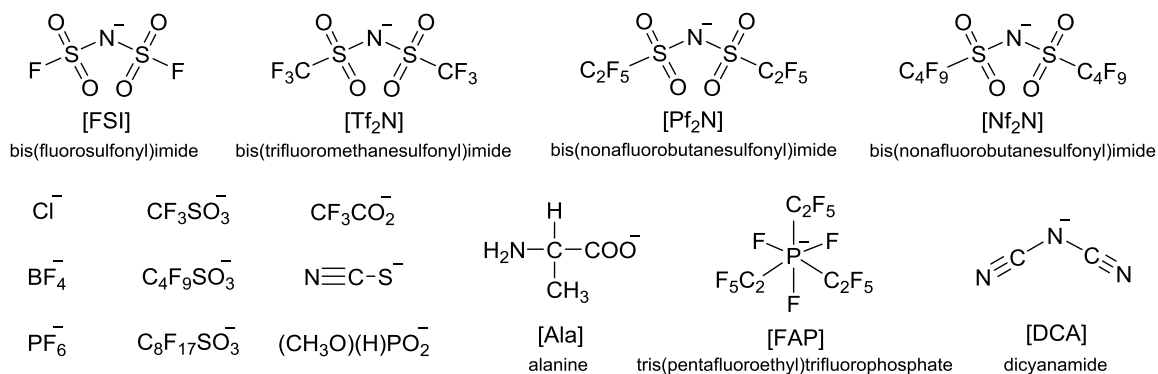$, [$P_{666,14}$][$Tf_2N$], [$P_{666,14}$][$Nf_2N$], [$P_{666,14}$]$CF_3CO_2$, [$P_{666,14}$]$CF_3SO_3$, [$P_{666,14}$]$C_8F_{17}SO_3$, [$P_{4446}$]$C_4F_9SO_3$, [$P_{4446}$]$C_8F_{17}SO_3$, and [$C_2mim$]$C_8F_{17}SO_3$ were prepared in our laboratory as follows.   The structure of the ILs were determined by $^1H$ NMR (α-400 or α-500, both from JEOL).

## Preparation and NMR analysis

1-Butyl-3-methylimidazolium bis(trifluoromethanesulfonyl)imide ($[C_4mim][Tf_2N]$)

Prior to the preparation, both $[C_4mim]Br$ and $Li[Tf_2N]$ were diluted tenfold with Milli-Q water. To an aqueous solution of $[C_4mim]Br$, an aqueous solution of $Li[Tf_2N]$ (1.1 molar of Br salts) was added.   The resulting solution was mixed with dichloromethane, and the dichloromethane fraction was collected.   The dichloromethane fraction was washed with Milli-Q water for 3 times, then evaporated to remove dichloromethane.   The remaining liquid was diluted with dichloromethane and then passed through a short column filled with activated aluminum oxide. After evaporation of dichloromethane, the remaining liquid was then dried in vacuum at 60 ℃ for at least 3 h to give colorless liquids.   $^1$H-NMR (400MHz, DMSO-$d_6$, $\delta$/ppm relative to Me$_4$Si): 0.91 (3H, t, $J$ = 7.3 Hz, CH$_2$C$H_3$), 1.22-1.31 (2H, m, CH$_2$C$H_2$CH$_3$), 1.73-1.80 (2H, m, CH$_2$C$H_2$CH$_2$), 3.85 (3H, s, NC$H_3$), 4.16 (2H, t, $J$ = 7.1 Hz, NC$H_2$CH$_2$), 7.70 and 7.76 (2H, t, $J$ = 1.6 and 1.8 Hz, NC$H$C$H$N), 9.10 (s, 1H, NC$H$N).

Tributyloctylphosphonium bis(trifluoromethanesulfonyl)imide ($[P_{4448}][Tf_2N]$)

Titled compound was prepared by the same procedure as that described above for $[C_4mim][Tf_2N]$ with a corresponding bromide salt; $[P_{4448}]Br$.   $^1$H-NMR (400MHz, CDCl$_3$, $\delta$/ppm relative to Me$_4$Si): 0.84 (3H, t, $J$ = 6.6 Hz, P(CH$_2$)$_7$C$H_3$), 0.92 (9H, t, $J$ = 9.6 Hz, P(CH$_2$)$_3$C$H_3$), 1.24-1.28 (8H, m, broad, P(CH$_2$)$_3$(C$H_2$)$_4$CH$_3$), 1.44 (16H, t, $J$ = 13.8 Hz, PCH$_2$C$H_2$C$H_2$), 2.06-2.14 (8H, m, PC$H_2$).

1-Butyl-1-methylpyrrolidinium bis(trifluoromethanesulfonyl)imide ($[Pyr_{14}][Tf_2N]$)

This salt was prepared by the same method as described above for $[C_4mim][Tf_2N]$ with a corresponding bromide salt; $[Pyr_{14}]Br$.   $^1$H-NMR (400MHz, CDCl$_3$, $\delta$/ppm relative to Me$_4$Si): 0.99-1.07 (3H, m, CH$_2$C$H_3$), 1.43-1.51 (2H, m, C$H_2$CH$_3$), 1.76-1.82 (2H, m, NCH$_2$C$H_2$), 2.30 (4H, t, $J$ = 12.6, C$H_2$CH$_2$NCH$_2$C$H_2$), 3.08 (3H, d, $J$ = 24.4, NC$H_3$), 3.30-3.39 (2H, m, NC$H_2$), 3.52-3.59 (4H, m, C$H_2$NC$H_2$).

1-Butyl-2,3-dimethylimidazolium bis(trifluoromethanesulfonyl)imide ($[C_4mmim][Tf_2N]$)

First, $[C_4mmim]Br$ was prepared as follow.   To 1,2-dimethylimidazole diluted tenfold with acetonitrile, 1-bromobutane (1.2 molar of 1,2-dimethylimidazole) was added dropwise at room temperature under N$_2$ atmosphere.   The resulting mixture was heated up to 70 ℃ and stirred for 48 h.   Removal of acetonitrile and unreacted precursors by evaporation yielded a yellow solid.   The resulting solid was recrystallized with ethyl acetate/acetonitrile 2/1 (v/v) solution. Recrystallization was repeated to give white crystals.   Then, Br anion of this salt was replaced with [Tf$_2$N] anion using the same procedure as described above for $[C_4mim][Tf_2N]$.   $^1$H-NMR

(500 MHz, CDCl$_3$, $\delta$/ppm relative to Me$_4$Si): 0.96 (3H, t, $J = 7.5$ Hz, CH$_2$C$H_3$), 1.33-1.41 (2H, m, CH$_2$C$H_2$CH$_3$), 1.74-1.80 (2H, m, CH$_2$C$H_2$CH$_2$), 2.60 (3H, s, NC$H_3$N), 3.79 (3H, s, NC$H_3$), 4.04 (2H, t, $J = 7.5$ Hz, NC$H_2$CH$_2$), 7.17 and 7.20 (2H, d, $J = 2.3$ and 1.7 Hz, NC$H$C$H$N).

1-(2-Hydroxyethyl)-3-methylimidazolium bis(trifluoromethanesulfonyl)imide ([C$_2$OHmim][Tf$_2$N])
A [C$_2$OHmim]Br was prepared by the same procedure as that described for [C$_4$mmim]Br with corresponding precursor, 1-butylimidazole and 2-bromoethanol under dry N$_2$ gas atmosphere. The obtained yellow solid was recrystallized with ethyl acetate/methanol 2/1 (v/v) solution. Recrystallization was repeated to give colorless crystals.    Br anion of this salt was replaced with [Tf$_2$N] anion using the same procedure as described for [C$_4$mim][Tf$_2$N].   $^1$H-NMR (400MHz, DMSO-$d_6$, $\delta$/ppm relative to Me$_4$Si): 3.73 (q, $J = 5.33$ Hz, 2H, CH$_2$C$H_2$OH), 3.87 (s, 3H, NC$H_3$), 4.21 (t, $J = 4.00$ Hz, 2H, NC$H_2$CH$_2$), 5.17 (t, $J = 6.00$ Hz, 1H, O$H$), 7.68 and 7.72 (d, $J = 2.00$ and 2.00 Hz, 2H, NC$H$C$H$N), 9.07 (s, 1H, NC$H$N).

1-Ethyl-3-methylimidazolium bis(fluorosulfonyl)imide ([C$_2$mim][FSI])
Titled compound was prepared by the same procedure as that for [C$_4$mim][Tf$_2$N] with corresponding imidazolium salts and lithium salts; [C$_2$mim]Cl and Li[FSI].   $^1$H-NMR (400MHz, DMSO-$d_6$, $\delta$/ppm relative to Me$_4$Si): 1.45 (3H, t, $J = 7.2$ Hz, CH$_2$C$H_3$), 3.88 (3H, s, NC$H_3$), 4.24 (2H, q, $J = 12.1$ Hz, NC$H_2$CH$_3$), 7.72 and 7.80 (2H, t, $J = 1.8$ and 1.8 Hz, NC$H$C$H$N), 9.13 (1H, s, NC$H$N).

1-Ethyl-3-methylimidazolium bis(nonafluorobutanesulfonyl)imide ([C$_2$mim][Nf$_2$N])
Titled compound was prepared by the same procedure as that for [C$_4$mim][Tf$_2$N] with corresponding imidazolium salts and lithium salts; [C$_2$mim]Cl and Li[Nf$_2$N].   $^1$H-NMR (400MHz, DMSO-$d_6$, $\delta$/ppm relative to Me$_4$Si): 1.41 (3H, t, $J = 7.4$ Hz, CH$_2$C$H_3$), 3.85 (3H, s, NC$H_3$), 4.19 (2H, q, $J = 7.3$ Hz, NC$H_2$CH$_3$), 7.69 and 7.78 (2H, t, $J = 2.0$ and 1.8 Hz, NC$H$C$H$N), 9.11 (1H, s, NC$H$N).

Trimethylsulfonium bis(trifluoromethanesulfonyl)imide ([S$_{111}$][Tf$_2$N])
This salt was prepared by the same method as described above for [C$_4$mim][Tf$_2$N] with a corresponding iodide salt; [S$_{111}$]I.   $^1$H-NMR (400MHz, DMSO-$d_6$, Me$_4$Si) $\delta_H = 2.81$ (9H, s, SC$H_3$).

1-Butyl-3-methylimidazolium trifluoromethanesulfonate ([C$_4$mim]CF$_3$SO$_3$)
First, [C$_4$mim]Br was diluted tenfold with Milli-Q water, and passed through a column filled with anion exchange resin (Amberlite IRN-78) to give an aqueous solution of [C$_4$mim]OH. To the resulting solution, aqueous CF$_3$SO$_3$H solution was added dropwise, and neutralised solution obtained was concentrated by evaporation. The crude material was dissolved in acetone and then passed through a short column filled with activated aluminum oxide.    Acetone was removed by evaporation and the resulting liquid was dried in vaccum at 60 $^o$C for at least 3 h. The purpose material was obtained as a colorless liquid.    $^1$H-NMR (400MHz, DMSO-$d_6$, $\delta$/ppm

relative to Me$_4$Si): 0.91 (3H, t, $J = 7.42$ Hz, CH$_2$C$H_3$), 1.24-1.30 (2H, m, CH$_2$C$H_2$CH$_2$), 1.74-1.80 (2H, m, CH$_2$C$H_2$CH$_2$), 3.85 (3H, s, NC$H_3$), 4.17 (2H, t, $J = 7.2$ Hz, NC$H_2$CH$_2$), 7.70 and 7.77 (2H, t, $J = 1.7$ and 1.7 Hz, NC$H$C$H$N), 9.10 (1H, s, NC$H$N).

1-Butyl-3-methylimidazolium CF$_3$CO$_2$ ([C$_4$mim]CF$_3$CO$_2$)

The salts was prepared by the same procedure as described above for [C$_4$mim]CF$_3$SO$_3$ with corresponding acid; CF$_3$CO$_2$H. $^1$H-NMR (500MHz, CDCl$_3$, Me$_4$Si) $\delta_H$ = 0.93 (3H, t, $J = 7.3$ Hz, CH$_2$C$H_3$), 1.29-1.38 (2H, m, CH$_2$C$H_2$CH$_2$), 1.80-1.88 (2H, m, CH$_2$C$H_2$CH$_2$), 4.00 (3H, s, NC$H_3$), 4.22 (2H, t, $J = 7.33$ Hz, NC$H_2$CH$_2$), 7.37 and 7.44 (2H, t, $J = 1.8$ and 1.8 Hz, NC$H$C$H$N), 10.12 (1H, s, NC$H$N).

1-Butyl-3-methylimidazolium alanine ([C$_4$mim][Ala])

This salt was prepared by the same procedure as described above for [C$_4$mim]CF$_3$SO$_3$ with corresponding imidazolium salt and acid; [C$_4$mim]Br and alanine. $^1$H-NMR (400MHz, DMSO-$d_6$, Me$_4$Si) $\delta_H$ = 0.87 (3H, t, $J = 7.6$ Hz, CH$_2$C$H_3$), 0.99 (3H, d, $J = 6.9$ Hz, CC$H_3$), 1.18-1.27 (2H, m, CH$_2$C$H_2$CH$_2$), 1.70-1.77 (2H, m, CH$_2$C$H_2$CH$_2$), 2.82 (1H, q, $J = 6.7$ Hz, C$H$), 3.85 (3H, s, NC$H_3$), 4.17 (2H, t, $J = 7.1$ Hz, NC$H_2$CH$_2$), 7.74 and 7.81 (2H, t, $J = 1.4$ and 1.6 Hz, NC$H$C$H$N), 9.80 (1H, s, NC$H$N).

Tetrabutylphosphonium alanine ([P$_{4444}$][Ala])

This salt was prepared by the same procedure as described above for [C$_4$mim]CF$_3$SO$_3$ with corresponding solution of phosphonium salt and acid; [P$_{4444}$]OH and alanine. $^1$H-NMR (500MHz, CDCl$_3$, Me$_4$Si) $\delta_H$ = 0.98 (12H, q, $J = 4.7$ Hz, P(CH$_2$)$_3$C$H_3$), 1.30 (3H, d, $J = 7.3$ Hz, CC$H_3$), 1.50-1.55 (16H, m, PCH$_2$C$H_2$C$H_2$), 2.39-2.46 (8H, m, PC$H_2$), 3.28 (1H, q, $J = 7.0$ Hz, C$H$).

1-Ethyl-3-methylimidazolium methylphosphonate ([C$_2$mim](CH$_3$O)(H)PO$_2$)

To 1-ethylimidazole diluted tenfold with THF, dimethyl phosphite (1.2 molar of 1-buthylimidazole) was added dropwise at room temperature under Ar atmosphere. The resulting mixture was heated up to 80 ℃ and stirred for 48 h. After removal of THF by evaporation, the resulting liquid was washed with an excess amount of dehydrated diethyl ether repeatedly. The residual liquid was dissolved in dichloromethane and the resulting solution was passed through a column filled with neutral activated alumina. After removal of dichloromethane by evaporation, residual liquid was dried in a vacuum at 60 ℃ for at least 3 h to give colorless liquids. $^1$H-NMR (400MHz, DMSO-$d_6$, $\delta$/ppm relative to Me$_4$Si): 1.42 (3H, t, $J = 7.2$ Hz, CH$_2$C$H_3$), 3.24 (3H, d, $J = 12.0$ Hz, POC$H_3$), 3.87 (3H, s, NC$H_3$), 4.22 (2H, q, $J = 7.3$ Hz, NC$H_2$CH$_3$), 6.20 (1H, d, $J = 810.8$ Hz (peaks were appeared on 5.18 and 7.21), P$H$), 7.77 and 7.86 (2H, s, NC$H$C$H$N), 9.50 (1H, s, NC$H$N).

## Appendix

**Trihexyl(tetradecyl)phosphonium bis(trifluoromethanesulfonyl)imide ([P$_{666,14}$][Tf$_2$N])**

This salt was prepared by the same method as described above for [C$_4$mim][Tf$_2$N] with a corresponding chloride salt; [P$_{666,14}$]Cl. $^1$H-NMR (400MHz, CDCl$_3$, $\delta$/ppm relative to Me$_4$Si): 0.86-0.91 (12H, m, C*H$_3$*), 1.26 and 1.31 (32H, broad, (C*H$_2$*)$_8$CH$_3$ and P(CH$_2$)$_3$C*H$_2$C*H$_2$*), 1.48 (16H, broad, PCH$_2$C*H$_2$C*H$_2$*), 2.09 (8H, broad, PC*H$_2$*).

**Trihexyl(tetradecyl)phosphonium bis(nonafluorobutanesulfonyl)imide ([P$_{666,14}$][Nf$_2$N])**

This salt was prepared by the same method as described above for [C$_4$mim][Tf$_2$N] with a corresponding chloride salt and lithium salt; [P$_{666,14}$]Cl and Li[Nf$_2$N].

**Trihexyl(tetradecyl)phosphonium CF$_3$CO$_2$ ([P$_{666,14}$]CF$_3$CO$_2$)**

The salts was prepared by the same procedure as described above for [C$_4$mim]CF$_3$SO$_3$ with corresponding chloride salt and acid; [P$_{666,14}$]Cl and CF$_3$CO$_2$H. $^1$H-NMR (400MHz, CDCl$_3$, Me$_4$Si) $\delta_H$ = 0.87-0.95 (12H, m, C*H$_3$*), 1.27-1.33 (32H, m, (C*H$_2$*)$_8$CH$_3$ and P(CH$_2$)$_3$C*H$_2$C*H$_2$*), 1.50-1.58 (16H, m, PCH$_2$C*H$_2$C*H$_2$*), 2.28-2.36 (8H, m, PC*H$_2$*).

**Trihexyl(tetradecyl)phosphonium CF$_3$SO$_3$ ([P$_{666,14}$]CF$_3$SO$_3$)**

Titled compound was prepared by the same procedure as described above for [C$_4$mim]CF$_3$SO$_3$ with corresponding chloride salt and acid; [P$_{666,14}$]Cl and CF$_3$SO$_3$H. $^1$H-NMR (400MHz, CDCl$_3$, Me$_4$Si) $\delta_H$ = 0.89-0.97 (12H, m, C*H$_3$*), 1.28-1.34 (32H, m, (C*H$_2$*)$_8$CH$_3$ and P(CH$_2$)$_3$C*H$_2$C*H$_2$*)), 1.50 (16H, broad, PCH$_2$C*H$_2$C*H$_2$*), 2.18-2.26 (8H, m, PC*H$_2$*).

**Trihexyl(tetradecyl)phosphonium C$_8$F$_{17}$SO ([P$_{666,14}$]C$_8$F$_{17}$SO$_3$)**

Titled compound was prepared by the same procedure as described above for [C$_4$mim]CF$_3$SO$_3$ with corresponding chloride salt and acid; [P$_{666,14}$]Cl and C$_8$F$_{17}$SO$_3$H. $^1$H-NMR (400MHz, CDCl$_3$, Me$_4$Si) $\delta_H$ = 0.88-0.93 (12H, m, C*H$_3$*), 1.27-1.34 (32H, m, (C*H$_2$*)$_8$CH$_3$ and P(CH$_2$)$_3$C*H$_2$C*H$_2$*), 1.50-1.58 (16H, m, PCH$_2$C*H$_2$C*H$_2$*), 2.19-2.26 (8H, m, PC*H$_2$*).

**Tributyl(hexyl)phosphonium C$_4$F$_9$SO$_3$ ([P$_{4446}$]C$_4$F$_9$SO$_3$)**

The salts was prepared by the same procedure as described above for [C$_4$mim]CF$_3$SO$_3$ with corresponding bromide salt and acid; [P$_{4446}$]Br and C$_4$F$_9$SO$_3$H. $^1$H-NMR (400MHz, CDCl$_3$, Me$_4$Si) $\delta_H$ = 0.89 (3H, t, $J$ = 7.2 Hz, P(CH$_2$)$_5$C*H$_3$*), 0.97 (9H, t, $J$ = 6.8 Hz, P(CH$_2$)$_3$C*H$_3$*), 1.29-1.33 (4H, m, P(CH$_2$)$_3$C*H$_2$C*H$_2$*), 1.48-1.55 (16H, m, PCH$_2$C*H$_2$C*H$_2$*), 2.16-2.24 (8H, m, PC*H$_2$*).

**Tributyl(hexyl)phosphonium C$_8$F$_{17}$SO$_3$ ([P$_{4446}$]C$_8$F$_{17}$SO$_3$)**

The salts was prepared by the same procedure as described above for [C$_4$mim]CF$_3$SO$_3$ with corresponding bromide salt and acid; [P$_{4446}$]Br and C$_8$F$_{17}$SO$_3$H. $^1$H-NMR (400MHz, CDCl$_3$, Me$_4$Si) $\delta_H$ = 0.89 (3H, t, $J$ = 6.9 Hz, P(CH$_2$)$_5$C*H$_3$*), 0.97 (9H, t, $J$ = 4.7 Hz, P(CH$_2$)$_3$C*H$_3$*), 1.29-1.35 (4H, m,

P(CH$_2$)$_3$C*H$_2$*C*H$_2$*), 1.48-1.55 (16H, m, PCH$_2$C*H$_2$*CH$_2$), 2.16-2.24 (8H, m, PC*H$_2$*).

1-Ethyl-3-methylimidazolium C$_4$F$_9$SO$_3$ ([C$_2$mim]C$_4$F$_9$SO$_3$)

The salts was prepared by the same procedure as described above for [C$_4$mim]CF$_3$SO$_3$ with corresponding chloride salt and acid; [C$_2$mim]Cl and C$_4$F$_9$SO$_3$H.  $^1$H-NMR (400MHz, DMSO-$d_6$, $\delta$/ppm relative to Me$_4$Si): 1.41 (3H, t, $J$ = 7.4 Hz, CH$_2$C*H$_3$*), 3.84 (3H, s, NC*H$_3$*), 4.19 (2H, q, $J$ = 7.3 Hz, NC*H$_2$*CH$_3$), 7.69 and 7.78 (2H, t, $J$ = 2.0 and 1.6 Hz, NC*H*C*H*N), 9.10 (1H, s, NC*H*N).

1-Ethyl-3-methylimidazolium C$_8$F$_{17}$SO$_3$ ([C$_2$mim]C$_8$F$_{17}$SO$_3$)

Titled compound was prepared by the same procedure as described above for [C$_4$mim]CF$_3$SO$_3$ with corresponding chloride salt and acid; [C$_2$mim]Cl and C$_8$F$_{17}$SO$_3$H. $^1$H-NMR (400MHz, DMSO-$d_6$, $\delta$/ppm relative to Me$_4$Si): 1.35-1.39 (3H, m, CH$_2$C*H$_3$*), 3.80 (3H, d, $J$ = 0.0 Hz, NC*H$_3$*), 4.12-4.18 (2H, m, NC*H$_2$*CH$_3$), 7.66 and 7.74 (2H, d, $J$ = 1.6 and 2.0 Hz, NC*H*C*H*N), 9.07 (1H, s, NC*H*N).
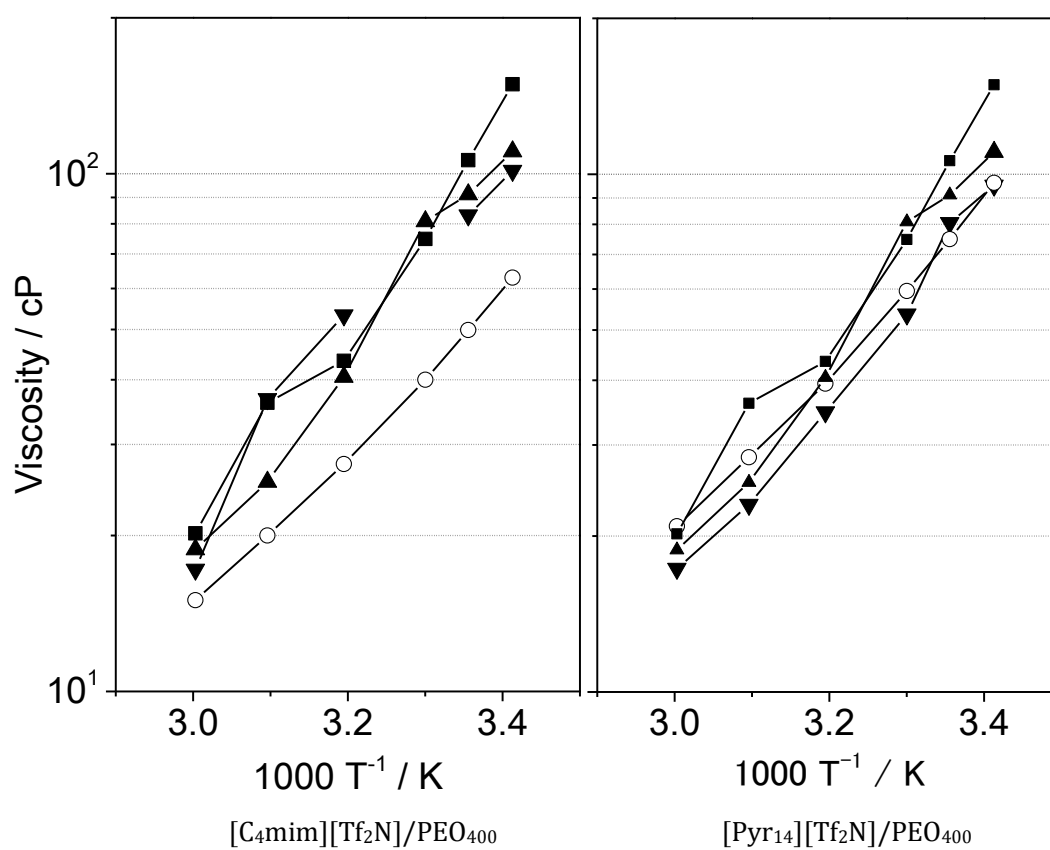
**Figure A2.**  Viscosity of the mixture of [C$_4$mim][Tf$_2$N]/PEO$_{400}$ and [Pyr$_{14}$][Tf$_2$N]/PEO$_{400}$.

**Table A1.** Concentration of 20N, 14H, 13H, 12H, and 8H in ILs and Kamlet-Taft parameter of the ILs.  The concentration are described in form of mole fraction evaluated by using thermal gravimetric analysis in chapter 4.  (○: soluble, ○*: soluble at 70 ℃, ×: insoluble at 70 ℃, and △: soluble at 70 ℃ and became solid after cooling)

| | Mole fraction / mmol mol$^{-1}$ | | | | | Kamlet-Taft parameter | |
| | 20N | 14H | 13H | 12H | 8H | $\alpha$ | $\beta$ |
|---|---|---|---|---|---|---|---|
| $[P_{666,14}][Tf_2N]$ | 3.1 | 24.9 | 173.4 | 520.7 | × | 0.33 | 0.47 |
| $[P_{666,14}]C_8F_{17}SO_3$ | 60.5 | 139.5 | ○ | ○ | × | 0.41 | 0.81 |
| $[C_2mim][Nf_2N]$ | 35.5 | 92.2 | ○ | ○ | △ | 0.76 | 0.22 |
| $[C_2mim][FSI]$ | - | 2.2 | 8.1 | 165.1 | × | - | - |
| $[C_2mim][FAP]$ | 5.7 | 18.3 | 48.0 | ○ | × | 0.81 | -0.02 |
| $[C_4mim]PF_6$ | - | 1.5 | - | ○ | △ | 0.77 | 0.41 |
| $[C_4mim]BF_4$ | - | 3.5 | - | ○ | ○* | 0.73 | 0.72 |
| $[C_4mim]CF_3SO_3$ | - | 6.6 | - | ○ | ○* | 0.63 | 0.46 |
| $[C_2OHmim][Tf_2N]$ | 3.3 | 5.2 | 28.4 | 176.5 | ○* | 1.14 | 0.28 |
| $[AAim][Tf_2N]$ | - | 7.7 | - | ○ | △ | 0.70 | 0.27 |
| $[C_4pri][Tf_2N]$ | - | 5.3 | - | ○ | △ | 0.64 | 0.12 |
| $[Pip_{14}][Tf_2N]$ | - | 7.8 | - | ○ | △ | 0.50 | 0.36 |
| $[Py_{14}][Tf_2N]$ | - | 10.8 | - | ○ | × | 0.49 | 0.23 |
| $[N_{4441}][Tf_2N]$ | - | 12.2 | - | ○ | △ | - | - |
| $[P_{4446}]C_4F_9SO_3$ | 17.7 | 36.4 | ○ | ○ | △ | 0.33 | 0.76 |
| $[C_2mim]C_4F_9SO_3$ | 19.0 | 28.8 | 147.5 | ○ | ○* | 0.77 | 0.47 |
| $[P_{4446}]C_8F_{17}SO_3$ | 101.4 | 208.6 | ○ | - | - | 0.36 | 0.81 |
| $[AAim]Cl$ | - | - | - | ○ | ○* | - | - |
| $[C_2mim][Tf_2N]$ | - | 6.0 | - | - | △ | - | - |